EUROPEAN ORGANIZATION FOR NUCLEAR RESEARCH (CERN)

CERN-EP-2022-008
2022/02/18

CMS-EXO-21-002

Inclusive nonresonant multilepton probes of new phenomena at $\sqrt{s} = 13\,\text{TeV}$

The CMS Collaboration*

Abstract

An inclusive search for nonresonant signatures of beyond the standard model (SM) phenomena in events with three or more charged leptons, including hadronically decaying τ leptons, is presented. The analysis is based on a data sample corresponding to an integrated luminosity of $138\,\text{fb}^{-1}$ of proton-proton collisions at $\sqrt{s} = 13\,\text{TeV}$, collected by the CMS experiment at the LHC in 2016–2018. Events are categorized based on the lepton and b-tagged jet multiplicities and various kinematic variables. Three scenarios of physics beyond the SM are probed, and signal-specific boosted decision trees are used for enhancing sensitivity. No significant deviations from the background expectations are observed. Lower limits are set at 95% confidence level on the mass of type-III seesaw heavy fermions in the range 845–1065 GeV for various decay branching fraction combinations to SM leptons. Doublet and singlet vector-like τ lepton extensions of the SM are excluded for masses below 1045 GeV and in the mass range 125–150 GeV, respectively. Scalar leptoquarks decaying exclusively to a top quark and a lepton are excluded below 1.12–1.42 TeV, depending on the lepton flavor. For the type-III seesaw as well as the vector-like doublet model, these constraints are the most stringent to date. For the vector-like singlet model, these are the first constraints from the LHC experiments. Detailed results are also presented to facilitate alternative theoretical interpretations.

Submitted to Physical Review D

*See Appendix A for the list of collaboration members

1 Introduction

The standard model (SM) of particle physics describes the known fundamental particles and their interactions, and has been extensively tested by experiments. There are strong indications, however, that the SM is incomplete, and beyond-the-SM (BSM) models are required to answer the open questions such as the origin of neutrino masses, the particle nature of dark matter, and the observed baryon asymmetry in the universe. A multitude of compelling BSM theories have been proposed with characteristic signatures that would modify the production of SM particles in proton-proton (pp) collisions. In particular, new BSM particles decaying via the weak interaction could produce the distinctive signature of an excess of events containing multiple final-state leptons above the SM expectations.

In this paper, we describe a search for anomalous production of events with at least three charged leptons (electrons, muons, and hadronically decaying τ leptons) using pp collision data at $\sqrt{s} = 13\,\text{TeV}$ collected by the CMS experiment at the CERN LHC during 2016 to 2018, corresponding to an integrated luminosity of $138\,\text{fb}^{-1}$. The final states analysed in this result include production of up to four light leptons, and up to three hadronically decaying τ leptons. The search is carried out in an inclusive fashion, encompassing a number of final states with numerous kinematic properties, which makes it sensitive to a broad range of BSM scenarios. Collision events are classified by the number of reconstructed objects, such as charged leptons and b-tagged jets (identified from b quark hadronization); kinematic properties, such as the momenta of individual objects; combined properties, such as the invariant mass of lepton pairs; and properties of the entire event, such as missing transverse momentum ($\vec{p}_{\text{T}}^{\,\text{miss}}$) or total hadronic energy. A set of model-independent signal regions (SRs) are defined without reference to any specific signature or model, but rather to minimize the SM background contributions. Results are presented in the form of detailed tables of observed and predicted background yields for these mutually exclusive SRs.

We consider three specific BSM models that address shortcomings of the SM and predict complementary nonresonant multilepton signatures. These BSM models are type-III seesaw heavy fermions [1–9], doublet and singlet vector-like extensions of the third-generation of leptons [10–16], and scalar leptoquarks coupled to a top quark and an SM lepton of any flavor [17–20]. For the first time, we carry out dedicated analyses for these models using a multivariate approach based on boosted decision trees (BDTs). In addition, the model-independent SRs are also used to set constraints on these models.

This paper is organized as follows. We describe the three BSM models in Section 2. Sections 3 and 4 describe the CMS detector and the data and simulation samples used in this search, respectively. Section 5 describes the reconstruction and identification of leptons, jets, and $\vec{p}_{\text{T}}^{\,\text{miss}}$. In Section 6, we outline the broad event selection, and in Section 7, we describe the background estimation techniques. Section 8 describes the model-independent search categories that span the multilepton phase space, as well as the model-specific event selections using BDTs. Section 9 describes the systematic uncertainties in the predictions. Section 10 presents the results of this search, and also discusses the procedure for future interpretations using the model-independent SRs and supporting information made available in a HEPDATA record [21].

2 Signal models

2.1 Type-III seesaw fermions

The observed nonzero neutrino masses and mixing among lepton flavors can be explained by a seesaw mechanism, which introduces new heavy particles coupled to the SM leptons [1–9]. In these models, the neutrino is a Majorana particle, and the neutrino mass arises via mixing with new massive fermions. We consider the type-III seesaw model [22] in this paper, which introduces an SU(2) triplet of heavy leptons, including Dirac charged leptons ($\Sigma^{\pm}$) and a Majorana neutral lepton (Σ^{0}).

At the LHC, these heavy fermions may be pair-produced through electroweak interactions in both charged-charged ($\Sigma^{\pm}\Sigma^{\mp}$) and charged-neutral ($\Sigma^{\pm}\Sigma^{0}$) modes. The seesaw fermions are assumed to mix with SM leptons, and decay to a W, Z, or Higgs boson (H) and an SM lepton (ν, or ℓ = e,μ,τ). The three production modes, combined with the nine possible combinations of boson-SM lepton decay yield 27 distinct signal production and decay modes. An example of the complete decay chain is $\Sigma^{\pm}\Sigma^{0} \to \mathrm{W}^{\pm}\nu\mathrm{W}^{\mp}\ell^{\pm} \to \ell^{\pm}\nu\nu\ell^{\mp}\nu\ell^{\pm}$. Two diagrams exemplifying the production and decay of Σ pairs that result in multilepton final states are shown in Fig. 1. Electroweak and low-energy precision measurements enforce an upper limit on the mixing angles of 10^{-4} across all lepton flavors [23, 24]. This bound allows for prompt decays of heavy fermions in the mass ranges accessible to collider experiments [25–29].

In this analysis, the $\Sigma^{\pm,0}$ are assumed to be degenerate in mass and their decays are assumed to be prompt. The effects of the radiative mass splitting between the neutral and charged heavy fermions are negligible. The Σ decay branching fractions to different bosons are determined solely by their masses. The free parameters are the Σ mass, m_{Σ}, and the Σ decay branching fractions to the SM lepton flavors, $\mathcal{B}_{\mathrm{e}}$, $\mathcal{B}_{\mu}$, and $\mathcal{B}_{\tau}$, where $\mathcal{B}_{\mathrm{e}} + \mathcal{B}_{\mu} + \mathcal{B}_{\tau} = 1$.

The most stringent limits on the type-III seesaw model come from a search conducted by the ATLAS Collaboration using the combined LHC data set from 2016–2018 at $\sqrt{s} = 13\,\mathrm{TeV}$ in multilepton final states with up to four electrons and muons [30]. The search excluded at 95% confidence level (CL) type-III seesaw fermions with masses below 910 GeV in the lepton-flavor-democratic scenario. Previous constraints in the same scenario by the CMS collaboration from a cut-based search using a comparable data set and in similar final states excluded type-III seesaw fermions with masses below 880 GeV at 95% CL [31].

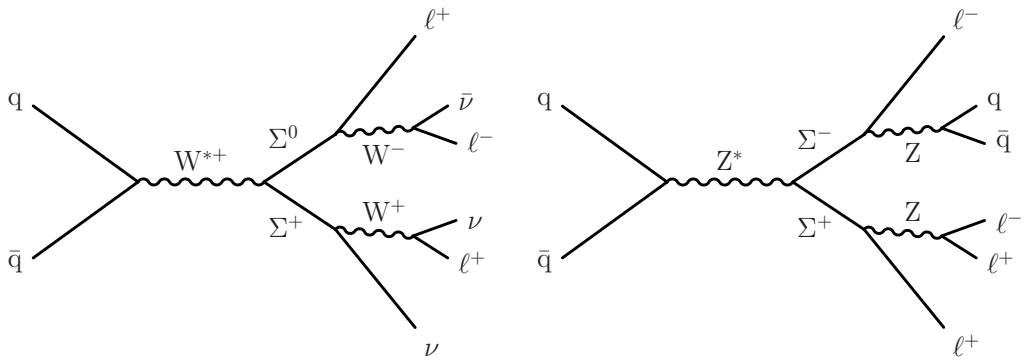

Figure 1: Example processes illustrating production and decay of type-III seesaw heavy fermion pairs at the LHC that result in multilepton final states.

2.2 Vector-like leptons

Vector-like fermions are hypothetical particles whose left- and right-handed components transform under conjugate representations of the SM gauge symmetries [10–13, 15], and hence their

masses are independent of the SM Higgs mechanism and are not constrained by electroweak precision measurements [14, 16]. Vector-like fermions arise in a wide variety of BSM scenarios, including, but not limited to, supersymmetric models [32–35], models with extra spatial dimensions [36, 37], and grand unified theories [38–40]. Extensions of the SM with one or more vector-like fermion families may provide a dark matter candidate [41–44], and account for the mass hierarchy between the different generations of particles in the SM via their mixings with the SM fermions [45–47]. Furthermore, vector-like leptons are also among the proposed solutions to the observed tensions between the experimental measurements and the SM prediction of the anomalous magnetic moment of the muon [34, 48–53].

In this paper, we consider two distinct models in which the vector-like leptons couple to the SM τ lepton [54, 55]. The vector-like doublet model contains an SU(2) doublet (τ',ν'), where the τ' and ν' are mass-degenerate at tree level and can be produced in pairs ($pp \to \tau'^{+}\tau'^{-}$ / $\nu'\overline{\nu'}$) or in association ($pp \to \tau'\nu'$). The decay modes are $\tau' \to Z\tau$ or $H\tau$, and $\nu' \to W\tau$, with the branching fractions of the τ' dependent on the mass $m_{\tau'}$. An example of the complete decay chain for the associated production would be $\nu'\tau'^{\pm} \to W^{\pm}\tau^{\mp}H\tau^{\pm} \to \ell^{\pm}\nu\tau^{\mp}b\bar{b}\tau^{\pm}$ and for the pair production would be $\nu'\overline{\nu'} \to W^{\pm}\tau^{\mp}W^{\pm}\tau^{\mp} \to \ell^{\pm}\nu\tau^{\mp}\ell^{\pm}\nu\tau^{\mp}$. In the vector-like singlet model, only a charged lepton (τ') is present. The τ' can decay to either $Z\tau$ or $H\tau$, or $W\nu$, with the branching fractions similarly governed by $m_{\tau'}$. Figure 2 shows two processes from the doublet and singlet models, which exemplify the production and decay of vector-like τ lepton pairs that result in multilepton final states.

Electroweak precision data constrain the mixing angle between vector-like leptons and SM leptons to be less than about 10^{-2}, permitting prompt decays for mass values that are close to the electroweak scale [56, 57]. We assume prompt decays of vector-like τ leptons; aside from this assumption, the analysis is insensitive to the precise values of the mixing angles.

The most stringent constraints on models with vector-like τ lepton doublets are from a search conducted by the CMS Collaboration [58] with 77 fb^{-1} of data collected in 2016–2017, which excludes them in the mass range of 120–790 GeV. The search is performed with multilepton final states consisting of up to four electrons and muons, and also an additional final state with two light leptons along with one hadronically decaying τ lepton. There are, so far, no direct constraints on the vector-like τ lepton singlet model from any of the LHC experiments. The L3 Collaboration at the LEP placed a lower bound of $\sim$100 GeV on the mass of additional heavy leptons [59].

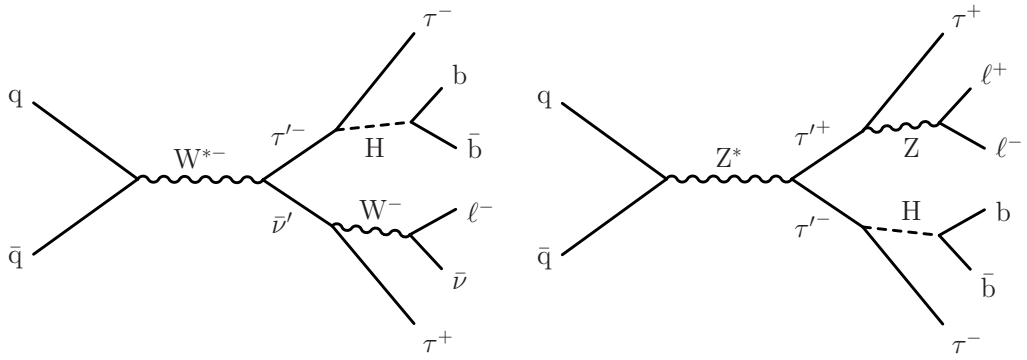

Figure 2: Example processes illustrating production and decay of doublet vector-like τ lepton pairs at the LHC that result in multilepton final states. The right diagram also illustrates the singlet scenario.

2.3 Leptoquarks

Leptoquarks are color-triplet scalar or vector bosons that carry nonzero baryon and lepton quantum numbers and fractional electric charge [18]. Such particles commonly emerge in grand unified theories, e.g., based on $SU(4)$ [60], $SU(5)$ [61], or $SO(10)$ [62] schemes, models with compositeness [63, 64], and R-parity violating supersymmetry models [65, 66].

In pp collisions at the LHC, scalar leptoquarks (S) could be pair-produced via strong interactions, with the production cross section depending only on the leptoquark mass, m_S, but not on the unknown Yukawa coupling. Depending on the nature of the Yukawa coupling, such leptoquarks are expected to decay either to an up-type quark and a charged lepton or to a down-type quark and a neutrino, with branching fractions β and $1-\beta$, respectively. We assume that the Yukawa couplings involve only one generation of quarks or leptons. The simultaneous coupling of leptoquarks to more than one generation of quarks or leptons that are not aligned with the SM Yukawa couplings may lead to quark or lepton flavor violation [20, 67].

In this analysis, we consider scalar leptoquarks [19] with electric charge of $-1/3|e|$, and a nonzero Yukawa coupling to the top quark and a single flavor of SM charged lepton. In a supersymmetric theory, these leptoquarks are right handed down-type squarks that couple to the top quark and charged leptons through leptonic-hadronic R parity violating interactions, where the down-type squarks are the scalar partners of the SM down-type quarks. We assume that only one flavor of charged lepton coupling dominates at a time, and hence consider leptoquark branching fractions $\mathcal{B}_{\mathrm{e}} = 1$, $\mathcal{B}_{\mu} = 1$, or $\mathcal{B}_{\tau} = 1$, for leptoquarks decaying into a top quark and a charged lepton of the first-, second-, or third-generation, respectively. We target the mass range from just above the top quark mass up to the TeV scale. Furthermore, the leptoquark decays are assumed to be prompt, and the coupling is assumed to satisfy $\lesssim$0.1, within the bounds on such Yukawa couplings from leptonic Z boson decays [19, 68]. As with the type-III seesaw and vector-like lepton models, the analysis is independent of the magnitude of the leptoquark Yukawa couplings aside from the assumption of prompt decays. Figure 3 shows two processes exemplifying the production and decay of leptoquark pairs that result in multilepton final states.

Leptoquarks with preferential couplings to third-generation fermions have been suggested among the possible extensions of the SM [69–73] motivated by a series of anomalies recently observed in charged- and neutral-current B meson decays, $\mathrm{b} \to \mathrm{c}\ell\nu$ [74–78] and $\mathrm{b} \to \mathrm{s}\ell\ell$ [79–81], respectively. The ATLAS and CMS Collaborations have conducted a number of searches for leptoquarks with flavor-diagonal and cross-generational couplings involving third-generation fermions [82–90]. The most stringent constraints on scalar leptoquarks with 100% branching fraction to a top quark and first-, second-, or third-generation lepton are set by ATLAS, excluding such particles with masses below 1.48, 1.47 TeV [82] and 1.43 TeV [83], respectively. Similarly, CMS has excluded scalar leptoquarks decaying to a top quark and a τ lepton or a bottom quark and a neutrino with equal branching fractions ($\beta = 0.5$) with masses below 950 GeV [87]. The final states include hadronically decaying top quark and τ lepton, b-tagged jet, and significant missing energy.

3 The CMS detector

The central feature of the CMS apparatus is a superconducting solenoid of 6 m internal diameter, providing a magnetic field of 3.8 T. Within the solenoid volume are a silicon pixel and strip tracker, a lead tungstate crystal electromagnetic calorimeter (ECAL), and a brass and scintillator hadron calorimeter (HCAL), each composed of a barrel and two endcap sections. Forward

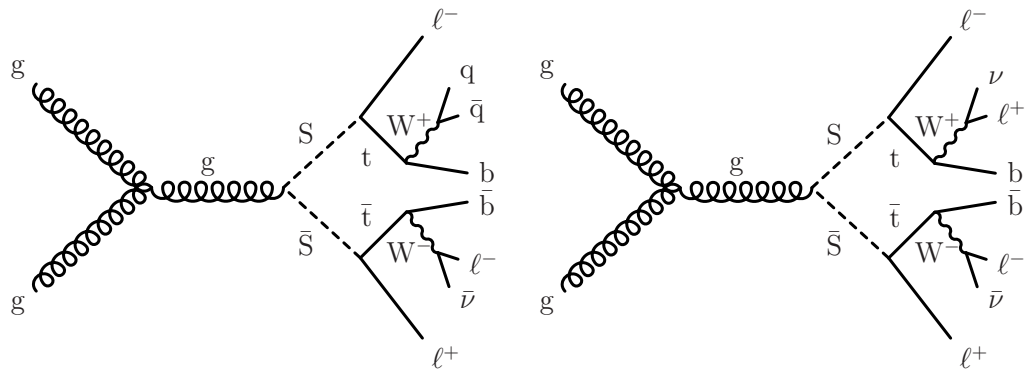

Figure 3: Example processes illustrating the production and decay of scalar leptoquark pairs in pp collisions at the LHC that result in multilepton final states.

calorimeters extend the pseudorapidity (η) coverage provided by the barrel and endcap detectors. Muons are detected in gas-ionization chambers embedded in the steel flux-return yoke outside the solenoid. A more detailed description of the CMS detector, together with a definition of the coordinate system used and the relevant kinematic variables, can be found in Ref. [91].

Events of interest are selected using a two-tiered trigger system. The first level, composed of custom hardware processors, uses information from the calorimeters and muon detectors to select events at a rate of around 100 kHz within a fixed latency of about 4 μs [92]. The second level, known as the high-level trigger, consists of a farm of processors running a version of the full event reconstruction software optimized for fast processing, and reduces the event rate to around 1 kHz before data storage [93].

4 Data samples and event simulation

The total integrated luminosity recorded by CMS in pp collisions at $\sqrt{s} = 13$ TeV corresponds to 138 fb^{-1}, with 36.3, 41.5, and 59.8 fb^{-1} recorded in the years 2016, 2017, and 2018, respectively. The data presented here are collected using a combination of isolated single-electron (-muon) triggers with corresponding transverse momentum (p_{T}) thresholds of 27 (24) GeV in 2016, and 32 (27) GeV in 2017, and 32 (24) GeV in 2018. The rates of signal and SM background processes that gives rise to isolated and nondisplaced leptons are estimated from Monte Carlo (MC) simulations, which incorporate detailed detector and pp collision properties.

The $\mathrm{Z}\gamma$, WZ, $\mathrm{t\bar{t}V}$, and triboson (VVV) backgrounds, where V denotes a W or Z boson, are generated using MADGRAPH5_aMC@NLO (versions 2.2.2 for 2016 data and 2.4.2 for 2017 and 2018 data) [94] at next-to-leading order (NLO) precision in perturbative quantum chromodynamics (QCD). The top quark mass used in all simulations is 172.5 GeV. The $\mathrm{Z}\gamma$ background includes all diagrams contributing to $\mathrm{pp} \to \ell\ell\gamma$, with photons from both initial-state radiation (ISR) and final-state radiation (FSR), and with an invariant mass cut of $m(\ell^+\ell^-) > 10$ GeV. The ZZ background contribution from quark-antiquark annihilation production is generated using POWHEG 2.0 [95–97] at NLO, whereas the contribution from gluon-gluon fusion production is generated at leading order (LO) using MCFM 7.0.1 [98]. The SM processes involving Higgs boson production are generated using POWHEG, MADGRAPH5_aMC@NLO and JHUGEN 7.0.11 [99–102] at NLO, for a Higgs boson mass of 125 GeV. Processes with a single top quark and a Z boson or with four top quarks are simulated using MADGRAPH5_aMC@NLO at NLO in QCD. Other small contributions from processes involving a single top quark and an electroweak or Higgs boson, two top quarks and two bosons, or three top quarks are simulated

using MADGRAPH5_aMC@NLO at LO in QCD. Simulated event samples for the Drell–Yan (DY) and $\mathrm{t\bar{t}}$ processes, which are used for systematic uncertainty studies and in the BDT training process, are generated at NLO with MADGRAPH5_aMC@NLO and POWHEG, respectively.

All signal samples are simulated at LO precision. The type-III seesaw and vector-like lepton samples are generated with MADGRAPH5_aMC@NLO 2.6.1, whereas the leptoquark samples are generated with PYTHIA 8.212 (8.230) in 2016 (2017 and 2018) [103]. The production cross sections for the type-III seesaw signal model are calculated at NLO plus next-to-leading logarithmic precision, assuming that the heavy leptons are SU(2) triplet fermions [104, 105]. Similarly, vector-like lepton and leptoquark cross sections are calculated at NLO precision [55, 106, 107]. In this paper, these higher-order cross sections are used in the analysis of these BSM models.

The NNPDF3.0 LO or NLO parton distribution function (PDF) sets [108] are used for all background and signal samples for 2016 data, with order matching that of the matrix element calculations. The NNPDF3.1 next-to-NLO order (NNLO) PDF set [109] is used for all 2017 and 2018 samples. To perform the parton showering, fragmentation, and hadronization of the matrix-level events in all samples, PYTHIA 8.212 is used with the event tune CUETP8M1 [110] for 2016, and PYTHIA 8.230 is used with the event tune CP5 [111] for 2017 and 2018. The MLM [112] or FxFx [113] jet matching schemes are used for MADGRAPH5_aMC@NLO samples at LO or NLO, respectively. The simulation of the response of the CMS detector to incoming particles is performed using the GEANT4 toolkit [114]. Additional inelastic pp interactions from the same or nearby bunch crossings (pileup) are simulated and incorporated in the MC samples.

5 Event reconstruction and particle identification

In each event, the candidate vertex with the largest total physics-object p_{T}^2 is taken to be the primary pp interaction vertex (PV). The physics objects are the jets, clustered using the anti-k_{T} algorithm [115, 116] with the tracks assigned to candidate vertices as inputs, and the associated $\vec{p}_{\mathrm{T}}^{\,\mathrm{miss}}$, which is the negative vector p_{T} sum of those jets.

The reconstruction and identification of individual particles in an event is based on the particle-flow (PF) algorithm [117], with an optimized combination of information from the various elements of the CMS detector. The energy of photons is obtained from the ECAL measurement. The energy of electrons is determined from the electron momentum at the PV as determined by the tracker, the energy of the corresponding ECAL cluster, and the energy sum of all bremsstrahlung photons spatially compatible with originating from the electron track. The momentum of muons is determined from the curvature of the corresponding track, and the energy is obtained from the momentum. The energy of charged hadrons is determined from a combination of their momentum measured in the tracker and the matching ECAL and HCAL energy deposits, corrected for the response function of the calorimeters to hadronic showers. Finally, the energy of neutral hadrons is obtained from the corresponding corrected ECAL and HCAL energies.

Electrons are reconstructed by geometrically matching charged-particle tracks from the tracking system with energy clusters deposited in the ECAL [118]. The electron momentum is estimated by combining the energy measurement in the ECAL with the momentum measurement in the tracker. The momentum resolution for electrons with $p_{\mathrm{T}} \approx 45\,\mathrm{GeV}$ from $\mathrm{Z} \to \mathrm{ee}$ decays ranges from 1.7 to 4.5%. It is generally better in the barrel region than in the endcaps, and also depends on the bremsstrahlung energy emitted by the electron as it traverses the material in front of the ECAL. To suppress undesired electrons originating from photon conversions in detector material, as well as the misidentification of hadrons, the electron candidates are required

to satisfy shower shape and track quality requirements, using the medium cut-based criteria described in Ref. [118]. Electrons used in this analysis are also required to satisfy $p_T > 10\,\text{GeV}$ and $|\eta| < 2.4$.

Muons are reconstructed from compatible tracks in the inner tracker and the muon detectors [119]. Additional track fit and matching quality criteria suppress the misidentification of hadronic showers that punch through the calorimeters and reach the muon system. Matching tracks measured in the inner tracker and the muon detectors results in a relative p_T resolution, for muons with p_T up to 100 GeV, of 1% in the barrel and 3% in the endcaps, and of better than 7% in the barrel for muons with p_T up to 1 TeV [119]. Muons used in this analysis must lie within the tracking system acceptance, $|\eta| < 2.4$, and are required to have $p_T > 10\,\text{GeV}$.

Hadronically decaying τ lepton candidates (τ_h) are reconstructed from jets, using the hadrons-plus-strips algorithm [120], which combines one or three tracks with energy deposits in the calorimeters, to identify the corresponding one- or three-prong τ lepton decay modes. Neutral pions from τ lepton decay are reconstructed as strips with variable size in η-ϕ from reconstructed electrons and photons, where the ϕ is azimuthal angle in radians and the strip size varies as a function of the p_T of the electron or photon candidate. The reconstructed τ_h candidate must satisfy $|\eta| < 2.3$ and $p_T > 20\,\text{GeV}$.

Jets are clustered using the anti-k_T algorithm [115] with a distance parameter of 0.4, as implemented in the FastJet package [116]. The minimum p_T threshold for the jets selected in this analysis is 30 GeV and the central axis of the jet is also required to be inside the tracking acceptance, $|\eta| < 2.4$. Jets are composite objects made up of several particles, hence the momentum is determined as the vectorial sum of all particle momenta, and is found from simulation to be, on average, within 5–10% of the true momentum over the whole p_T spectrum and detector acceptance. Additional pp interactions within the same or nearby bunch crossings can contribute additional tracks and calorimetric energy depositions, increasing the apparent jet momentum. To mitigate the effect of the charged-particle contribution from pileup on reconstructed jets, a charged hadron subtraction technique is employed, which removes the energy of charged hadrons not originating from the PV [117]. In addition, the impact of neutral pileup particles in jets is mitigated by an event-by-event jet-area-based correction of the jet four-momenta [121–123]. Aside from pileup contamination removal, additional quality criteria are applied to each jet to remove those potentially mismeasured because of instrumental effects or reconstruction failures [124]. Finally, the qualifying jets must lie outside a cone of $\Delta R \equiv \sqrt{(\Delta\eta)^2 + (\Delta\phi)^2} = 0.4$ around a selected muon, electron, or τ_h candidate, where $\Delta\phi$ is the ϕ angle between the jet and lepton.

Jet energy corrections are derived from simulation studies so that the average measured energy of jets matches that of particle level jets. In situ measurements of the p_T balance in dijet, photon+jet, leptonically decaying Z+jet, and multijet events are used to determine any residual differences between the jet energy scale in data and in simulation, and appropriate corrections are made to the jet p_T [123].

The reconstructed jets originating from b hadrons are identified using the medium working point of the DeepCSV b tagging algorithm [125]. This working point has an identification efficiency of 60–75% for b quark jets, depending on jet p_T and η, and a misidentification probability of about 10% for c quark jets and about 1% for light-quark and gluon jets.

The vector $\vec{p}_T^{\,\text{miss}}$ is defined as the negative vector p_T sum of all the PF candidates in an event, and its magnitude is denoted as p_T^{miss} [126]. The pileup-per-particle identification algorithm [127] is applied to reduce the pileup dependence of the $\vec{p}_T^{\,\text{miss}}$ observable. The $\vec{p}_T^{\,\text{miss}}$ is computed from

the PF candidates weighted by their probability to originate from the PV, and is modified to account for corrections to the energy scale of the reconstructed jets in the event.

The leptons that are produced from the decays of the SM bosons W, Z, H (either directly, or via an intermediate τ lepton) are referred to as prompt leptons, and are often indistinguishable in momentum and isolation from those produced in signal events. Thus, the SM processes giving rise to three or more isolated leptons, such as WZ, ZZ, $t\bar{t}V$, VVV, and Higgs boson production, constitute the irreducible backgrounds in this analysis. On the other hand, reducible backgrounds come from SM processes in which the jets are misidentified as leptons, or where the leptons originate from heavy-quark decays. Some examples of such backgrounds are Z+jets or $t\bar{t}$+jets production, in which the prompt leptons are accompanied by leptons that are within or near jets, hadrons that traverse the HCAL and reach the muon detectors, or hadronic showers with large electromagnetic energy fractions. Leptons from such sources are referred to as misidentified leptons, and SM background processes with such misidentified leptons are collectively labeled as "MisID" backgrounds in the subsequent discussion.

The reducible backgrounds are significantly suppressed by applying stringent requirements on the lepton isolation and displacement. For electron and muon candidates, the relative isolation is defined as the scalar p_T sum, normalized to the lepton p_T, of photon and hadron PF objects within a cone of radius ΔR around the lepton. For electrons, the relative isolation is required to be less than $0.0478 + 0.506\,\text{GeV}/p_T$ in the barrel ($|\eta| < 1.479$) and less than $0.0658 + 0.963\,\text{GeV}/p_T$ in the endcap ($|\eta| > 1.479$), with $\Delta R = 0.3$. The relative isolation for muons is required to be less than 0.15 with $\Delta R = 0.4$. The isolation quantities are also corrected for contributions from particles originating from pileup vertices. In addition to the isolation requirement, electrons in the barrel must satisfy $|d_z| < 0.1\,\text{cm}$ and $|d_{xy}| < 0.05\,\text{cm}$, and in the endcap $|d_z| < 0.2\,\text{cm}$ and $|d_{xy}| < 0.1\,\text{cm}$, where d_z and d_{xy} are the longitudinal and transverse impact parameters of electrons with respect to the PV, respectively. Similarly, muons must satisfy $|d_z| < 0.1\,\text{cm}$ and $|d_{xy}| < 0.05\,\text{cm}$. For both electrons and muons, the three-dimensional impact parameter significance, the impact parameter value divided by its uncertainty, must be less than 10, 12, and 9 in 2016, 2017, and 2018 data, respectively. All selected electrons within a cone of $\Delta R < 0.05$ of a selected muon are discarded in order to reduce bremsstrahlung contributions from muons.

For τ leptons, the DEEPTAU [128] algorithm is used to distinguish genuine hadronic tau lepton decays from jets originating from the hadronization of quarks or gluons, as well as from electrons or muons. Information from all individual reconstructed particles near the τ_h axis is combined with properties of the τ_h candidate and the event. In addition to this multivariate requirement, τ_h candidates must satisfy $|d_z| < 0.2\,\text{cm}$. All selected τ_h candidates within a cone of $\Delta R < 0.5$ of a selected electron or muon are also discarded to suppress misidentified tau leptons.

Additionally, to suppress misidentified leptons originating from heavy-flavor decays, leptons are discarded if a b-tagged jet with $p_T > 10\,\text{GeV}$ and $|\eta| < 2.5$ is found within a cone of radius $\Delta R < 0.4$ around the lepton.

These lepton reconstruction and selection requirements result in typical efficiencies of 40–85%, 65–90%, and 20–50% for electrons, muons, and τ_h leptons, respectively, depending on lepton p_T and η.

6 Event selection

We consider seven distinct final states (channels) based on the number of light leptons and τ_h candidates. These seven channels are orthogonal, and are defined as:

- $\geq$4 light leptons and any number of τ_h candidates (4L),
- exactly 3 light leptons and $\geq$1 τ_h candidates (3L1T),
- exactly 3 light leptons and no τ_h candidates (3L),
- exactly 2 light leptons and $\geq$2 τ_h candidates (2L2T),
- exactly 2 light leptons and exactly 1 τ_h candidates (2L1T),
- exactly 1 light lepton and $\geq$3 τ_h candidates (1L3T), and
- exactly 1 light lepton and exactly 2 τ_h candidates (1L2T).

In the 4L channel, only the leading four light leptons in p_T are used in the subsequent analysis. Likewise, in the 3L1T, 2L2T, and 1L3T channels, only the leading 1, 2, and 3 τ_h candidates are used, respectively. In each channel, at least one muon with $p_T > 26$ (29) GeV in 2016 and 2018 (2017) or at least one electron with $p_T > 30$ (35) GeV in 2016 (2017 and 2018) is required, with the thresholds set in order to be consistent with the triggers used.

The events in these seven channels are further classified based on several event properties. This classification is used to enhance sensitivity to particular signal decay chains, or to define dedicated selections to help constrain the SM backgrounds. The quantities are defined below.

- Scalar momentum sums: We define L_T as the scalar p_T sum of all charged leptons that constitute the channel. For example, in the 4L channel, L_T is calculated from the leading four light leptons in p_T, while for the 3L1T channel, it is calculated from the three light leptons and the leading τ_h. We define H_T as the scalar p_T sum of all jets. Additionally, the scalar sum of L_T, H_T, and p_T^{miss} is defined as S_T. The quantity L_T+p_T^{miss} is also of interest. For the signal models considered in this analysis, high signal mass hypotheses give rise to events with high L_T, H_T, p_T^{miss}, and S_T.
- Charge and flavor combinations: We count the number OSSFn as distinct opposite-sign (electric charge) same-flavor lepton pairs in an event. Specific lepton pairs are labeled as OSSF (opposite-sign, same-flavor) and OSDF (opposite-sign, different-flavor). We define Q_ℓ as the sum of charges of all leptons in the event.
- Invariant and transverse masses: We define M_ℓ as the invariant mass of all leptons in the event, and M_{min} as the minimum invariant mass of all dilepton pairs in the event, irrespective of charge or flavor. Additionally, the invariant mass of leptons i and j is defined as M^{ij}. The transverse mass for a single lepton i is defined as $M_T^i = (2p_T^{miss}p_T^i[1-\cos(\vec{p}_T^{miss}, \vec{p}_T^i)])^{1/2}$, where p_T^i is the p_T of lepton i. Similarly, M_T^{ij} is defined as the transverse mass calculated with the p_T^{miss} and the resultant 4-momentum sum of lepton i and j. The lepton indices run over up to 4 leptons, in descending p_T order.

  We define the M_{OSSF} variable in a given event as the OSSF dielectron or dimuon mass closest to the Z boson mass at 91 GeV [129], subject to some additional constraints, and label events with M_{OSSF} within 15 GeV of the Z boson mass (76–106 GeV mass window) as OnZ. Throughout this paper, OSSF1 or OSSF2 events that are not OnZ are labeled as OffZ. In the 3L event with a distinct OSSF pair (such as in $e^+e^-\mu^+$, $\mu^+\mu^-e^-$), the event is classified as BelowZ, OnZ, or AboveZ if the $M_{OSSF} < 76$ GeV, within 76–106 GeV, or >106 GeV, respectively. In the 3L events with two nondistinct

OSSF pairs (such as in $e^+e^-e^+$), the events are classified as OnZ if either pair satisfies M_{OSSF} within 76–106 GeV, as BelowZ if both pairs have masses <76 GeV, or as AboveZ if both pairs have masses >106 GeV. In cases where one pair has mass <76 GeV and the other pair has mass >106 GeV, the event is classified as MixedZ.

In 3L OSSF1 events, the M_T variable is defined as M_T^i, where the lepton i is not part of the M_{OSSF} pair. In events with three electrons or three muons, the M_{OSSF} and M_T variables are chosen simultaneously so that the event is OnZ, and M_T is in the range 50–150 GeV, where this is kinematically possible. Similarly, in 4L OSSF2 events with four electrons or muons, M_{OSSF} is chosen to give the maximum number of nonoverlapping OSSF pairs with masses within the Z boson mass window. Such events are labeled as Single- or Double-OnZ, respectively, depending on whether they have one or two nonoverlapping OnZ OSSF pairs. Additionally, the p_T of the M_{OSSF} lepton pair is defined as p_T^{OSSF}.

The signal models and the SM backgrounds can have multiple W and Z bosons in the decay chains. The invariant and transverse mass quantities aid in defining regions to isolate these specific decays. The M_{OSSF} and M_T variables primarily isolate events with $Z \to \ell\ell$ and $W \to \ell\nu$ decays, respectively, while M_T^{ij} is useful in describing signal events with two visible leptons and p_T^{miss}, such as $\nu' \to W\tau \to \ell\tau\nu$ in the vector-like lepton doublet model.

- Angular quantities: We define ΔR_{min} as the minimum ΔR between all the dilepton pairings in an event, irrespective of charge or flavor. Similarly, $\Delta R_{min}^{\tau_h}$ is defined as the minimum ΔR between any dilepton pair, where at least one of the leptons is a τ_h candidate. The quantities $\Delta\phi^{ij}$ and $\Delta\eta^{ij}$ are defined as the azimuthal angle or pseudorapidity difference between the i^{th} and j^{th} lepton, whereas $\Delta\phi^i$ is defined to denote the opening azimuthal angle between lepton i and $\vec{p}_T^{miss}$. These are quantities that help to characterize the topology of the signal and background events.
- Counts: We define N_j as the multiplicity of jets and N_b as the multiplicity of b-tagged jets satisfying the selection criteria defined earlier.

Finally, all events with $M_{min} < 12$ GeV, $\Delta R_{min} < 0.2$, or $\Delta R_{min}^{\tau_h} < 0.5$ are vetoed in order to suppress contributions due to low-mass resonances (J/ψ, Υ) and low-ΔR FSR photons.

7 Background estimation

A set of control regions (CRs) dominated by the primary background processes is used for the purpose of SM background determination. A summary of all the CR definitions is provided in Table 1. These CRs are utilized to develop and verify a mixture of methods based on both MC simulations and data: normalizing simulated samples for the dominant irreducible SM processes, deriving any residual corrections to the simulated samples, and developing the background estimates based on data for the reducible background contributions. The CRs consist of the following selections: 4L events with two OSSF OnZ pairs and no b jets (4L ZZ CR); 3L events with an OSSF OnZ pair, $M_T < 150$ GeV, and $p_T^{miss} < 125$ GeV (3L OnZ CR); 3L OffZ events with a trilepton mass OnZ and no b jets (3L $Z\gamma$ CR); and 2L1T events with an OSSF OnZ pair and $p_T^{miss} < 100$ GeV (2L1T MisID τ CR). The 3L OnZ CR is further split into three subregions with the following criteria: $p_T^{miss} < 100$ GeV, $M_T < 50$ GeV, and $N_b = 0$ (3L MisID e/μ CR); $50 < M_T < 150$ GeV, minimum lepton $p_T > 20$ GeV, and $N_b = 0$ (3L WZ CR); and $p_T^{miss} < 125$ GeV, $M_T < 150$ GeV, minimum lepton $p_T > 20$ GeV, $N_b > 0$, $N_j > 2$, and $S_T > 350$ GeV (3L $t\bar{t}Z$ CR). Events satisfying any of the CR selection criteria are not considered

in the SRs.

Table 1: A summary of control regions for the irreducible SM processes $Z\gamma$, WZ, $t\bar{t}Z$, and ZZ, and for the misidentified lepton backgrounds. The p_T^{miss}, M_T, the minimum 3L lepton p_T (p_T^3), and S_T are in units of GeV. The 3L OnZ CR is further split into 3L MisID e/μ CR, 3L WZ CR, and 3L $t\bar{t}Z$ CR.

CR name	OSSFn	M_{OSSF}	N_b	p_T^{miss}	M_T	p_T^3	Other selections
2L1T MisID τ	OSSF1	OnZ	—	<100	—	—	—
3L $Z\gamma$	OSSF1	BelowZ	0	—	—	—	Trilepton mass OnZ
3L OnZ	OSSF1	OnZ	—	<125	<150	—	—
3L MisID e/μ	OSSF1	OnZ	0	<100	<50	—	—
3L WZ	OSSF1	OnZ	0	<125	50–150	>20	—
3L $t\bar{t}Z$	OSSF1	OnZ	≥1	<125	<150	>20	$N_j > 2$, $S_T > 350$
4L ZZ	OSSF2	Double-OnZ	0	—	—	—	—

7.1 Irreducible backgrounds

The irreducible backgrounds, as described earlier, arise from processes in which all reconstructed leptons originate from decays of SM bosons. These contributions are estimated using simulated event samples, after normalization and validation in dedicated CRs in data for the major WZ, ZZ, $Z\gamma$, and $t\bar{t}Z$ processes. The normalization correction factors and associated uncertainties, which include both statistical and systematic contributions, take into account the contamination of events from other processes, and are applied to the corresponding background estimates in the SRs. The measurements for the diboson processes are largely independent because of the high purity of the corresponding CRs. Since these backgrounds make significant contributions to the $t\bar{t}Z$-enriched CR, the normalization correction for this process is measured after the corresponding corrections have been obtained for the other backgrounds.

The $ZZ \to 4\ell$ process is the primary background component in the channels with four leptons. The fraction of ZZ events in the 4L ZZ CR is greater than 99%. We consider the $qq \to ZZ \to 4\ell$ and $gg \to ZZ \to 4\ell$ processes collectively, and observe relative normalization uncertainties of 4–5% in each of the three data-taking periods. These uncertainties are dominated by the statistical uncertainties, as the contamination from background processes other than ZZ is negligible in this CR.

The $WZ \to 3\ell\nu$ process is the primary irreducible background source for channels with three leptons. This background is normalized to data in the 3L WZ CR, where the minimum lepton p_T threshold is raised to 20 GeV to suppress the misidentified lepton contributions, and the selection yields a set of events $> 75\%$ pure in WZ. We observe relative normalization uncertainties in the range 3–6% across the three data-taking periods for the $WZ \to 3\ell\nu$ process, which include the statistical and systematic components due to subtraction of background processes other than WZ.

The ZZ and WZ simulation samples are reweighted as functions of the jet multiplicity as well as the visible diboson p_T to match the simulated distributions to those of the data in these CRs, where the visible diboson p_T is defined as the vector p_T sum of the charged leptons in the event. This accounts for missing higher-order QCD and electroweak corrections, and yields an improved description of leptonic and hadronic quantities of interest in this analysis.

Production of $t\bar{t}Z$ is a major irreducible SM background process for all channels with $N_b > 0$.

This background is normalized to data in the 3L $t\bar{t}Z$ CR selection, which is orthogonal to the 3L WZ CR and the misidentified lepton CR selections. Similarly to the selection in the 3L WZ CR, the minimum lepton p_T threshold is raised to 20 GeV to suppress the misidentified lepton contributions, and the selection yields a set of events ∼60% pure in $t\bar{t}Z$. Including the statistical and systematic uncertainties due to subtraction of other background processes, we measure relative normalization uncertainties in the range of 20–30% across the three data-taking periods for the $t\bar{t}Z$ process.

A smaller background contribution arises from ISR or FSR photons that convert asymmetrically such that only one of the resultant leptons is reconstructed in the detector, or from misidentifying on-shell photons as electrons. The dominant source of such backgrounds, collectively referred to as the conversion background, is DY events with an additional photon.The cross section of this process is normalized in a dedicated 3L $Z\gamma$ CR, consisting of BelowZ trilepton events with $N_b = 0$, where the mass of the trilepton system is within 15 GeV of the Z boson mass. The CR targets $Z \to \ell\ell + \gamma$ events, where, for example, the photon converts in the detector and one of the four leptons is too soft to satisfy our lepton selection criteria. This selection yields a set of events $> 70\%$ pure in $Z\gamma$. We obtain relative normalization uncertainties of about 10% across the three data-taking periods, where the quoted value includes the statistical and systematic components due to subtraction of background processes other than $Z\gamma$, as well as a flavor-dependent component due to varying fractions of internal and external conversions as a function of electron multiplicity in the events.

Other irreducible processes that are not normalized in a dedicated CR in data are estimated from simulation samples and normalized to their theoretical cross sections.

In the following figures, diboson backgrounds from WZ and ZZ processes are denoted as "VV", whereas the $t\bar{t}Z$ and $t\bar{t}W$ contributions are labeled as "$t\bar{t}V$". Background processes involving a lepton conversion, particularly the $Z\gamma$ process, are labeled as "Conv." Other irreducible backgrounds estimated using simulation consist of triboson, Higgs boson, and other rare SM contributions, and are collectively referred to as "Rare" backgrounds.

7.2 Misidentified lepton backgrounds

The misidentified lepton backgrounds are estimated via a three- or four-dimensional implementation of a matrix method [130], based on the lepton multiplicity in the targeted signal selections in data. The matrix method defines a set of sideband regions for each SR based on the isolation properties of the selected lepton objects in each event. Leptons in the SR selections satisfy the tight lepton definitions given in Section 5, whereas the sideband selections are defined by loose criteria with relaxed isolation requirements ($<$1.0 relative isolation for electrons and muons, and a relaxed working point of the DEEPTAU algorithm for τ_h), but are otherwise identical to the tight lepton criteria. Therefore, for a 3 (4) lepton event in an SR, the matrix method uses an additional 7 (15) nonoverlapping sideband regions with at least one lepton failing the tight isolation criteria. The sideband regions are therefore orthogonal to the SRs by construction. The probabilities with which prompt- and misidentified lepton candidates pass the tight selection, given that they satisfy the loose selection, are denoted as prompt and misidentification rates, respectively. These are measured as a function of various kinematic features of leptons and hadronic properties of events that impact the lepton isolation. These rates are used in the extrapolation from the sideband regions to the SR. This extrapolation is performed for each event, where the contamination due to prompt leptons that fail the tight lepton selection criteria is also corrected for. Because of the isolation requirements used in the single-lepton triggers, background contributions with up to 2 (3) simultaneous misidentified

leptons in 3 (4) lepton events can be predicted by this implementation of the matrix method. The fraction of signal events where all lepton candidates are misidentified is found to be negligible in simulation based studies.

The prompt rates are measured using a "tag-and-probe" method [131] in various dilepton event selections. In data, prompt rates for electrons and muons are studied in a DY-enriched OnZ OSSF ee and $\mu\mu$ events, respectively. Similarly, prompt rates for τ_h candidates are studied in a DY-enriched set of opposite-sign $e\tau_h$ and $\mu\tau_h$ events. In simulation, the prompt rates are measured in DY and $t\bar{t}$ MC samples, using reconstructed leptons kinematically matched to generator-level prompt leptons ($\Delta R < 0.2$). The measured prompt rates are primarily parametrized as a function of the lepton p_T and $|\eta|$. Prompt rates for electrons and muons vary from about 65% at $p_T \sim 10$ GeV to about 95% at 40 GeV and above. For one- (three-) prong τ_h candidates, the prompt rates are about 50–70% (30–70%) in the p_T range of 20–50 GeV. The final prompt rates for all lepton flavors are based on the DY-enriched data measurements, and the differences between rates derived from DY and $t\bar{t}$ MC simulations are taken as an estimate of the associated systematic uncertainty, accounting for the dependence of prompt rates on hadronic activity. Prompt rate uncertainties are found to be unimportant in the matrix method, and the corresponding impact on the misidentified lepton background estimate is negligible.

The DY+jets and $t\bar{t}$+jets processes are the dominant SM contributions to the total misidentified lepton background in multilepton events. However, different gluon, light quark, and heavy quark compositions, as well as different event kinematic properties of these two processes, yield misidentification rates that may differ by up to 50% from each other for a given lepton flavor. Therefore, dedicated data and MC measurements are performed for both processes. A variant of the tag-and-probe method is used for the measurement of the misidentification rates. In both 3L and 2L1T MisID CRs, the OnZ leptons are taken as the tag leptons, and the additional lepton is taken as the misidentified lepton probe, e.g., eeμ and $\mu\mu\mu$ events are used to measure muon misidentification rates, while eeτ_h and $\mu\mu\tau_h$ events are used to measure the τ_h misidentification rates. In measurements conducted in data, contributions due to prompt probe leptons are estimated and subtracted using MC simulation. Misidentification rates obtained in simulated $t\bar{t}$+jets samples are verified in dedicated data CRs enriched in such contributions, where one lepton is required to fail the three-dimensional impact parameter significance requirement or the b tag veto described in Section 5.

The lepton misidentification rates are also parametrized as functions of the lepton p_T and $|\eta|$. The τ_h rates are further split for one- and three-prong objects. The central value of the misidentification rates for each lepton flavor is corrected for the recoil of the event, where the recoil is defined as a function of the vector sum of the p_T of all other leptons, jets, and p_T^{miss} in the event. These recoil-based corrections improve the modeling of misidentified lepton backgrounds in DY+jets events, in which the misidentified lepton often originates from a jet recoiling against the leptonically decaying Z boson system. Similarly, the misidentification rates are corrected as a function of the multiplicity of tracks originating from the PV and the jet multiplicity.

The final misidentification rates for all lepton flavors are obtained by a weighted average of the DY- and $t\bar{t}$-based measurements. These are evaluated according to the expected DY-$t\bar{t}$ composition of the MisID background, as obtained from simulated samples in each SR category and for each b-tagged jet multiplicity. These DY and $t\bar{t}$ MC samples use normalization factors measured in dedicated dilepton control regions. Half of the difference between rates derived from DY- and $t\bar{t}$-based measurements is assigned as a systematic uncertainty to allow for inaccurate modeling of the expected background composition. Typical electron and muon misidentification rates, relative to the loose selection, are in the range of 5–30%, whereas those of τ_h objects

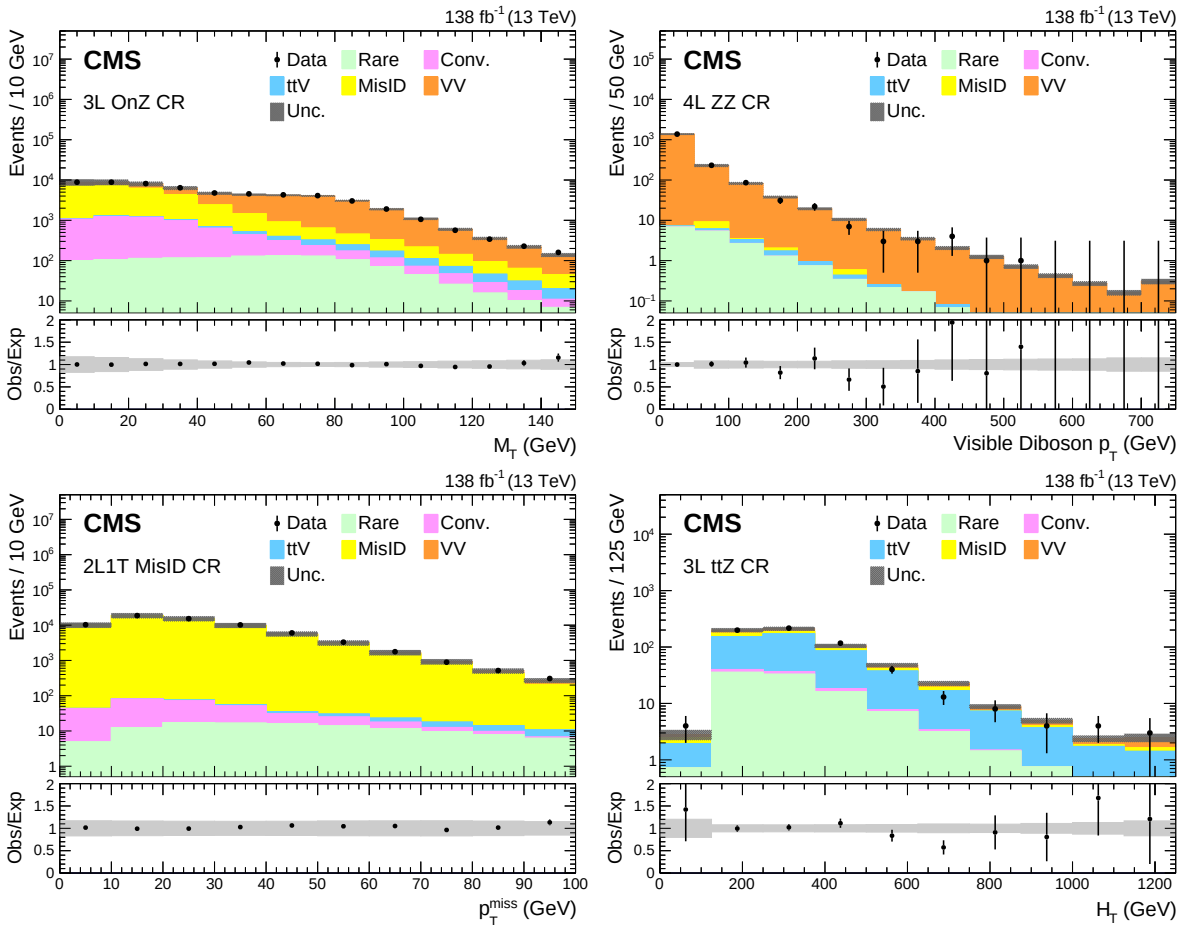

Figure 4: The distributions of M_{T} in 3L OnZ CR (upper left), visible diboson p_{T} in 4L ZZ CR (upper right), $p_{\mathrm{T}}^{\mathrm{miss}}$ in 2L1T MisID CR (lower left), and H_{T} in 3L $\mathrm{t\bar{t}Z}$ CR (lower right) events. The rightmost bin contains the overflow events in each distribution. The lower panel shows the ratio of observed events to the total expected background prediction. The gray band on the ratio represents the sum of statistical and systematic uncertainties in the SM background prediction.

are found to be in the range of 1–15%.

Figure 4 shows a selection of kinematic distributions in the various control regions, with the sum of statistical and systematic uncertainties in the SM background prediction, as described in Section 9. The data are observed to be in agreement with the SM prediction.

8 Signal regions

The multilepton events that have been selected in the seven channels following the description in Sections 5 and 6 are now categorized into two alternative SRs. This categorization is done either in a model-independent way, based on the characteristics of the SM backgrounds, or in a model-dependent way, based on the output of BDTs trained specifically for particular signal hypotheses.

Figure 5 illustrates L_{T}, $p_{\mathrm{T}}^{\mathrm{miss}}$, and H_{T} distributions in the full multilepton phase space, and the M_{OSSF} distribution in channels with at least one OSSF light lepton pair. In each distribution, a benchmark signal hypothesis distribution is overlaid to allow a comparison of shapes between

signal and background. The plots include the sum of statistical and systematic uncertainties in the SM background prediction, as described in Section 9, and the data are found to be in agreement with the SM prediction.

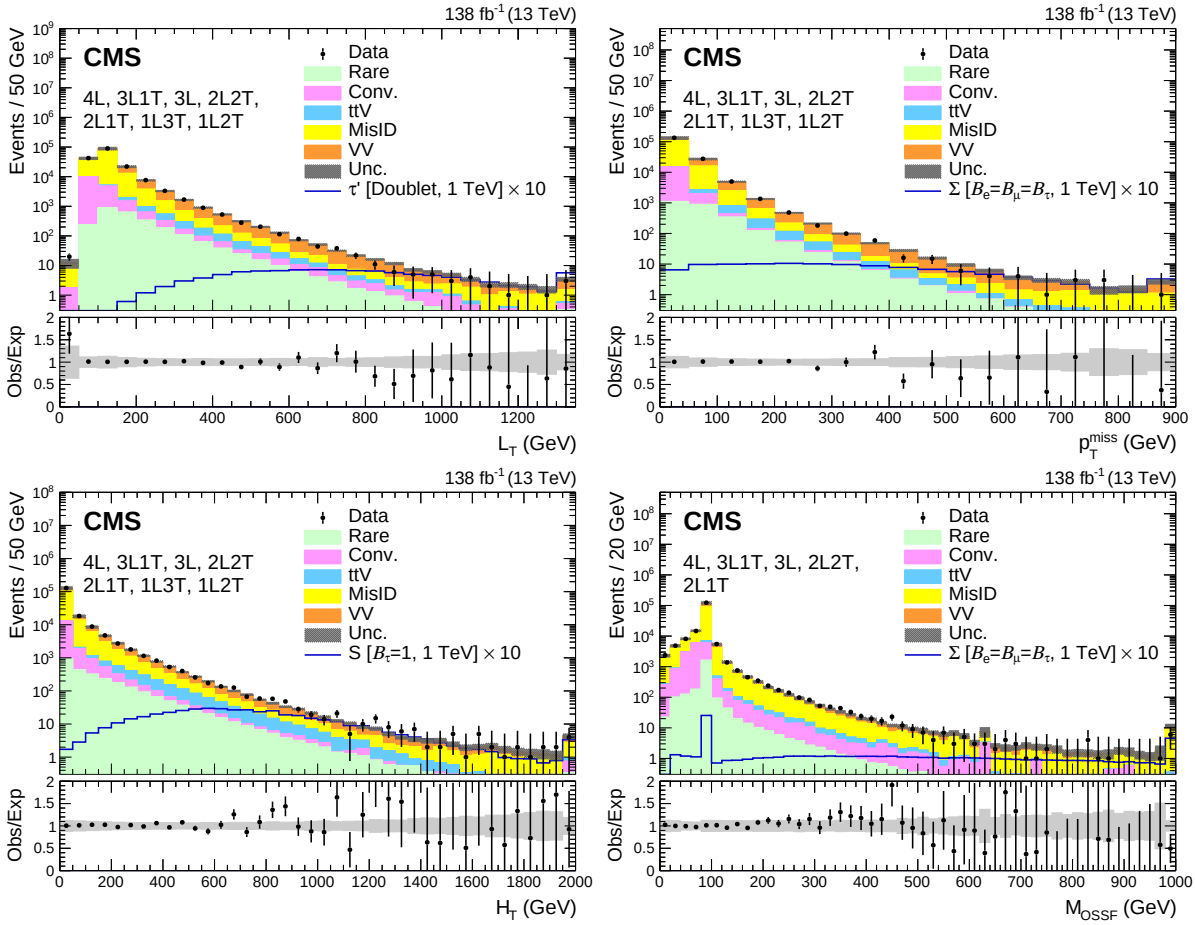

Figure 5: The distributions of L_T (upper left), p_T^{miss} (upper right), and H_T (lower left) in all seven multilepton channels, and M_{OSSF} (lower right) in channels with at least one light lepton pair (4L, 3L1T, 3L, 2L2T, and 2L1T). The rightmost bin contains the overflow events in each distribution. The lower panel shows the ratio of observed events to the total expected background prediction. The gray band on the ratio represents the sum of statistical and systematic uncertainties in the SM background prediction. As illustrative examples, a signal hypothesis for the production of the vector-like τ lepton in the doublet scenario of $m_{\tau'} = 1$ TeV and a scalar leptoquark coupled to a top quark and a τ lepton of $m_S = 1$ TeV are overlaid in the L_T and H_T distributions respectively. Similarly, a signal hypothesis for the production of the type-III seesaw heavy fermions in the flavor-democratic scenario of $m_\Sigma = 1$ TeV is overlaid for the p_T^{miss} and M_{OSSF} distributions.

8.1 Model-independent selections

The model-independent SRs are defined by splitting the channels into various lepton charge and flavor combinations, mass variables, and kinematic regions depending on the dominant SM background processes. This categorization allows the complete utilization of multilepton events collected, such that any event that does not populate a CR contributes to an SR. Explicitly, events selected for the CRs, which are used in the estimation of major SM backgrounds as described in Section 7, are not used in any of the SRs.

Table 2: Fundamental scheme of event categorization, as a function of lepton charge combinations and mass variables. The mass categorizations refer to masses of OSSF pairs if present, and of OSDF pairs otherwise, as explained in the text. For categorization purposes, all possible opposite-sign dielectron and dimuon pair masses in the event are considered, whereas only the largest mass in the event is considered for all other opposite-sign pairs. Only the dielectron and dimuon pairs are considered to tag events as OnZ. The 1L3T OSSF0 and OSSF1 events are combined into a single category. Disallowed categories are marked with "—".

		OSSF0			OSSF1				OSSF2		
		BelowZ	AboveZ	SS	OnZ	BelowZ	AboveZ	MixedZ	Single-OnZ	Double-OnZ	OffZ
3L	Low p_T/M_T	A1	A1	A2	A3	A4	A5	A6	—	—	—
	High p_T/M_T	A7	A7	A8	A9	A10	A11	A12	—	—	—
2L1T	Low p_T	B1	B2	B3	B4	B5	B6	—	—	—	—
	High p_T	B7	B8	B9	B10	B11	B12	—	—	—	—
1L2T		C1	C2	C3	—	C4	C5	—	—	—	—
4L		D1	D1	D1	D2	D3	D3	D3	D4	D5	D6
3L1T		E1	E1	E1	E2	E3	E3	E3	—	—	—
2L2T		F1	F1	F1	F2	F2	F2	—	F3	—	F4
1L3T		G1	G1	G1	—	G1	G1	—	—	—	—

The SRs are designed to separate regions where signs of BSM models could appear from regions dominant in SM background processes. The most easily distinguishable feature is the presence of a Z boson candidate, determined using OSSFn and M_{OSSF}. The ZZ and the WZ processes can be separated by additional requirements on M_T in the event. Similarly, the MisID background can be separated using the minimum lepton p_T. Further selections on N_b give SR regions that have significant contributions from $t\bar{t}Z$.

Based on the idea of the broad categorization described above, we have a fundamental scheme with 43 orthogonal selections labeled A1–G1, as summarized in Table 2. The primary classification is done based on OSSFn, with n being 2, 1, or 0. We also define another scheme, labeled the advanced scheme, which builds on the fundamental scheme, but adds further categories. Each of the 43 fundamental scheme categories is first split into up to three b tag multiplicity regions. The categories with 0 b tag, 1 b tag, and 2 or more b tag multiplicities are denoted by 0B, 1B, and 2B respectively, in all the subsequent tables and figures. Furthermore, each category in a given b tag multiplicity region is split in up to four bins, using a binary low/high p_T^{miss} criterion and an H_T requirement. This results in a total of 204 orthogonal categories.

Events where an OSSF light lepton pair is not found, but an OSSF $\tau\tau$ pair is found, are categorized as BelowZ or AboveZ with respect to the Z pole mass (91 GeV) using the $\tau\tau$ pair mass. This is done since a resonance will not appear at the Z pole mass because of the neutrino emitted in the τ lepton decays. In OSSF0 events, an OSDF pair is sought, and the event is categorized as BelowZ or AboveZ (as for $\tau\tau$ events) based on the OSDF pair with the largest mass. Events with no OSSF or OSDF pairs are classified as same-sign (SS) events.

The 3L channel is further split into two categories, based on the value of either M_T or the minimum lepton p_T. In the 3L OnZ channel, an $M_T > 125$ GeV criterion is used for a binary low or high classification, whereas a lepton $p_T > 25$ GeV criterion is used for the rest of the 3L channel. The 2L1T channel is split into a similar binary classification based on the τ_h candidate $p_T > 50$ GeV criterion.

In order to be sensitive to a large class of BSM models in each of the 43 categories of the fundamental scheme, an L_T+p_T^{miss} distribution is obtained in 200 GeV wide bins, with the last bin being inclusive for all higher values. This results in 156 L_T+p_T^{miss} bins. The combined spectrum (across all 43 categories) gives the fundamental L_T+p_T^{miss} table. The width of bins in the spec-

trum is chosen to provide smooth and monotonic expected background behavior, while still retaining sensitivity to nonresonant models. The first and last bins of the L_T+p_T^{miss} distribution are chosen with the requirement that the per-bin expected background yield is more than 0.5 events to ensure robustness in statistical interpretations.

The second table, labeled the fundamental S_T table, is identical to the first table except that we use the S_T distribution in each category, where S_T is the scalar sum of L_T, H_T, and p_T^{miss}, also in 200 GeV wide bins, resulting in 257 bins. This table provides sensitivity to signal models with energetic jets, such as leptoquarks, whereas the L_T+p_T^{miss} table is optimized for models without significant hadronic activity, such as vector-like lepton and type-III seesaw scenarios.

For the third and final table, we use S_T as the final discriminating variable, binned in 200 GeV increments, in the advanced scheme categorization resulting in 805 bins. This table, labeled the advanced S_T table, provides improved sensitivity to a wide array of BSM signals with masses at the electroweak scale.

The binning in all the schemes is described in Tables 3–6. Each table is produced separately for each year of data collection, resulting in a total of 468 bins in the fundamental L_T+p_T^{miss} table scheme, 771 bins in the fundamental S_T table scheme, and 2415 bins in the advanced S_T table scheme, for the combined 2016–2018 data set.

Table 3: The binning of L_T+p_T^{miss} and S_T distributions for the fundamental scheme in the 3L channel, and the binning of S_T distribution for the advanced scheme in the 3L channel. The categorization is described in Table 2. The ranges, as well the p_T^{miss} and H_T requirements, are given in GeV. The first bins in the L_T+p_T^{miss} or S_T range contain the underflow, the last bins contain the overflow.

	Fundamental Tables				Advanced Table				Advanced Table			Advanced Table	
	L_T+p_T^{miss}		S_T		0B				1B			2B	
Cat.	Range	Bins	Range	Bins	p_T^{miss}	H_T	S_T Range	Bins	p_T^{miss}	S_T Range	Bins	S_T Range	Bins
A1	[0, 800]	1–4	[50, 1650]	1–8	<125	<150	[100, 700]	1–3	<125	[100, 1100]	189–193	[50, 1250]	291–296
					<125	>150	[200, 1000]	4–7					
					>125	<150	[250, 650]	8–9	>125	[150, 1350]	194–199		
					>125	>150	[350, 1150]	10–13					
A2	[50, 450]	5–6	[150, 750]	9–11	—	—	[150, 750]	14–16	—	—	—	—	—
A3	[50, 1650]	7–14	[150, 2750]	12–24	>125	<150	[50, 1450]	17–23	>125	[300, 2100]	200–208	[350, 1750]	297–303
					>125	>150	[250, 2650]	24–35					
A4	[100, 900]	15–18	[50, 1850]	25–33	<125	<150	[50, 650]	36–38	<125	[0, 1200]	209–214	[100, 1300]	304–309
					<125	>150	[150, 1350]	39–44					
					>125	<150	[100, 700]	45–47	>125	[100, 1500]	215–221		
					>125	>150	[300, 1500]	48–53					
A5	[150, 1150]	19–23	[0, 1800]	34–42	<125	<150	[0, 1000]	54–58	<125	[100, 1100]	222–226	[100, 1300]	310–315
					<125	>150	[150, 1150]	59–63					
					>125	<150	[100, 900]	64–67	>125	[200, 1200]	227–231		
					>125	>150	[300, 1300]	68–72					
A6	[50, 850]	24–27	[0, 1400]	43–49	<125	<150	[50, 650]	73–75	<125	[150, 950]	232–236	[300, 1100]	316–319
					<125	>150	[200, 1000]	76–79					
					>125	<150	[200, 800]	80–82	>125	[350, 1150]	237–239		
					>125	>150	[500, 1100]	83–85					
A7	[0, 1000]	28–32	[150, 1750]	50–57	<125	<150	[50, 650]	86–88	<125	[150, 1150]	240–244	[150, 1350]	320–325
					<125	>150	[150, 950]	89–92					
					>125	<150	[150, 750]	93–95	>125	[350, 1350]	245–249		
					>125	>150	[350, 1350]	96–100					
A8	[100, 500]	33–34	[50, 650]	58–60	—	—	[50, 650]	101–103	—	—	—	—	—
A9	[150, 1350]	35–40	[150, 2150]	61–70	<125	<150	[150, 2150]	104–108	<125	[300, 1300]	250–254	[450, 1250]	326–329
					<125	>150	[400, 1800]	109–115					
					>125	<150	[200, 1000]	116–119	>125	[350, 1350]	255–259		
					>125	>150	[500, 1700]	120–125					
A10	[100, 1100]	41–45	[0, 1800]	71–79	<125	<150	[0, 800]	126–129	<125	[150, 1150]	260–264	[250, 1250]	330–334
					<125	>150	[200, 1400]	130–135					
					>125	<150	[150, 950]	136–139	>125	[300, 1300]	265–269		
					>125	>150	[300, 1500]	140–145					
A11	[0, 1400]	46–52	[50, 2050]	80–89	<125	<150	[50, 1250]	146–151	<125	[200, 1400]	270–275	[200, 1600]	335–341
					<125	>150	[200, 1600]	152–158					
					>125	<150	[200, 1200]	159–163	>125	[300, 1500]	276–281		
					>125	>150	[400, 1800]	164–170					
A12	[100, 1100]	53–57	[150, 1750]	90–97	<125	<150	[100, 900]	171–174	<125	[100, 1100]	282–286	[350, 1150]	342–345
					<125	>150	[250, 1450]	175–180					
					>125	<150	[300, 900]	181–183	>125	[500, 1300]	287–290		
					>125	>150	[450, 1450]	184–188					

Table 4: The binning of L_T+p_T^{miss} and S_T distributions for the fundamental scheme in the 2L1T channel, and the binning of S_T distribution for the advanced scheme in the 2L1T channel. The categorization is described in Table 2. The ranges, as well as the p_T^{miss} and H_T requirements, are given in GeV. The first bins in the L_T+p_T^{miss} or S_T range contain the underflow, and the last bins contain the overflow.

	Fundamental Tables				Advanced Table 0B				Advanced Table 1B			Advanced Table 2B	
Cat.	L_T+p_T^{miss} Range	Bins	S_T Range	Bins	p_T^{miss}	H_T	S_T Range	Bins	p_T^{miss}	S_T Range	Bins	S_T Range	Bins
B1	[100, 700]	58–60	[100, 1300]	98–103	<100	<150	[150, 550]	346–347	<100	[0, 800]	489–492	[150, 950]	571–574
					<100	>150	[250, 850]	348–350					
					>100	<150	[0, 600]	351–353	>100	[100, 1100]	493–497		
					>100	>150	[350, 1150]	354–357					
B2	[50, 850]	61–64	[0, 1600]	104–111	<100	<150	[50, 650]	358–360	<100	[50, 1050]	498–502	[150, 1150]	575–579
					<100	>150	[300, 1100]	361–364					
					>100	<150	[200, 800]	365–367	>100	[250, 1250]	503–507		
					>100	>150	[300, 1300]	368–372					
B3	[100, 500]	65–66	[150, 750]	112–114	—	—	[150, 750]	373–375	—	—	—	—	—
B4	[150, 950]	67–70	[0, 1800]	115–123	>100	<150	[50, 750]	376–379	>100	[200, 1200]	508–512	[250, 1050]	580–583
					>100	>150	[400, 1600]	380–385					
B5	[100, 700]	71–73	[50, 1250]	124–129	<100	<150	[150, 550]	386–387	<100	[50, 850]	513–516	[50, 1050]	584–588
					<100	>150	[100, 1100]	388–392					
					>100	<150	[0, 600]	393–395	>100	[100, 900]	517–520		
					>100	>150	[300, 1100]	396–399					
B6	[0, 1000]	74–78	[150, 1550]	130–136	<100	<150	[50, 850]	400–403	<100	[150, 1150]	521–525	[250, 1050]	589–592
					<100	>150	[200, 1200]	404–408					
					>100	<150	[200, 800]	409–411	>100	[250, 1250]	526–530		
					>100	>150	[300, 1300]	412–416					
B7	[100, 700]	79–81	[50, 1250]	137–142	<100	<150	[150, 550]	417–418	<100	[100, 700]	531–533	[400, 800]	593–594
					<100	>150	[150, 750]	419–421					
					>100	<150	[150, 550]	422–423	>100	[250, 1050]	534–537		
					>100	>150	[350, 1150]	424–427					
B8	[0, 1000]	82–86	[150, 1750]	143–150	<100	<150	[150, 750]	428–430	<100	[100, 1100]	538–542	[350, 1350]	595–599
					<100	>150	[250, 1050]	431–434					
					>100	<150	[150, 950]	435–438	>100	[250, 1450]	543–548		
					>100	>150	[250, 1450]	439–444					
B9	[100, 500]	87–88	[100, 700]	151–153	—	—	[100, 700]	445–447	—	—	—	—	—
B10	[250, 1250]	89–93	[200, 2000]	154–162	>100	<150	[100, 1100]	448–452	>100	[250, 1250]	549–553	Incl.	600
					>100	>150	[400, 2000]	453–460					
B11	[100, 900]	94–97	[50, 1450]	163–169	<100	<150	[100, 700]	461–463	<100	[100, 900]	554–557	[250, 950]	601–603
					<100	>150	[250, 1050]	464–467					
					>100	<150	[150, 750]	468–470	>100	[250, 1050]	558–561		
					>100	>150	[400, 1200]	471–474					
B12	[50, 1050]	98–102	[150, 1750]	170–177	<100	<150	[100, 900]	475–478	<100	[200, 1000]	562–565	[400, 1000]	604–606
					<100	>150	[350, 1150]	479–482					
					>100	<150	[300, 900]	483–485	>100	[350, 1350]	566–570		
					>100	>150	[600, 1200]	486–488					

Table 5: The binning of L_T+p_T^{miss} and S_T distributions for the fundamental scheme in the 1L2T channel, and the binning of S_T distribution for the advanced scheme in the 1L2T channel. The categorization is described in Table 2. The ranges, as well as the p_T^{miss} and H_T requirements, are given in GeV. The first bins in the L_T+p_T^{miss} or S_T range contain the underflow, and the last bins contain the overflow.

	Fundamental Tables				Advanced Table 0B				Advanced Table 1B			Advanced Table 2B	
	L_T+p_T^{miss}		S_T										
Cat.	Range	Bins	Range	Bins	p_T^{miss}	H_T	S_T Range	Bins	p_T^{miss}	S_T Range	Bins	S_T Range	Bins
C1	[100, 500]	103–104	[100, 900]	178–181	<75	<75	[0, 400]	607–608	<75	[100, 500]	657–658	[200, 600]	684–685
					<75	>75	[200, 600]	609–610					
					>75	<75	Incl.	611	>75	[100, 700]	659–661		
					>75	>75	[150, 750]	612–614					
C2	[150, 750]	105–107	[100, 1100]	182–186	<75	<75	[150, 750]	615–616	<75	[50, 650]	662–664	[100, 900]	686–689
					<75	>75	[100, 700]	617–619					
					>75	<75	[150, 750]	620–622	>75	[200, 800]	665–667		
					>75	>75	[300, 900]	623–625					
C3	[50, 450]	108–109	[150, 550]	187–188	—	—	[150, 550]	626–627	—	—	—	—	—
C4	[50, 850]	110–113	[100, 1700]	189–196	<75	<75	[0, 600]	628–630	<75	[0, 800]	668–671	[200, 1000]	690–693
					<75	>75	[150, 950]	631–634					
					>75	<75	[150, 750]	635–637	>75	[150, 1150]	672–676		
					>75	>75	[150, 1350]	638–643					
C5	[50, 850]	114–117	[150, 1350]	197–202	<75	<75	[0, 600]	644–646	<75	[150, 750]	677–679	[200, 800]	694–696
					<75	>75	[250, 850]	647–649					
					>75	<75	[50, 650]	650–652	>75	[200, 1000]	680–683		
					>75	>75	[300, 1100]	653–656					

Table 6: The binning of L_T+p_T^{miss} and S_T distributions for the fundamental scheme in the 4L, 3L1T, 2L2T, and 1L3T channels, and the binning of S_T distribution for the advanced scheme in the 4L, 3L1T, 2L2T, and 1L3T channels. The categorization is described in Table 2. The ranges, as well as the p_T^{miss} and H_T requirements, are given in GeV. The first bins in the L_T+p_T^{miss} or S_T range contain the underflow, and the last bins contain the overflow. For the 3L1T and 2L2T channels, multiple categories in the 1B or 2B selections are combined. These bins are marked with a single- or a double-dagger. For the 1L3T channel, all the b tag categories are combined and the corresponding bins are marked with an asterisk.

	Fundamental Tables				Advanced Table 0B				Advanced Table 1B			Advanced Table 2B	
	L_T+p_T^{miss}		S_T										
Cat.	Range	Bins	Range	Bins	p_T^{miss}	H_T	S_T Range	Bins	p_T^{miss}	S_T Range	Bins	S_T Range	Bins
D1	Incl.	118	Incl.	203	—	—	Incl.	697	—	—	—	—	—
D2	[150, 950]	119–122	[0, 1400]	204–210	<75	<50	[150, 550]	698–699	<75	[200, 800]	739–741	[400, 1000]	765–767
					<75	>50	[200, 1000]	700–703					
					>75	<50	[100, 700]	704–706	>75	[300, 1100]	742–745		
					>75	>50	[250, 1050]	707–710					
D3	[150, 750]	123–125	[150, 950]	211–214	<75	<50	[0, 400]	711–712	—	[250, 850]	746–748	Incl.	768
					<75	>50	Incl.	713					
					>75	—	Incl.	714					
D4	[50, 1250]	126–131	[100, 1500]	215–221	<75	<50	[0, 1000]	715–719	<75	[100, 900]	749–752	[250, 1050]	769–772
					<75	>50	[150, 1150]	720-724					
					>75	<50	[150, 750]	725–727	>75	[250, 1050]	753–756		
					>75	>50	[400, 1200]	728–731					
D5	[100, 700]	132–134	[50, 1050]	222–226	—	—	—	—	<75	[100, 900]	757–760	Incl.	773
					—	—	—	—	>75	Incl.	761		
D6	[0, 800]	135–138	[100, 1100]	227–231	<75	<50	[0, 600]	732–734	—	[150, 750]	762–764	Incl.	774
					<75	>50	[150, 750]	735–737					
					>75	—	Incl.	738					
E1	[100, 500]	139–140	[250, 650]	232–233	—	—	Incl.	775	—	[150, 950]	795–798 †	[250, 850]	802–804 †
E2	[100, 900]	141–144	[50, 1250]	234–238	—	—	[100, 1100]	776–780	—	[150, 950]	795–798 †	[250, 850]	802–804 †
E3	[150, 750]	145–147	[0, 1000]	239–244	—	—	[0, 800]	781–784	—	[150, 950]	795–798 †	[250, 850]	802–804 †
F1	Incl.	148	[50, 450]	245–246	—	—	Incl.	785	—	[200, 800]	799–801 ‡	Incl.	805 ‡
F2	[150, 550]	149–150	[100, 700]	247–249	—	—	[150, 550]	786–787	—	[200, 800]	799–801 ‡	Incl.	805 ‡
F3	[100, 700]	151–153	[150, 950]	250–253	—	—	[100, 900]	788–791	—	[200, 800]	799–801 ‡	Incl.	805 ‡
F4	[150, 550]	154–155	[200, 800]	254–256	—	—	[150, 550]	792–793	—	[200, 800]	799–801 ‡	Incl.	805 ‡
G1	Incl.	156	Incl.	257	—	—	Incl.	794*	—	Incl.	794*	Incl.	794*

8.2 Model-dependent selections

The model-dependent SRs are defined by employing BDTs that are trained to discriminate a specific signal from the SM backgrounds. We have used the BDT implementation from the TMVA package [132]. Individual BDTs for specific model scenarios and for each year of data collection are trained to discriminate the signal process from the major SM backgrounds (WZ, ZZ, DY, $t\bar{t}$, and $Z\gamma$).

8.2.1 Discriminant training

The BDT training process consider all multilepton events that pass the event selection, and are performed separately for each year of data collection. Events passing the CR selections are removed from the training process, but are used to validate the modeling of BDT input variables and the outputs of the trained BDTs.

For each of the three data-taking periods, BDTs are trained using statistically independent simulated event samples of signal and background from the other two periods. The misidentified lepton background contributions used for training the BDT are taken from the DY and $t\bar{t}$ MC samples; hence the training does not employ the sideband events in data used to predict the misidentified lepton backgrounds.

The properties of the targeted BSM models vary considerably across the probed 0.1 to 2.0 TeV mass range, and may depend explicitly on lepton flavor. To address this, we define small windows in signal mass, combining a few neighboring signal mass hypotheses in a single training, yielding three mass-range-specific BDTs for each signal.

For the vector-like lepton model, a single BDT is trained using both the doublet and singlet scenarios. For the type-III seesaw model, separate BDTs are trained for the flavor-democratic ($\mathcal{B}_e = \mathcal{B}_\mu = \mathcal{B}_\tau$) scenario and for the $\mathcal{B}_\tau = 1$ scenario. Similarly, for the leptoquark model, two separate BDTs are trained for the models with couplings to τ leptons ($\mathcal{B}_\tau = 1$) and light leptons ($\mathcal{B}_e + \mathcal{B}_\mu = 1$).

A combination of up to 48 object- and event-level quantities are used as input variables to the model-specific trainings. These include p_T, invariant masses, angular variables, lepton charge and flavor, and b-tagged jet multiplicities, as described in Section 6. A full list of the quantities used in the BDT training process is provided in Table 7.

Table 7: Input variables used for the BDTs trained for the various BSM models. Note that the indices i, j run over the leptons of all flavors ($i, j = 1, 2, 3, 4$) in a given event. If a given variable is not defined in a given channel, the variable is set to a nonphysical default value for signal and background processes, and plays no role in training.

Variable type	Used for		
	All signals	Vector-like lepton	Seesaw and leptoquarks
Event	H_T, p_T^{miss}, N_b, M_ℓ	Q_ℓ	L_T, p_T^i/L_T, L_T/S_T, H_T/S_T, p_T^{miss}/S_T
Lepton	p_T^i, p_T^{OSSF}		
Angular	ΔR_{min}	Max, Min: $\Delta\phi^i$, Max, Min: $\Delta\phi^{ij}$	Max: $\Delta\eta^{ij}$
Mass	M_T^i	M^{ij}, M_T^{12}, M_T^{13}, M_T^{23}	

All BDTs used for each BSM model have 800 trees with a maximum depth of 10, and utilize a minimum node size of 1.5% with 10 steps during node cut optimization. The *GradientBoost* algorithm is chosen for boosting the trees. The BDT hyperparameters, as well as the choices of training strategy described here have been optimized to give the largest background rejection for a given signal efficiency in the training samples. This optimization is done while ensuring

that the performance of the BDTs in orthogonal testing data sets matches the training performance, and that the performance in testing data sets does not change significantly for small changes in the BDT hyperparameters.

To summarize, for the vector-like lepton model, three mass ranges and thus three BDTs are trained per year of data taking. For the type-III seesaw and leptoquark models, three mass ranges with two flavor scenarios in each range are considered, giving six BDTs each per year.

8.2.2 Discriminant application

The BDT of a given signal model training provides a score in the range of $(-1, 1)$, with the interval close to 1 associated with the highest sensitivity to the signal. Therefore, we define a number of variable-width regions across the BDT score, with narrower regions defined on the high score side. To further increase signal sensitivity, the BDT scores in the three-lepton (3L, 2L1T, 1L2T) channels are combined into a single distribution; similarly the BDT scores in the four-lepton (4L, 3L1T, 2L2T, 1L3T) channels are combined into one distribution as well. This procedure is applied to each year separately in order to achieve optimal signal-to-noise ratio, with bin widths chosen in each year to obtain uniformly increasing expected background yields. This defines the BDT regions in which we perform counting experiments.

We denote signal-specific BDTs by *SS*, *VLL*, and *LQ* for the type-III seesaw, vector-like lepton, and leptoquark models, respectively. The various mass ranges are denoted by *L* (low), *M* (medium), and *H* (high). For each signal mass hypothesis, the performance from every mass-range BDT of that signal model is considered, and the BDT that gives the best expected exclusion is chosen for that mass in the evaluation. Occasionally this leads to mismatched training and application mass ranges. For example, a vector-like τ lepton of $m_{\tau'} = 500\,\text{GeV}$ is used in the *VLL-M* training, but the best expected performance at $m_{\tau'} = 500\,\text{GeV}$ is achieved from the *VLL-H* training, and therefore is used for its application. This behavior can be attributed to the larger acceptance and population of events from higher mass samples in the tails of sensitive variables such as L_T, p_T^miss etc., which benefits the signal versus background separation. A summary of all these mass ranges for the individual BDTs used in the training and for the application for each model can be found in Table 8.

Table 8: Signal mass points as used in the training of BDTs and the masses for which the specific trained BDT is applied in the SRs according to the best sensitivity. The labels *L*, *M*, and *H* denote low, medium, and high mass ranges, respectively.

BDT	Trained using masses (GeV)	Applied for masses (GeV)
Type-III seesaw		
SS-L	200, 300	200, 300
SS-M	400, 550, 700, 850	400, 550
SS-H	1000, 1250	700 and higher
Vector-like lepton		
VLL-L	100, 150, 200	100, 150, 200
VLL-M	300, 500	250, 300, 350, 400
VLL-H	650, 700, 800	450 and higher
Leptoquarks		
LQ-L	300, 400	300, 400
LQ-M	500, 600, 700	500, 600, 700
LQ-H	1200, 1300, 1400	800 and higher

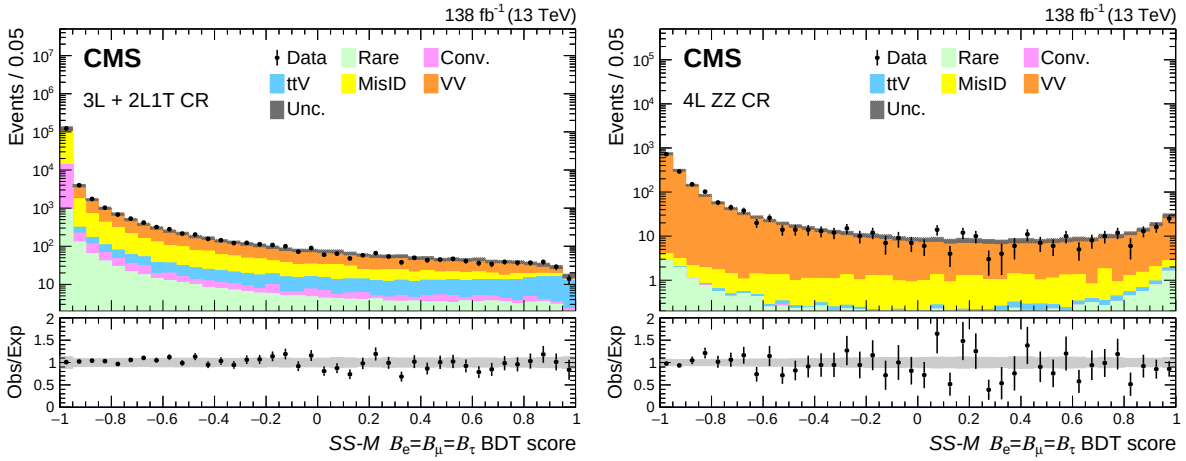

Figure 6: Distributions of BDT score from the *SS-M* $\mathcal{B}_e = \mathcal{B}_\mu = \mathcal{B}_\tau$ BDT are shown for the 3L+2L1T CR (left), and the 4L ZZ CR (right). The 3L+2L1T CR consists of the 3L OnZ, 3L Zγ, and 2L1T MisID CRs. The lower panel shows the ratio of observed events to the total expected background prediction. The gray band on the ratio represents the sum of statistical and systematic uncertainties in the SM background prediction.

Figure 6 shows the output from the *SS-M* BDT in the flavor-democratic scenario, with statistical and systematic uncertainties in the SM background prediction, as described in Section 9. The BDT output is shown in the 4L ZZ CR, and in the combined 3L OnZ, 3L Zγ and 2L1T MisID CRs, and the data are observed to be in good agreement with the expected SM background prediction.

9 Systematic uncertainties

All background and signal estimates have uncertainties due to the finite number of events in simulated samples or data sidebands. These statistical uncertainties are typically small, as we utilize large MC samples or data sidebands, but are nonetheless propagated to the analysis.

The fractional inclusive normalization uncertainties for WZ, Zγ, t$\bar{\text{t}}$Z, and ZZ backgrounds are 3–5, 10, 15–25, and 4–5% respectively, in all three years of data collection. For all other background processes, a 50% flat systematic uncertainty is assigned to the theoretical cross section estimates at LO or NLO to cover any higher-order effects, as well as the renormalization and factorization scale uncertainties.

Systematic uncertainties arise from the corrections applied to the background and signal simulations for lepton reconstruction, isolation, and trigger efficiencies; b tagging efficiency; pileup modeling; electron and jet energy resolution; and electron, muon, τ leptons, jet, and unclustered energy scale measurements. The uncertainties in such corrections typically correspond to 1–10% variation in the simulation-based irreducible background and signal yields across all SRs. Similarly, uncertainties due to choices of factorization and renormalization scales [133] and PDFs [108, 109] are also evaluated for signal and dominant irreducible background processes, yielding variations smaller than 10% in the SRs. The uncertainties in the diboson p_T and jet multiplicity modeling in the WZ and ZZ MC samples typically yield variations in the range of 5–15 and 5–30%, respectively. The electron charge misidentification rate is also corrected in a dedicated DY-enriched dielectron selection of data events, and a 30% relative uncertainty is assigned to it. The integrated luminosities of the 2016, 2017, and 2018 data-taking periods are individually known with uncertainties in the 1.2–2.5% range [134–136], while the total 2016–

2018 integrated luminosity has an uncertainty of 1.6%.

The uncertainty in the misidentified lepton background, which is estimated from data via the matrix method, is dominated by the uncertainties in the lepton misidentification rates. The relative statistical uncertainties in the measurement of the misidentification rates are typically in the 10–30% range. As we use an extrapolation of electron and muon misidentification rate measurements for $p_{\mathrm{T}} > 50\,\mathrm{GeV}$ and τ_{h} misidentification rate measurements for $p_{\mathrm{T}} > 80\,\mathrm{GeV}$, we double these uncertainties and assign a flat 60% relative uncertainty for all high-p_{T} leptons. In summary, lepton misidentification rates have typical relative uncertainties of 10, 30, and 60% in the low, medium, and high lepton p_{T} regions, respectively, where low is defined as ($10 < p_{\mathrm{T}} < 20\,\mathrm{GeV}$ for light leptons, $10 < p_{\mathrm{T}} < 30\,\mathrm{GeV}$ for τ_{h}), medium is ($20 < p_{\mathrm{T}} < 50\,\mathrm{GeV}$ for light leptons, $30 < p_{\mathrm{T}} < 80\,\mathrm{GeV}$ for τ_{h}), and high is ($p_{\mathrm{T}} > 50\,\mathrm{GeV}$ for light leptons, $p_{\mathrm{T}} > 80\,\mathrm{GeV}$ for τ_{h}). These result in variations in the range of 20–50% of the misidentified lepton background contribution estimates, and these nuisances are also kept uncorrelated in each of the three data-taking periods. In addition, we consider process-dependent uncertainties in the lepton misidentification rates. These are estimated by comparing the misidentification rates observed in the DY- and $\mathrm{t\bar{t}}$-enriched measurements, and are typically in the range of 5–25% and correlated across the data-taking periods.

In order to account for different compositions of misidentified lepton origins in multilepton events with and without b-tagged jets, the systematic uncertainties in the misidentified lepton backgrounds in different table categories and b-tagged jet multiplicities, as well as BDT regions, are taken to be uncorrelated. The uncertainties in the diboson p_{T} and jet multiplicity modeling in the WZ and ZZ MC samples are taken to be uncorrelated between the different channels. All other systematic uncertainties are taken to be correlated across all table categories, BDT regions, and channels.

The uncertainty sources, the affected processes, the resulting uncertainty in the yield of those processes, and the correlations across the data-taking periods are summarized in Table 9.

10 Results

The L_{T}+$p_{\mathrm{T}}^{\mathrm{miss}}$ distributions of the fundamental table scheme for all channels with the combined 2016–2018 data set are shown in Fig. 7, where each histogram bin corresponds to an orthogonal L_{T}+$p_{\mathrm{T}}^{\mathrm{miss}}$ bin in regions defined by the fundamental table scheme. Similarly, the S_{T} distributions of the fundamental table scheme and the advanced table scheme are shown in Fig. 8, and Figs. 9–12, respectively.

The BDT region distributions for the two highest mass BDTs for the 3-lepton channels (3L, 2L1T, 1L2T) and the 4-lepton channels (4L, 3L1T, 2L2T, 1L3T) with the combined 2016–2018 data set for the type-III seesaw model with $\mathcal{B}_{\mathrm{e}} = \mathcal{B}_{\mu} = \mathcal{B}_{\tau}$ and $\mathcal{B}_{\tau} = 1$ couplings are shown in Figs. 13–14 and 15–16, respectively. Similarly, distributions for the doublet vector-like lepton, leptoquarks with $\mathcal{B}_{\tau} = 1$ couplings, and leptoquarks with $\mathcal{B}_{\mathrm{e}} + \mathcal{B}_{\mu} = 1$ couplings are shown in Figs. 17–18, 19–20, and 21–22, respectively.

Across all the channels considered, we find agreement between the data and the predictions of the SM background. No significant excess of data consistent with the models we probe is observed. We perform goodness-of-fit tests in each of the model-independent SR table schemes based on the saturated model method [137] to quantify the deviations between the background-only hypothesis and the observed data. The fundamental L_{T}+$p_{\mathrm{T}}^{\mathrm{miss}}$, S_{T}, and the advanced S_{T} schemes have global p-values [138] of 0.67, 0.53, and 0.11, respectively, consistent with the

Table 9: Sources, magnitudes, effective variations, and correlation properties of systematic uncertainties in the SRs. Uncertainty sources marked as "Yes" in the Correlation column have their nuisance parameters correlated across the 3 years of data collection.

Uncertainty source	Magnitude	Type	Processes	Variation	Correlation
Statistical	1–100%	per event	All MC samples	1–100%	No
Integrated luminosity	1.2–2.5%	per event	Conv./Rare/Signal	1.2–2.5%	Yes
Electron/Muon reco., ID, and iso. efficiency	1–5%	per lepton	All MC samples	2–5%	No
τ_h reco., ID, and iso. efficiency	5–15%	per lepton	All MC samples	5–25%	No
Lepton displacement efficiency	1–2%	per lepton	All MC samples	3–5%	No
Trigger efficiency	1–4%	per lepton	All MC samples	<3%	No
b tagging efficiency	1–10%	per jet	All MC samples	2–5%	No
Pileup	5%	per event	All MC samples	<3%	Yes
PDF, fact./renorm. scale	<20%	per event	All MC samples	<10%	Yes
Jet energy scale	1–10%	per jet	All MC samples	<5%	No
Unclustered energy scale	1–25%	per event	All MC samples	<2%	No
Electron energy scale and resolution	<2%	per lepton	All MC samples	<5%	Yes
Muon energy scale and resolution	2%	per lepton	All MC samples	<5%	No
τ_h energy scale	<10%	per lepton	All MC samples	<5%	No
Electron charge misidentification	30%	per lepton	All MC samples	<25%	No
WZ normalization	3–5%	per event	WZ	3–5%	No
ZZ normalization	4–5%	per event	ZZ	4–5%	No
$t\bar{t}Z$ normalization	15–25%	per event	$t\bar{t}Z$	15–25%	No
Conversion normalization	10–50%	per event	$Z\gamma$/Conv.	10–50%	No
Rare normalization	50%	per event	Rare	50%	No
Prompt and misidentification rates	20–60%	per lepton	MisID	20–50%	No
DY-$t\bar{t}$ process dependence	5–25%	per lepton	MisID	5–25%	Yes
Diboson jet multiplicity modeling	<30%	per event	WZ/ZZ	5–30%	No
Diboson p_T modeling	<30%	per event	WZ/ZZ	5–15%	No

background-only hypotheses.

Apart from the global agreement, we report the most significant local deviations as seen in the three model-independent schemes in the combined 2016–2018 data set, without considering the look-elsewhere effect [139]. The largest local excess in the fundamental L_T+p_T^{miss} table is found in the bin 16 (3L, A4 category, OSSF1 BelowZ, low minimum lepton p_T, $300 < L_T+p_T^{miss} < 500\,GeV$), resulting in a data excess of 2.7 standard deviations. We also observe a local deficit of approximately 1.7 standard deviations in the bin 143 (3L1T, E3 category, OSSF1 OnZ, $500 < L_T+p_T^{miss} < 700\,GeV$). For the fundamental S_T table, we observe the largest local excess of around 2.3 standard deviations in the bin 78 (3L, A10 category, OSSF1 BelowZ, high minimum lepton p_T, $1400 < S_T < 1600\,GeV$) in the combined 2016–2018 data set, and similarly we also have a local deficit of 1.9 standard deviations in the bin 236 (3L1T, E2 category, OSSF1 OnZ, $650 < S_T < 850\,GeV$). Finally, the largest local excess in the advanced S_T table is found in the bin 600 (2L1T, B10 category, OSSF1 OnZ, high τ_h p_T, 2B, Inclusive) resulting in an excess of 2.5 standard deviations, and the largest local deficits are observed in bins 40 (3L, A4 category, OSSF1 BelowZ, low minimum lepton p_T, 0B, low p_T^{miss}, high H_T, $350 < S_T < 550\,GeV$) and 714 (4L, D3 category, OSSF1 OffZ, 0B, high p_T^{miss}, Inclusive) with 2.0 standard deviations each. These extreme local deviations are generally driven by excesses or deficits in a single year of data-taking, and are not found to be consistent across all three data-taking periods. All other local deviations are measured to be less significant.

The three model-independent SR table schemes are used separately to calculate the upper limits on the production cross section for the three BSM models considered here. For each of the three separate table schemes, the corresponding bins from Tables 3–6 are treated as counting experiments in each data-taking period, and are fitted simultaneously with bins for each of the three years of data collection in the statistical analysis. Similarly, the BDT regions corresponding to

the 3- and 4-lepton channels for a specific BDT variable (depending on the model, mass-range, and flavor scenario) are treated as counting experiments in each data-taking period, and are fitted simultaneously for each of the three years of data collection.

To calculate the upper limits, we use a modified frequentist approach with the CL_s [140–143] criterion, with a test statistic based on the binned profile likelihood, in the asymptotic approximation. The upper limits are calculated at 95% CL. The systematic uncertainties and their correlations as described in Section 9 are incorporated in the likelihood as nuisance parameters with log-normal probability density functions. The statistical uncertainties in the signal and background estimates are modeled with gamma functions. Finally, we present the cross section limit at a particular mass point from the table scheme or the BDT training that gives the best expected limit. The details for each model are discussed in the subsequent paragraphs.

As a general remark, the model-independent advanced S_T table schemes are more sensitive than the lowest-mass BDT training process for all the models. This is because at low signal masses, the training process is degraded by the low signal yield and the similar kinematic properties of signal and SM processes.

Figure 23 shows the observed and expected cross section limits for the production of the type-III seesaw heavy fermions in the flavor-democratic scenario. The observed (expected) lower limit on m_Σ in this scenario is 980 (1060) GeV. The best expected limit is given by the advanced S_T table scheme for $m_\Sigma < 350$ GeV, and by the BDT regions for higher signal mass values. For arbitrary Σ decay branching fractions to SM lepton flavors, subject to the constraint that $\mathcal{B}_e + \mathcal{B}_\mu + \mathcal{B}_\tau = 1$, the observed and expected lower limits on m_Σ in the plane defined by $\mathcal{B}_e$ and $\mathcal{B}_\tau$ are shown in Fig. 24. These limits are given by the *SS-H* $\mathcal{B}_\tau = 1$ BDT when $\mathcal{B}_\tau \geq 0.9$, and by the *SS-H* $\mathcal{B}_e = \mathcal{B}_\mu = \mathcal{B}_\tau$ BDT for the other decay branching fraction combinations. The strongest constraints are when $\mathcal{B}_\mu = 1$ ($m_\Sigma > 1065$ GeV), while the weakest are when $\mathcal{B}_\tau = 0.8$, $\mathcal{B}_e = 0.2$ ($m_\Sigma > 845$ GeV). This behavior is expected because of the greater efficiency of reconstructing and identifying muons versus τ_h candidates in the experiment.

Figure 25 shows the observed and expected cross section limits for the doublet and singlet vector-like lepton models. For the doublet model, vector-like τ leptons are excluded up to a mass $m_{\tau'}$ of to 1045 GeV, where the expected mass exclusion is 975 GeV. The best expected limit for $m_{\tau'} < 280$ GeV is given by the advanced S_T table scheme, and by the BDT regions for larger masses. For the singlet model, the best expected limits are given by the advanced S_T table over the entire mass range. Singlet vector-like τ leptons are excluded in the mass interval from 125 to 150 GeV, while the expected exclusion range is from 125 to 170 GeV.

The cross section limits for the leptoquark model are shown in Fig. 26. For a leptoquark S exclusively coupling to a top quark and a muon, the observed (expected) lower limit on the mass of pair produced leptoquarks is 1420 (1460) GeV. For the top quark and electron decay scenario, the observed (expected) lower limit on m_S is 1340 (1370) GeV, while for the top quark and τ lepton decay scenario, the lower limit is 1120 (1235) GeV. The advanced S_T table gives the best expected limit for m_S less than 400, 400, and 500 GeV for the $\mathcal{B}_e = 1$, $\mathcal{B}_\mu = 1$, and $\mathcal{B}_\tau = 1$ scenarios, respectively, while the BDT regions give the best expected limits above these thresholds.

The results presented here can be reinterpreted to provide constraints on other BSM models. We provide the requisite information in a HEPDATA record [21], as detailed in the following description. Specifically, given a specific BSM model, a particular model-independent scheme should be selected. The fundamental L_T+p_T^{miss} table scheme will be sensitive to BSM models produced primarily via electroweak interactions, while the advanced S_T table scheme will be

more sensitive for models which populate final states with several jets, which may or may not arise from b quarks. Following the choice of a scheme, the signal yield for the model should be obtained in the various categories of the scheme. This signal yield can be calculated using generator-level quantities. However, there will be a significant correction arising from detector effects, primarily the lepton reconstruction and identification efficiencies. We provide detailed efficiency maps for electrons, muons and τ_h, where the provided efficiency is that for a generator level lepton to be both reconstructed and identified as described in this analysis. In addition, we also provide the product of acceptance and efficiency for each probed signal model in this paper. We find that the yield calculated from generator-level quantities corrected by the efficiency maps agrees with the final analysis yields within 20% for the channels with light leptons (4L, 3L) and within 30% for channels that involve a τ_h (3L1T, 2L2T, 2L1T, 1L3T, 1L2T).

The obtained BSM model yields in the various categories can then be used along with the SM backgrounds, the background covariance matrix, and the observations to arrive at constraints for the model in the simplified likelihood framework [144].

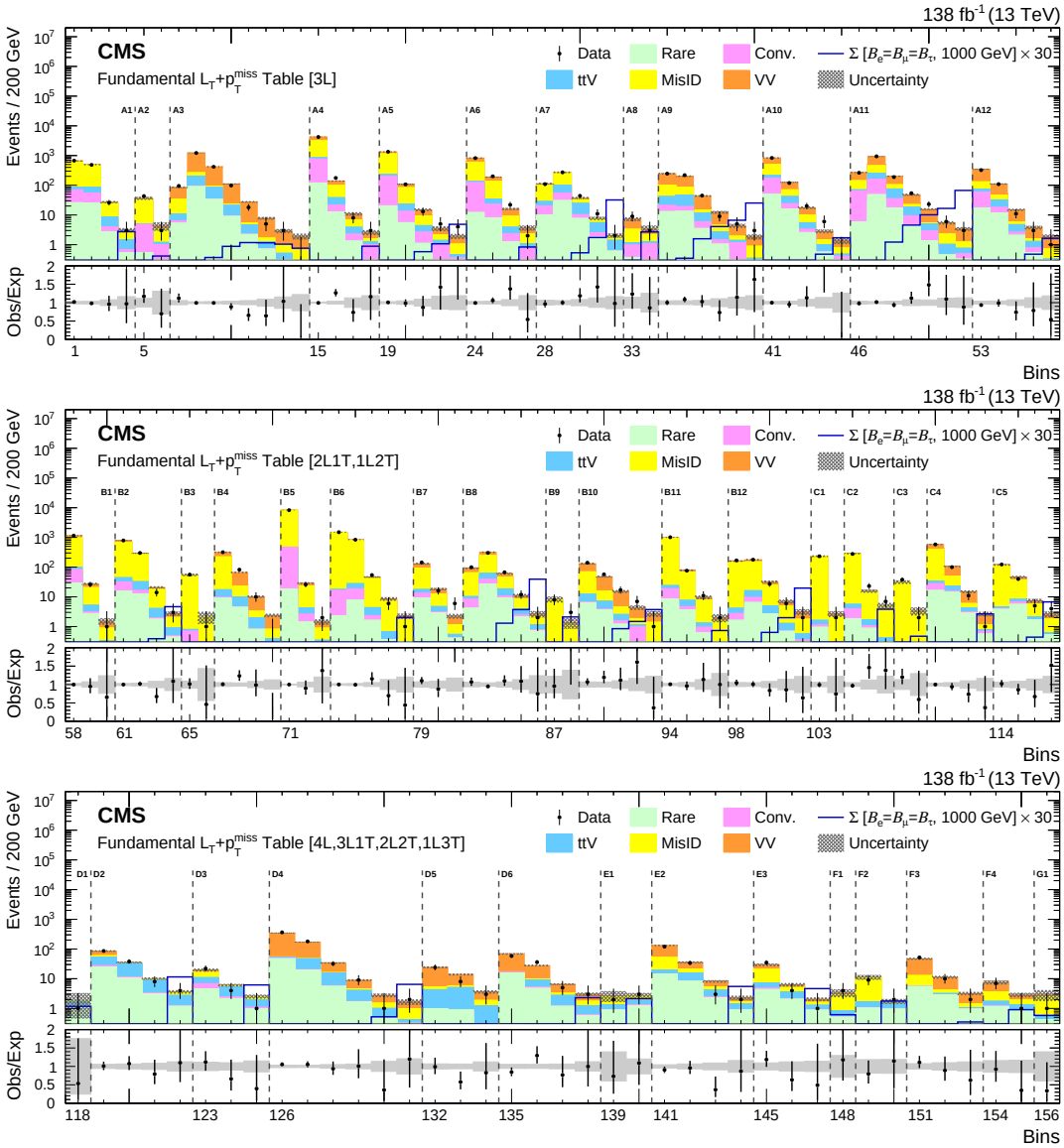

Figure 7: The SR distributions of the fundamental $L_T+p_T^{miss}$ table for the combined 2016–2018 data set. The detailed description of the bin numbers can be found in Tables 3–6. The lower panel shows the ratio of observed events to the total expected background prediction. The gray band on the ratio represents the sum of statistical and systematic uncertainties in the SM background prediction. The expected SM background distributions and the uncertainties are shown after fitting the data under the background-only hypothesis. For illustration, an example signal hypothesis for the production of the type-III seesaw heavy fermions in the flavor-democratic scenario for $m_\Sigma = 1$ TeV, before the fit, is also overlaid.

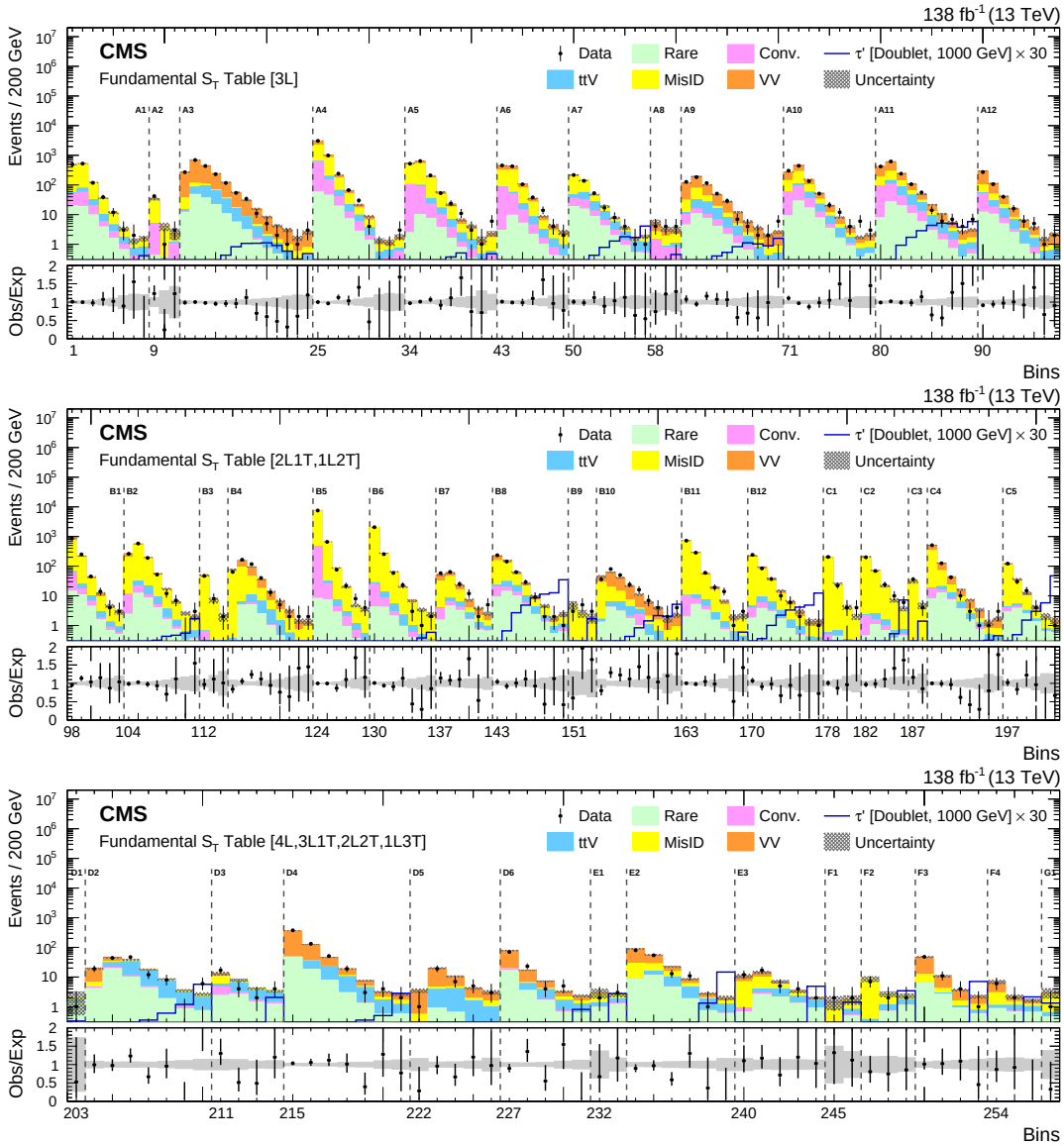

Figure 8: The SR distributions of the fundamental S_T table for the combined 2016–2018 data set. The detailed description of the bin numbers can be found in Tables 3–6. The lower panel shows the ratio of observed events to the total expected background prediction. The gray band on the ratio represents the sum of statistical and systematic uncertainties in the SM background prediction. The expected SM background distributions and the uncertainties are shown after fitting the data under the background-only hypothesis. For illustration, an example signal hypothesis for the production of the vector-like τ lepton in the doublet scenario for $m_{\tau'} = 1$ TeV, before the fit, is also overlaid.

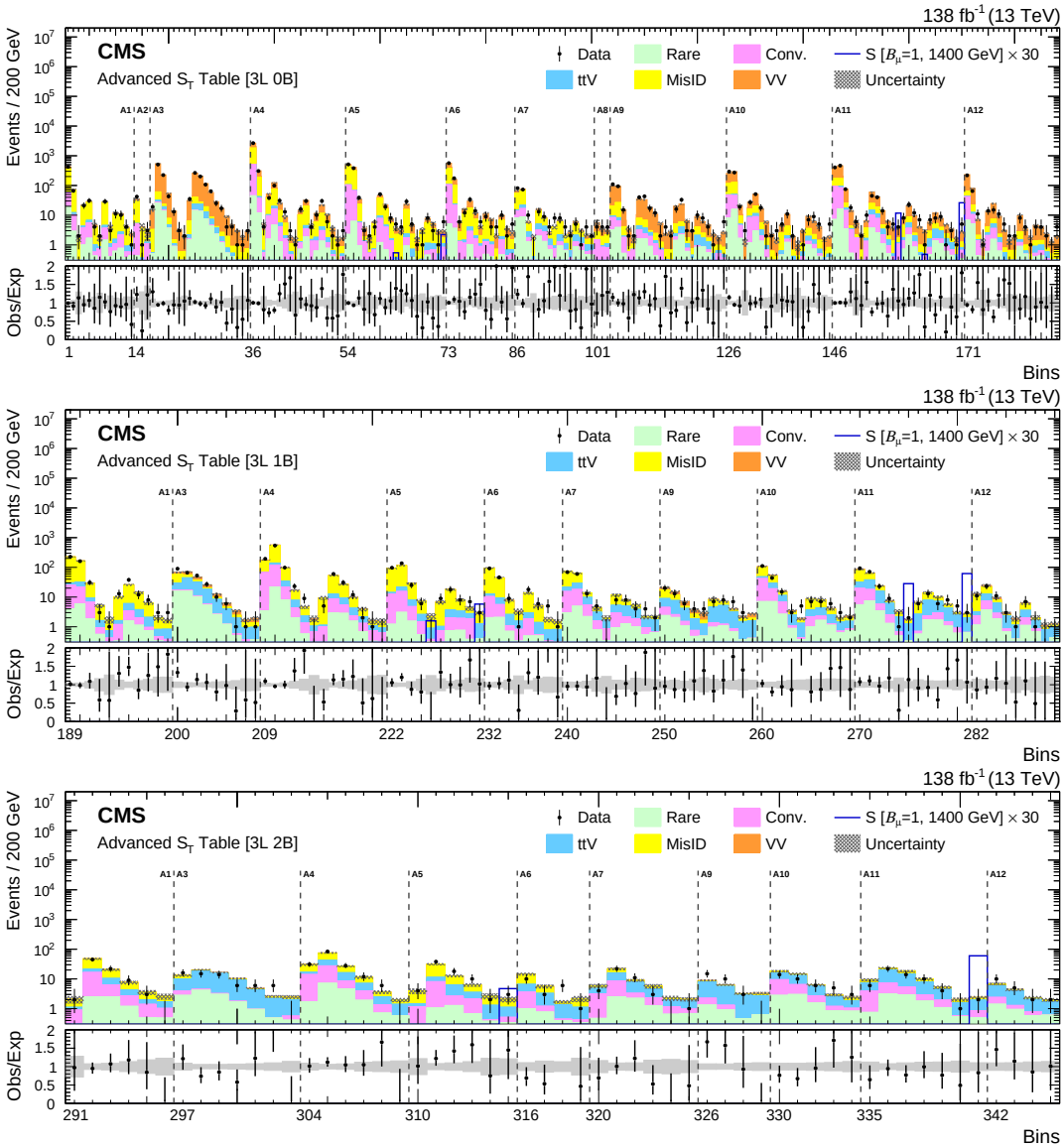

Figure 9: The 3L SR distributions of the advanced S_T table for the combined 2016–2018 data set. The detailed description of the bin numbers can be found in Table 3. The lower panel shows the ratio of observed events to the total expected background prediction. The gray band on the ratio represents the sum of statistical and systematic uncertainties in the SM background prediction. The expected SM background distributions and the uncertainties are shown after fitting the data under the background-only hypothesis. For illustration, an example signal hypothesis for the production of the scalar leptoquark coupled to a top quark and a muon for $m_S = 1.4$ TeV, before the fit, is also overlaid.

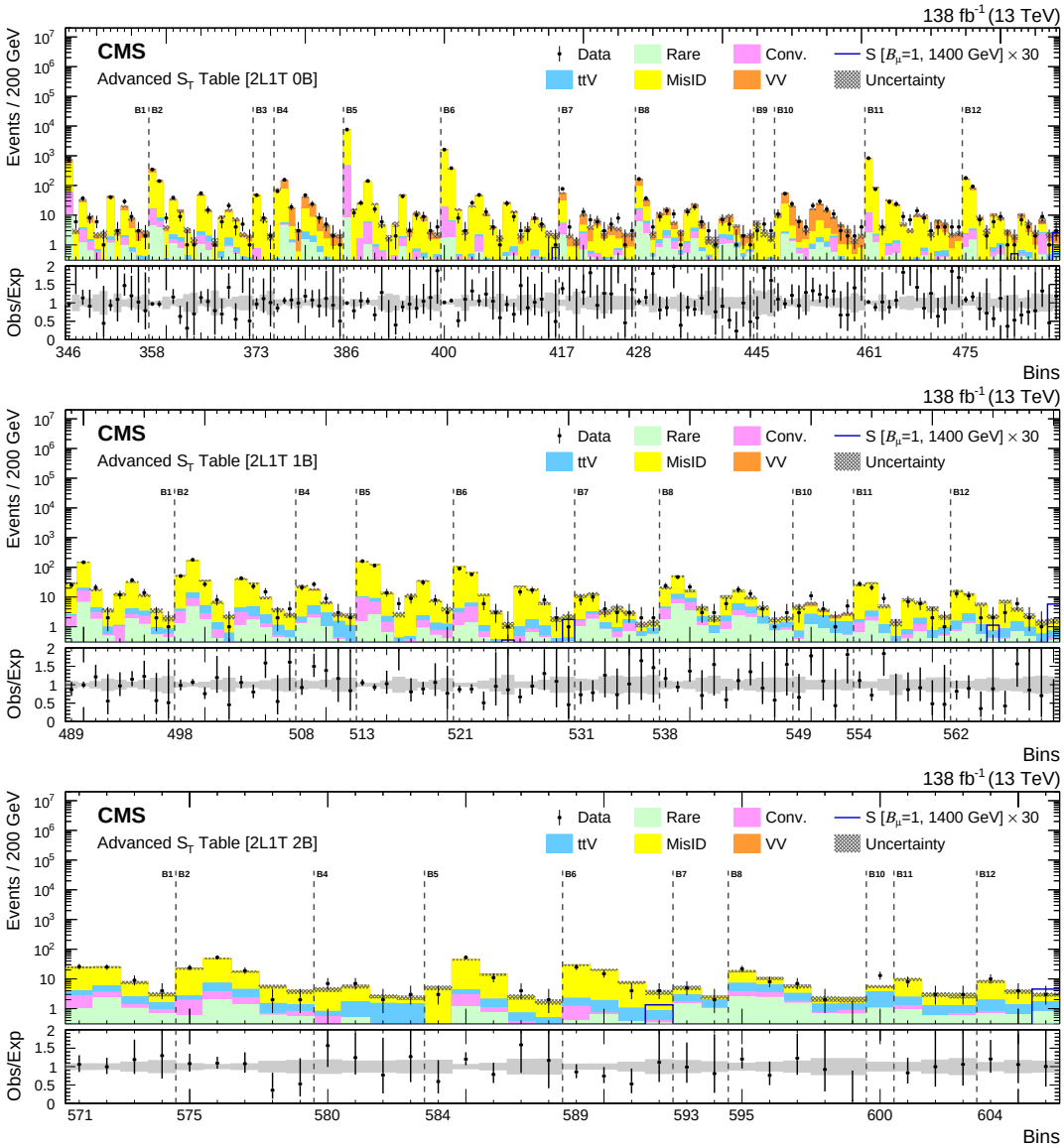

Figure 10: The 2L1T SR distributions of the advanced S_T table for the combined 2016–2018 data set. The detailed description of the bin numbers can be found in Table 4. The lower panel shows the ratio of observed events to the total expected background prediction. The gray band on the ratio represents the sum of statistical and systematic uncertainties in the SM background prediction. The expected SM background distributions and the uncertainties are shown after fitting the data under the background-only hypothesis. For illustration, an example signal hypothesis for the production of the scalar leptoquark coupled to a top quark and a muon for $m_S = 1.4$ TeV, before the fit, is also overlaid.

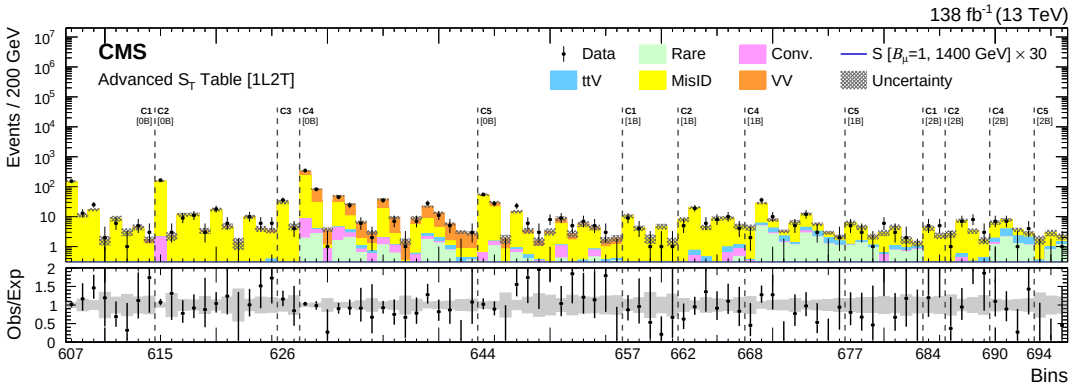

Figure 11: The 1L2T SR distribution of the advanced S_{T} table for the combined 2016–2018 data set. The detailed description of the bin numbers can be found in Table 5. The lower panel shows the ratio of observed events to the total expected background prediction. The gray band on the ratio represents the sum of statistical and systematic uncertainties in the SM background prediction. The expected SM background distributions and the uncertainties are shown after fitting the data under the background-only hypothesis. An example signal hypothesis for the production of the scalar leptoquark coupled to a top quark and a muon for $m_{\mathrm{S}} = 1.4\,\mathrm{TeV}$, before the fit, is also overlaid. For this category, the signal yield is negligible and is not visible in the figure.

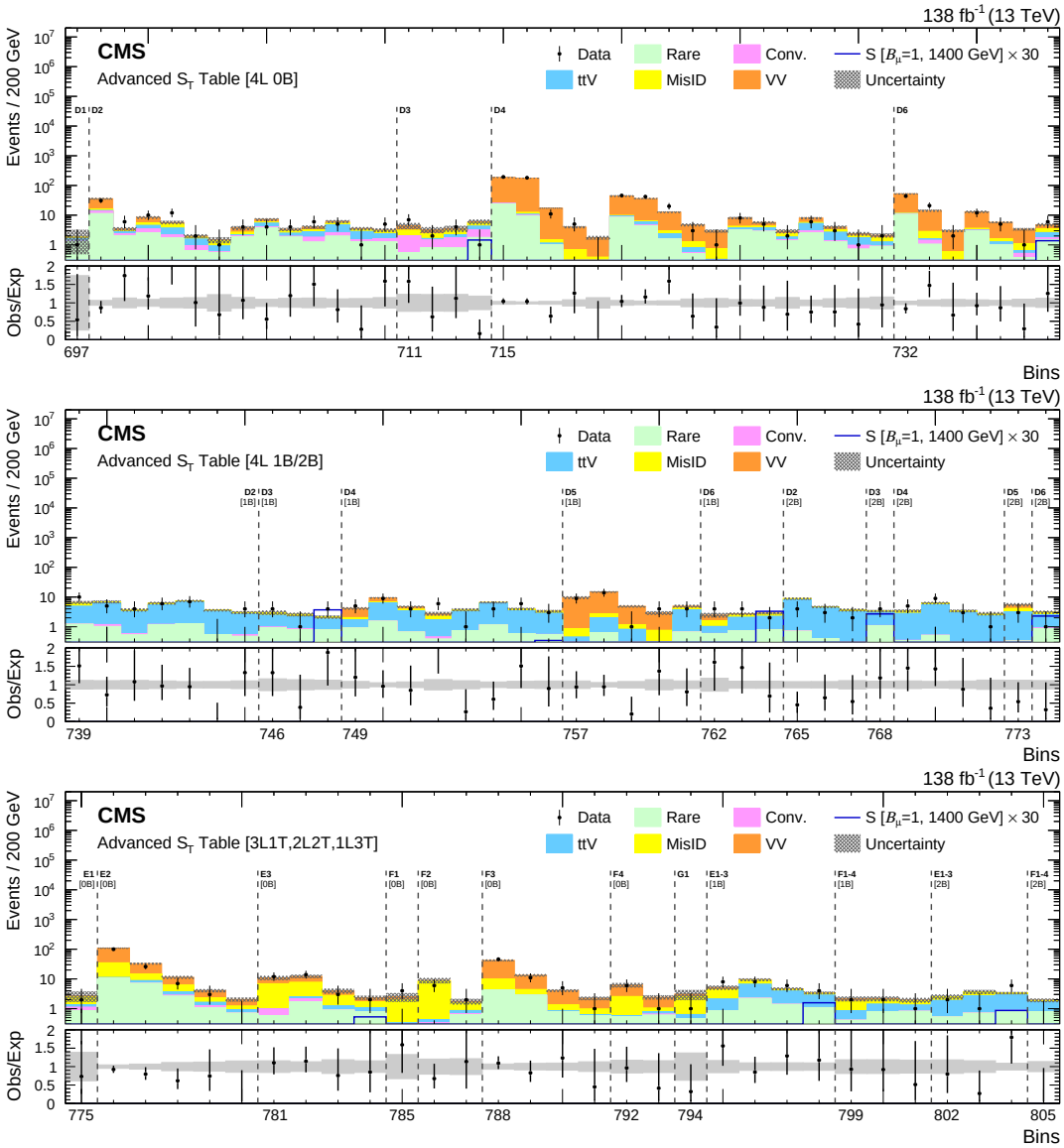

Figure 12: The 4L, 3L1T, 2L2T and 1L3T SR distributions of the advanced S_T table for the combined 2016–2018 data set. The detailed description of the bin numbers can be found in Table 6. The lower panel shows the ratio of observed events to the total expected background prediction. The gray band on the ratio represents the sum of statistical and systematic uncertainties in the SM background prediction. The expected SM background distributions and the uncertainties are shown after fitting the data under the background-only hypothesis. For illustration, an example signal hypothesis for the production of the scalar leptoquark coupled to a top quark and a muon for $m_S = 1.4$ TeV, before the fit, is also overlaid.

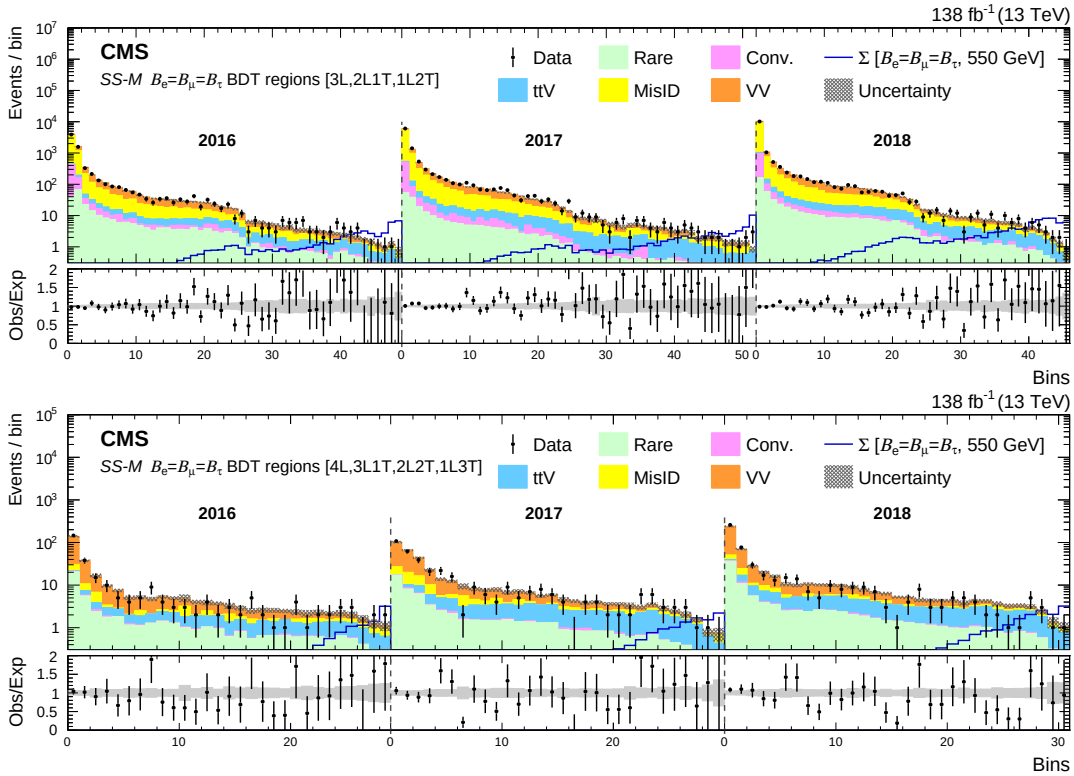

Figure 13: The *SS-M* $\mathcal{B}_e = \mathcal{B}_\mu = \mathcal{B}_\tau$ BDT regions for the 3-lepton (upper) and 4-lepton (lower) channels for the 2016–2018 data sets. The lower panel shows the ratio of observed events to the total expected background prediction. The gray band on the ratio represents the sum of statistical and systematic uncertainties in the SM background prediction. The expected SM background distributions and the uncertainties are shown after fitting the data under the background-only hypothesis. For illustration, an example signal hypothesis for the production of the type-III seesaw heavy fermions in the flavor-democratic scenario for $m_\Sigma = 550\,\text{GeV}$, before the fit, is also overlaid.

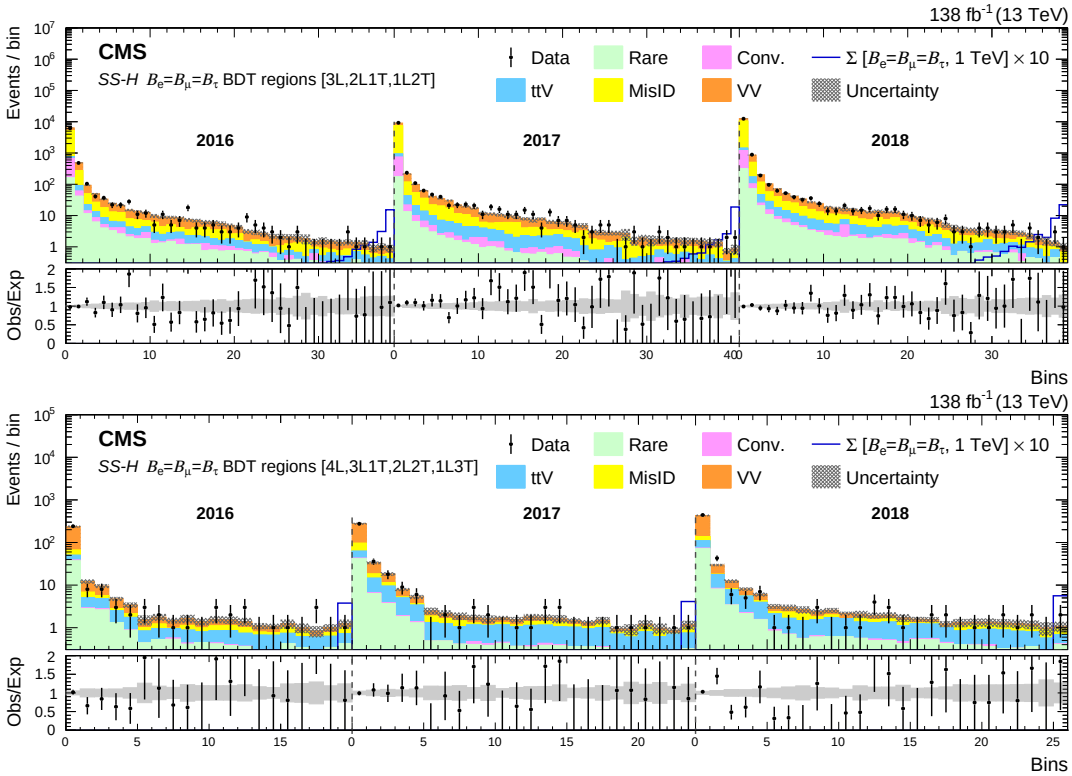

Figure 14: The *SS-H* $\mathcal{B}_e = \mathcal{B}_\mu = \mathcal{B}_\tau$ BDT regions for the 3-lepton (upper) and 4-lepton (lower) channels for the 2016–2018 data sets. The lower panel shows the ratio of observed events to the total expected background prediction. The gray band on the ratio represents the sum of statistical and systematic uncertainties in the SM background prediction. The expected SM background distributions and the uncertainties are shown after fitting the data under the background-only hypothesis. For illustration, an example signal hypothesis for the production of the type-III seesaw heavy fermions in the flavor-democratic scenario for $m_\Sigma = 1$ TeV, before the fit, is also overlaid.

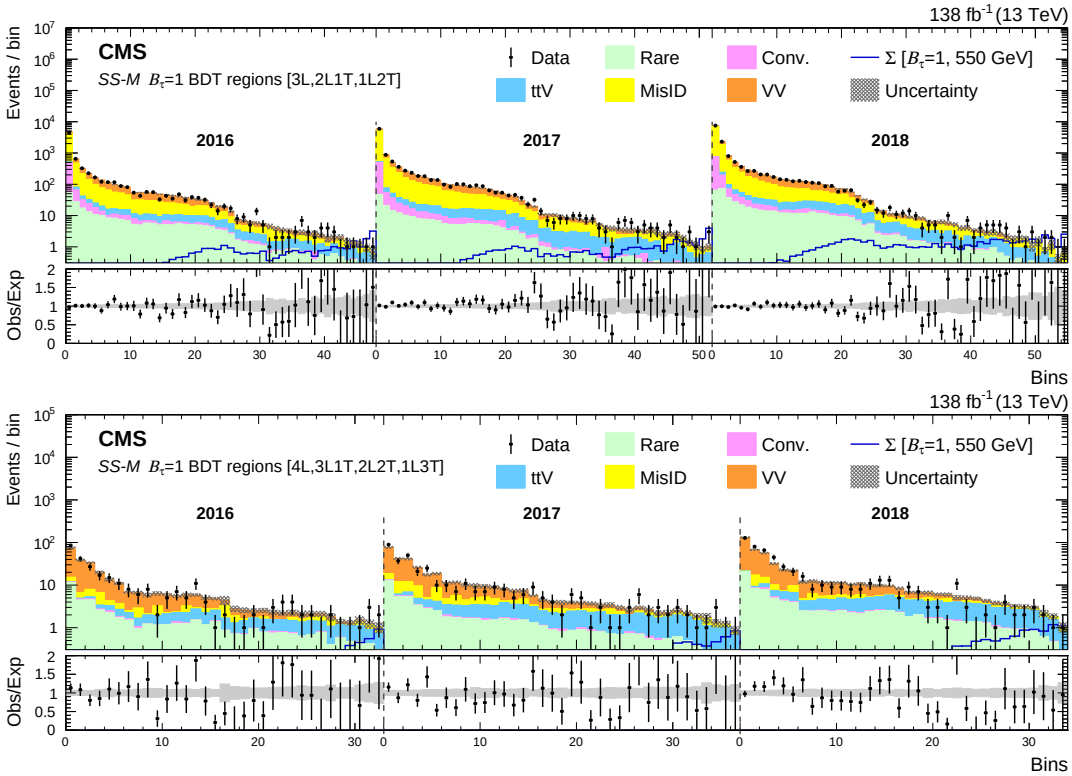

Figure 15: The *SS-M* $\mathcal{B}_\tau = 1$ BDT regions for the 3-lepton (upper) and 4-lepton (lower) channels for the 2016–2018 data sets. The lower panel shows the ratio of observed events to the total expected background prediction. The gray band on the ratio represents the sum of statistical and systematic uncertainties in the SM background prediction. The expected SM background distributions and the uncertainties are shown after fitting the data under the background-only hypothesis. For illustration, an example signal hypothesis for the production of the type-III seesaw heavy fermions in the scenario with mixing exclusively to τ lepton for $m_\Sigma = 550\,\text{GeV}$, before the fit, is also overlaid.

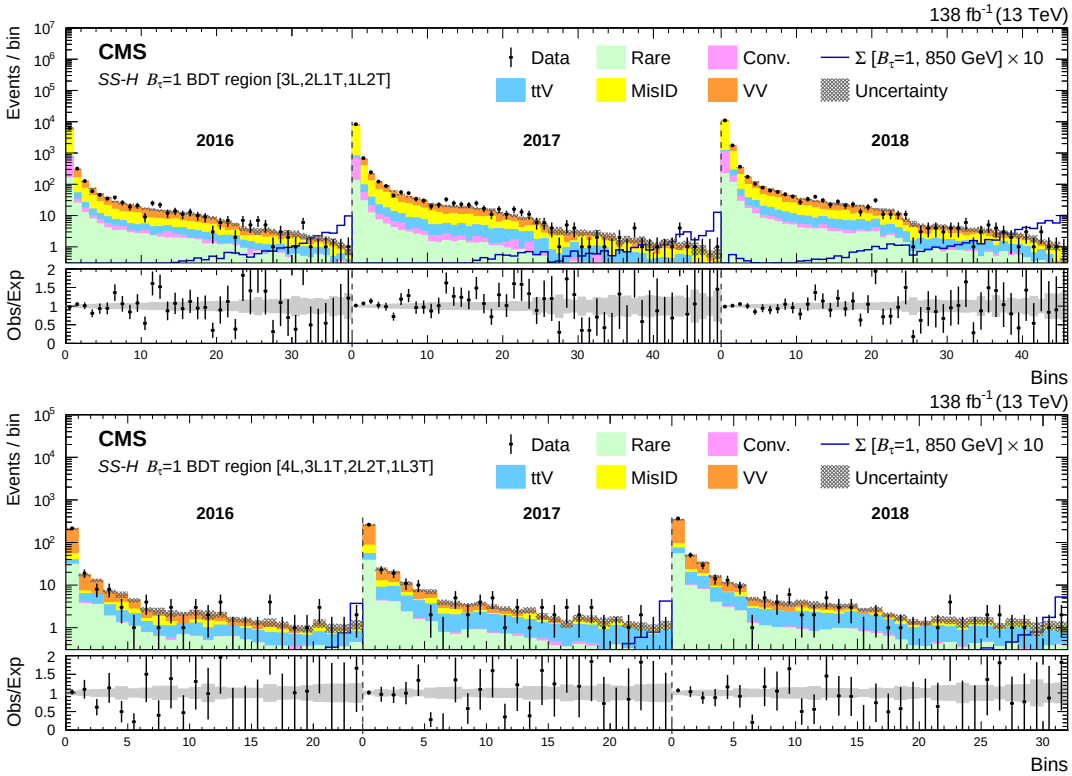

Figure 16: The *SS-H* $\mathcal{B}_\tau = 1$ BDT regions for the 3-lepton (upper) and 4-lepton (lower) channels for the 2016–2018 data sets. The lower panel shows the ratio of observed events to the total expected background prediction. The gray band on the ratio represents the sum of statistical and systematic uncertainties in the SM background prediction. The expected SM background distributions and the uncertainties are shown after fitting the data under the background-only hypothesis. For illustration, an example signal hypothesis for the production of the type-III seesaw heavy fermions in the scenario with mixing exclusively to τ lepton for $m_\Sigma = 850\,\text{GeV}$, before the fit, is also overlaid.

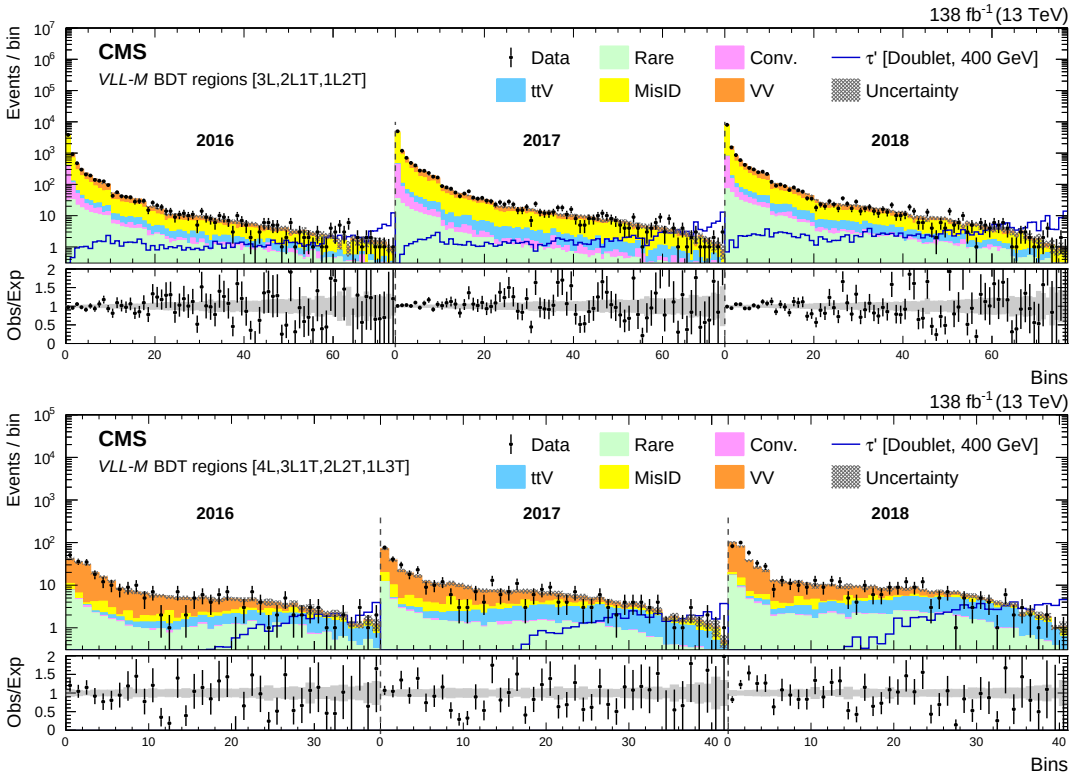

Figure 17: The *VLL-M* BDT regions for the 3-lepton (upper) and 4-lepton (lower) channels for the 2016–2018 data sets. The lower panel shows the ratio of observed events to the total expected background prediction. The gray band on the ratio represents the sum of statistical and systematic uncertainties in the SM background prediction. The expected SM background distributions and the uncertainties are shown after fitting the data under the background-only hypothesis. For illustration, an example signal hypothesis for the production of the vector-like τ lepton in the doublet scenario for $m_{\tau'} = 400\,\text{GeV}$, before the fit, is also overlaid.

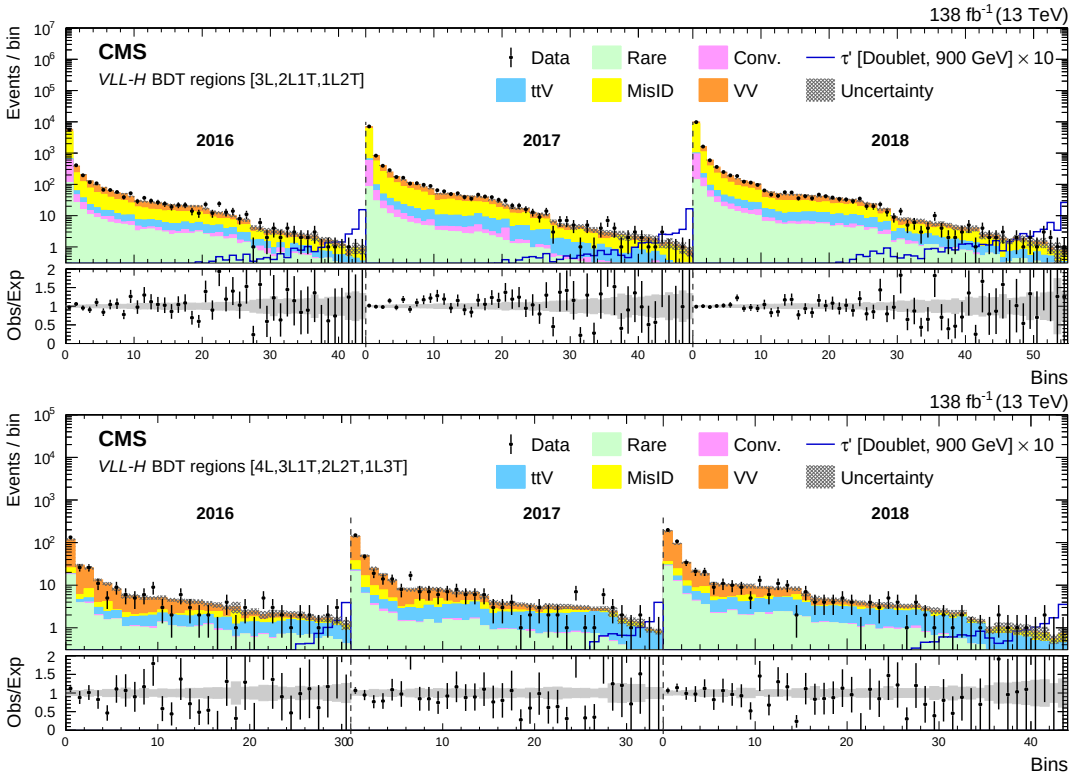

Figure 18: The *VLL-H* BDT regions for the 3-lepton (upper) and 4-lepton (lower) channels for the 2016–2018 data sets. The lower panel shows the ratio of observed events to the total expected background prediction. The gray band on the ratio represents the sum of statistical and systematic uncertainties in the SM background prediction. The expected SM background distributions and the uncertainties are shown after fitting the data under the background-only hypothesis. For illustration, an example signal hypothesis for the production of the vector-like τ lepton in the doublet scenario for $m_{\tau'} = 900\,\text{GeV}$, before the fit, is also overlaid.

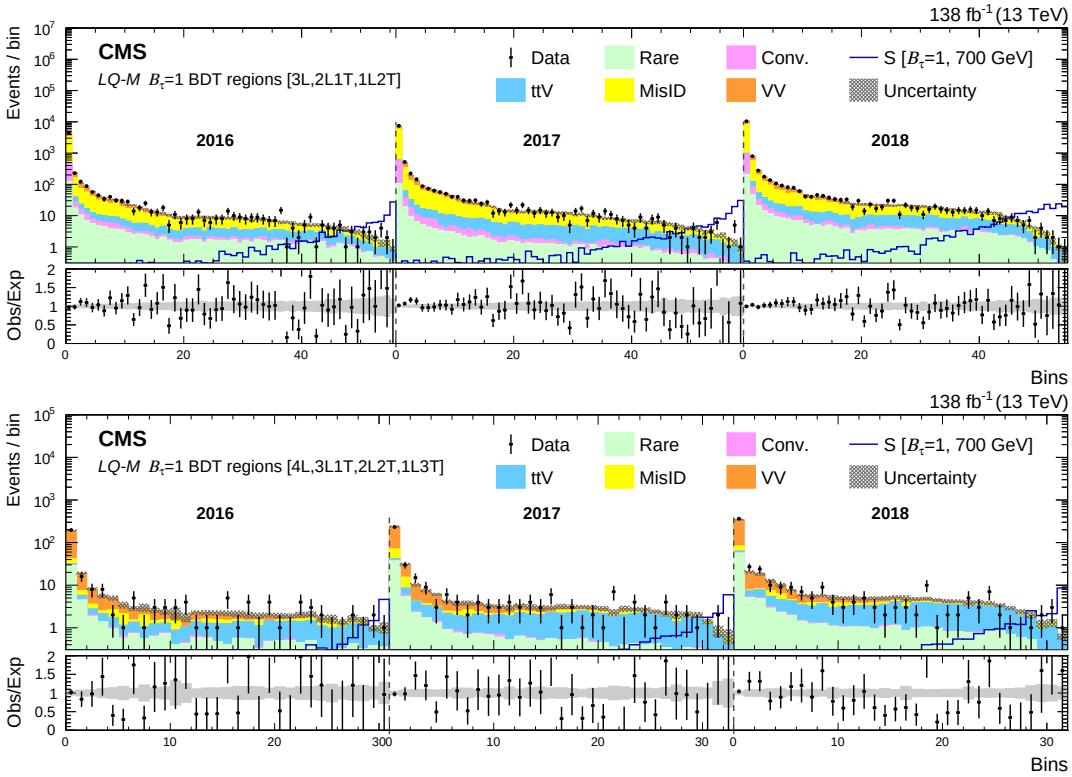

Figure 19: The *LQ-M* $\mathcal{B}_\tau = 1$ BDT regions for the 3-lepton (upper) and 4-lepton (lower) channels for the 2016–2018 data sets. The lower panel shows the ratio of observed events to the total expected background prediction. The gray band on the ratio represents the sum of statistical and systematic uncertainties in the SM background prediction. The expected SM background distributions and the uncertainties are shown after fitting the data under the background-only hypothesis. For illustration, an example signal hypothesis for the production of the scalar leptoquark coupled to a top quark and a τ lepton for $m_S = 700\,\text{GeV}$, before the fit, is also overlaid.

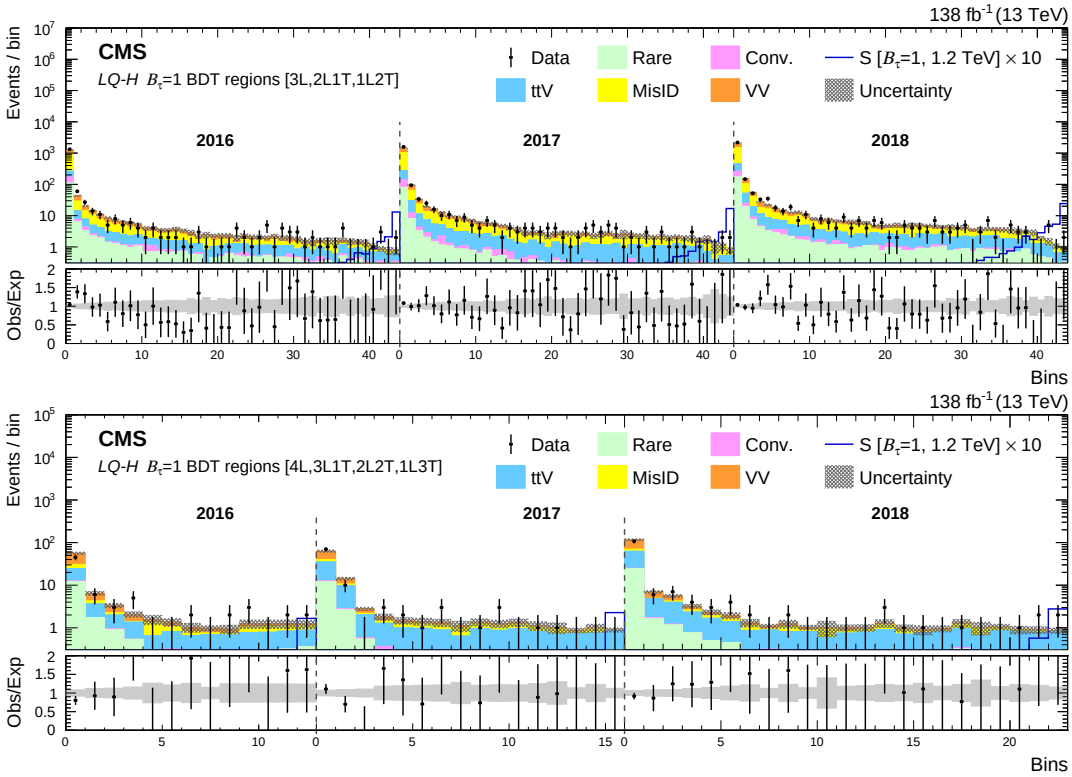

Figure 20: The *LQ-H* $\mathcal{B}_\tau = 1$ BDT regions for the 3-lepton (upper) and 4-lepton (lower) channels for the 2016–2018 data sets. The lower panel shows the ratio of observed events to the total expected background prediction. The gray band on the ratio represents the sum of statistical and systematic uncertainties in the SM background prediction. The expected SM background distributions and the uncertainties are shown after fitting the data under the background-only hypothesis. For illustration, an example signal hypothesis for the production of the scalar leptoquark coupled to a top quark and a τ lepton for $m_S = 1.2\,\text{TeV}$, before the fit, is also overlaid.

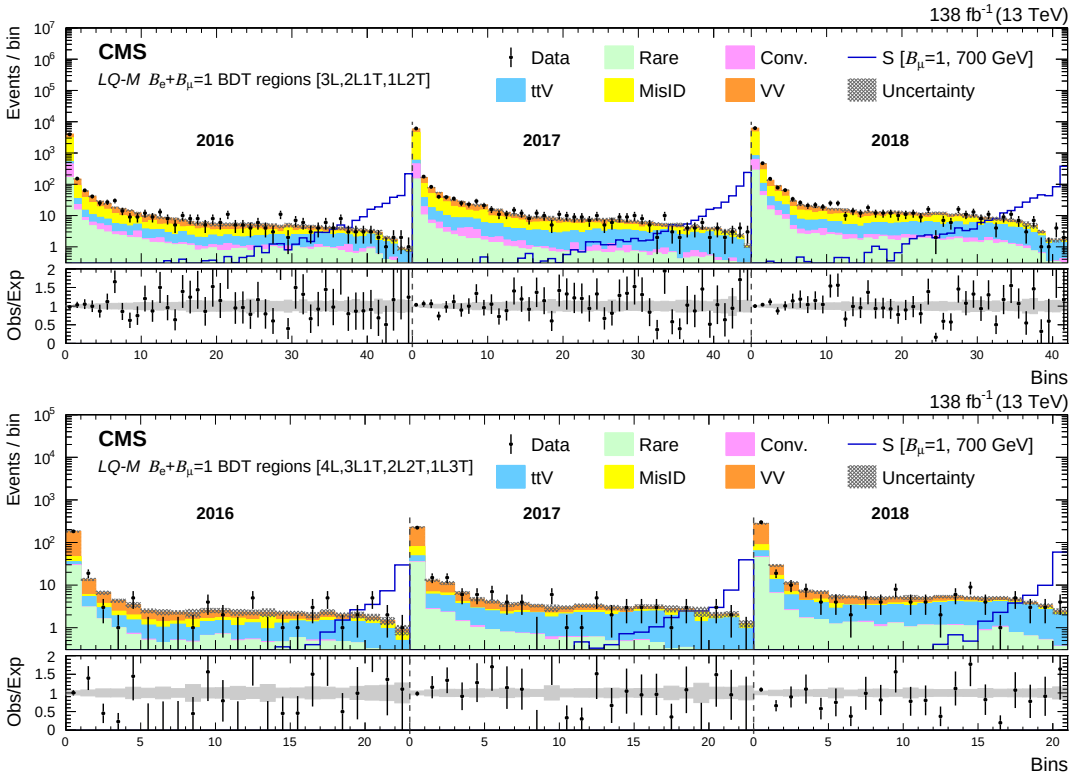

Figure 21: The *LQ-M* $\mathcal{B}_e + \mathcal{B}_\mu = 1$ BDT regions for the 3-lepton (upper) and 4-lepton (lower) channels for the 2016–2018 data sets. The lower panel shows the ratio of observed events to the total expected background prediction. The gray band on the ratio represents the sum of statistical and systematic uncertainties in the SM background prediction. The expected SM background distributions and the uncertainties are shown after fitting the data under the background-only hypothesis. For illustration, an example signal hypothesis for the production of the scalar leptoquark coupled to a top quark and a muon for $m_S = 700\,\text{GeV}$, before the fit, is also overlaid.

Figure 22: The *LQ-H* $\mathcal{B}_{\mathrm{e}} + \mathcal{B}_{\mu} = 1$ BDT regions for the 3-lepton (upper) and 4-lepton (lower) channels for the 2016–2018 data sets. The lower panel shows the ratio of observed events to the total expected background prediction. The gray band on the ratio represents the sum of statistical and systematic uncertainties in the SM background prediction. The expected SM background distributions and the uncertainties are shown after fitting the data under the background-only hypothesis. For illustration, an example signal hypothesis for the production of the scalar leptoquark coupled to a top quark and an electron for $m_{\mathrm{S}} = 1.4\,\mathrm{TeV}$, before the fit, is also overlaid.

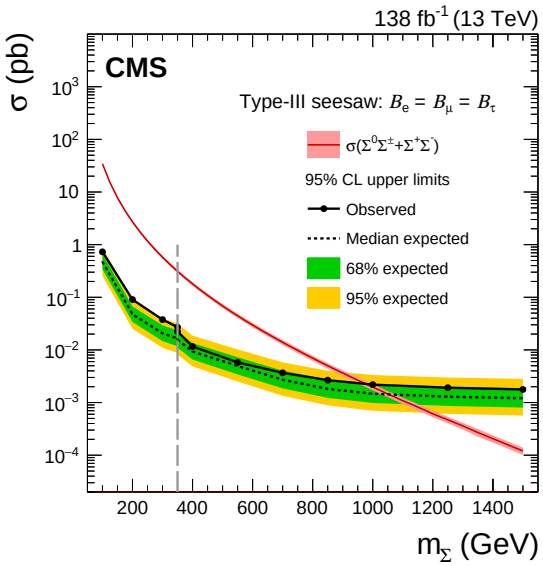

Figure 23: Observed and expected upper limits at 95% CL on the production cross section for the type-III seesaw fermions in the flavor-democratic scenario using the table schemes and the BDT regions of the *SS-M* and the *SS-H* $\mathcal{B}_e = \mathcal{B}_\mu = \mathcal{B}_\tau$ BDTs. To the left of the vertical dashed gray line, the limits are shown from the advanced S_T table, and to the right the limits are shown from the BDT regions.

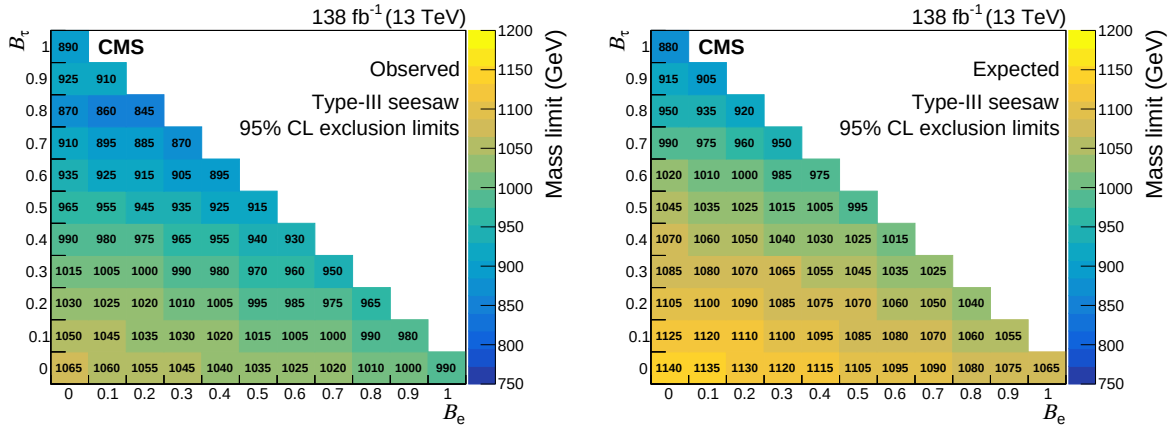

Figure 24: Observed (left) and expected (right) lower limits at 95% CL on the mass of the type-III seesaw fermions in the plane defined by $\mathcal{B}_e$ and $\mathcal{B}_\tau$, with the constraint that $\mathcal{B}_e + \mathcal{B}_\mu + \mathcal{B}_\tau = 1$. These limits arise from the *SS-H* $\mathcal{B}_\tau = 1$ BDT when $\mathcal{B}_\tau \geq 0.9$, and by the *SS-H* $\mathcal{B}_e = \mathcal{B}_\mu = \mathcal{B}_\tau$ BDT for the other decay branching fraction combinations.

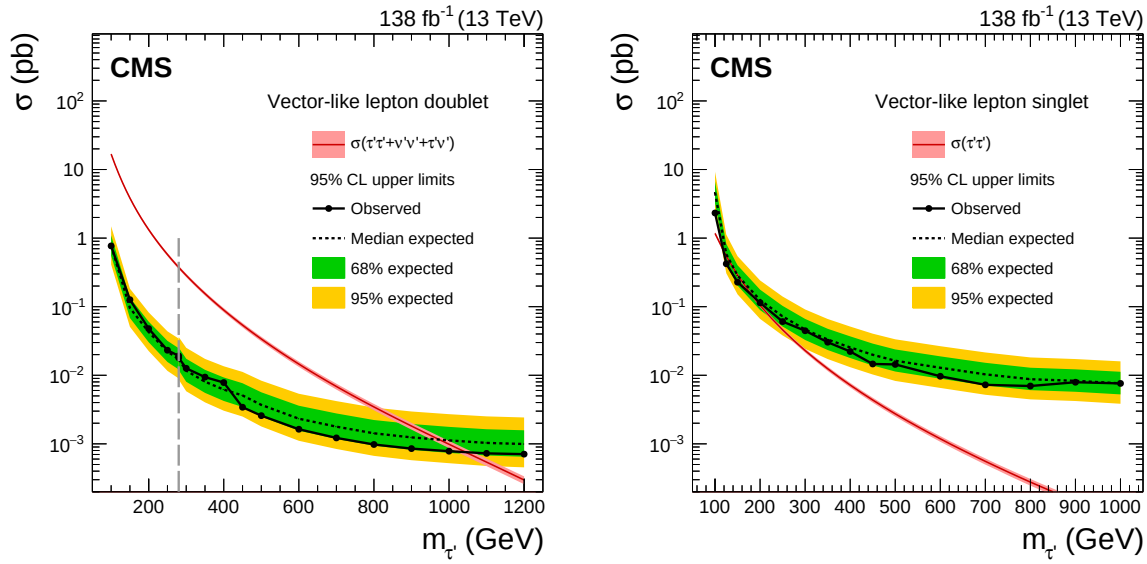

Figure 25: Observed and expected upper limits at 95% CL on the production cross section for the vector-like τ leptons: doublet model (left), and singlet model (right). For the doublet vector-like lepton model, to the left of the vertical dashed gray line, the limits are shown from the advanced S_{T} table, while to the right the limits are shown from the BDT regions. For the singlet vector-like lepton model, the limit is shown from the advanced S_{T} table for all masses.

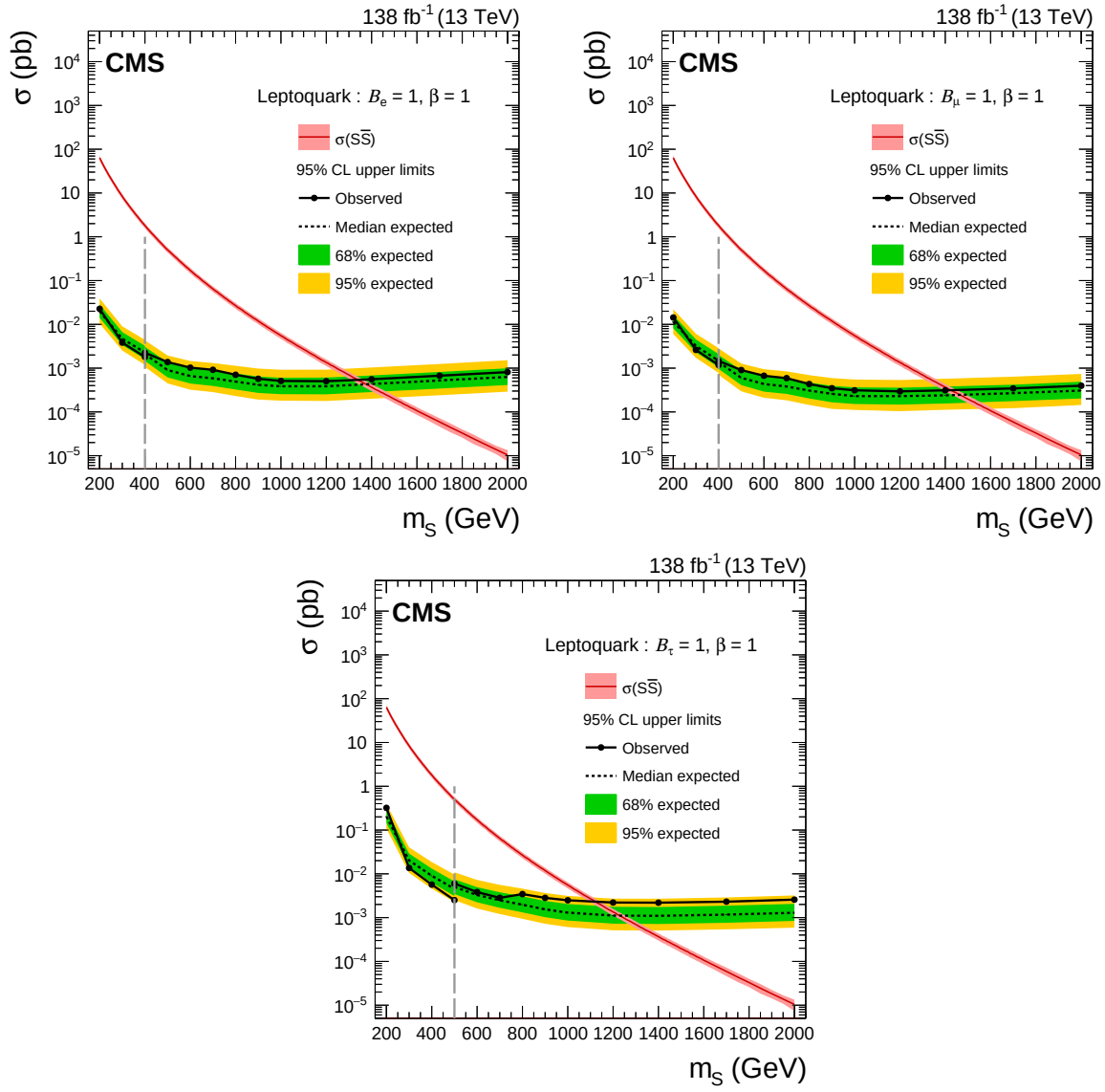

Figure 26: Observed and expected upper limits at 95% CL on the production cross section for the scalar leptoquarks: $\mathcal{B}_{e} = 1$ (upper left), $\mathcal{B}_{\mu} = 1$ (upper right), and $\mathcal{B}_{\tau} = 1$ (lower). In each figure, the limits to the left of the vertical dashed gray line are shown from the advanced S_{T} table, and to the right are shown from the BDT regions.

11 Summary

A search has been performed for physics beyond the standard model (SM), using multilepton events in proton-proton collision data at $\sqrt{s} = 13\,\text{TeV}$, collected in 2016–2018 by the CMS experiment at the LHC, corresponding to an integrated luminosity of $138\,\text{fb}^{-1}$. The search is carried out in seven orthogonal channels based on the number of light leptons and hadronically decaying τ leptons. Three model-independent schemes are used to define signal regions for the search. In addition, for each model scenario considered, a boosted decision tree is used to define model-specific signal regions. In all cases, the observations are found to be consistent with the expectations from the SM processes. Constraints are set on the production cross section of a number of beyond the SM signal models predicting a variety of multilepton final states.

Type-III seesaw heavy fermions are excluded at 95% confidence level (CL) with masses below 980 GeV (expected 1060 GeV), assuming flavor-democratic mixings with SM leptons, and below 990 GeV (expected 1065 GeV), 1065 GeV (expected 1140 GeV), and 890 GeV (expected 880 GeV), assuming mixings exclusively with electron, muon, and τ lepton flavors, respectively. Lower limits on the masses of the heavy fermions are also presented for various decay branching fractions of the heavy fermions to the different SM lepton flavors. These are the most stringent constraints on the type-III seesaw heavy fermions to date.

In the vector-like lepton doublet model, vector-like τ leptons are excluded at 95% CL with masses below 1045 GeV, with an expected exclusion of 975 GeV. These are the most stringent constraints on the doublet model. For the singlet model, vector-like τ leptons are excluded in the mass range from 125 to 150 GeV, while the expected exclusion range is from 125 to 170 GeV. These are the first constraints from the LHC on the singlet model.

Scalar leptoquarks coupled to top quarks and individual lepton flavors are also probed. In the scenario with the leptoquark coupling to a top quark and a τ lepton, leptoquarks with masses below 1120 GeV are excluded at 95% CL (expected 1235 GeV). For the decay to a top quark and an electron, leptoquarks are excluded with masses below 1340 GeV (expected 1370 GeV), and for the decay into a top quark and a muon, masses below 1420 GeV (expected 1460 GeV) are excluded.

Acknowledgments

We congratulate our colleagues in the CERN accelerator departments for the excellent performance of the LHC and thank the technical and administrative staffs at CERN and at other CMS institutes for their contributions to the success of the CMS effort. In addition, we gratefully acknowledge the computing centers and personnel of the Worldwide LHC Computing Grid and other centers for delivering so effectively the computing infrastructure essential to our analyses. Finally, we acknowledge the enduring support for the construction and operation of the LHC, the CMS detector, and the supporting computing infrastructure provided by the following funding agencies: BMBWF and FWF (Austria); FNRS and FWO (Belgium); CNPq, CAPES, FAPERJ, FAPERGS, and FAPESP (Brazil); MES and BNSF (Bulgaria); CERN; CAS, MoST, and NSFC (China); MINCIENCIAS (Colombia); MSES and CSF (Croatia); RIF (Cyprus); SENESCYT (Ecuador); MoER, ERC PUT and ERDF (Estonia); Academy of Finland, MEC, and HIP (Finland); CEA and CNRS/IN2P3 (France); BMBF, DFG, and HGF (Germany); GSRI (Greece); NKFIA (Hungary); DAE and DST (India); IPM (Iran); SFI (Ireland); INFN (Italy); MSIP and NRF (Republic of Korea); MES (Latvia); LAS (Lithuania); MOE and UM (Malaysia); BUAP, CINVESTAV, CONACYT, LNS, SEP, and UASLP-FAI (Mexico); MOS (Montenegro); MBIE (New Zealand); PAEC (Pakistan); MSHE and NSC (Poland); FCT (Portugal); JINR (Dubna); MON,

RosAtom, RAS, RFBR, and NRC KI (Russia); MESTD (Serbia); MCIN/AEI and PCTI (Spain); MOSTR (Sri Lanka); Swiss Funding Agencies (Switzerland); MST (Taipei); ThEPCenter, IPST, STAR, and NSTDA (Thailand); TUBITAK and TAEK (Turkey); NASU (Ukraine); STFC (United Kingdom); DOE and NSF (USA).

Individuals have received support from the Marie-Curie program and the European Research Council and Horizon 2020 Grant, contract Nos. 675440, 724704, 752730, 758316, 765710, 824093, 884104, and COST Action CA16108 (European Union); the Leventis Foundation; the Alfred P. Sloan Foundation; the Alexander von Humboldt Foundation; the Belgian Federal Science Policy Office; the Fonds pour la Formation à la Recherche dans l'Industrie et dans l'Agriculture (FRIA-Belgium); the Agentschap voor Innovatie door Wetenschap en Technologie (IWT-Belgium); the F.R.S.-FNRS and FWO (Belgium) under the "Excellence of Science – EOS" – be.h project n. 30820817; the Beijing Municipal Science & Technology Commission, No. Z191100007219010; the Ministry of Education, Youth and Sports (MEYS) of the Czech Republic; the Deutsche Forschungsgemeinschaft (DFG), under Germany's Excellence Strategy – EXC 2121 "Quantum Universe" – 390833306, and under project number 400140256 - GRK2497; the Lendület ("Momentum") Program and the János Bolyai Research Scholarship of the Hungarian Academy of Sciences, the New National Excellence Program ÚNKP, the NKFIA research grants 123842, 123959, 124845, 124850, 125105, 128713, 128786, and 129058 (Hungary); the Council of Science and Industrial Research, India; the Latvian Council of Science; the Ministry of Science and Higher Education and the National Science Center, contracts Opus 2014/15/B/ST2/03998 and 2015/19/B/ST2/02861 (Poland); the Fundação para a Ciência e a Tecnologia, grant CEECIND/01334/2018 (Portugal); the National Priorities Research Program by Qatar National Research Fund; the Ministry of Science and Higher Education, projects no. 0723-2020-0041 and no. FSWW-2020-0008 (Russia); MCIN/AEI/10.13039/501100011033, ERDF "a way of making Europe", and the Programa Estatal de Fomento de la Investigación Científica y Técnica de Excelencia María de Maeztu, grant MDM-2017-0765 and Programa Severo Ochoa del Principado de Asturias (Spain); the Stavros Niarchos Foundation (Greece); the Rachadapisek Sompot Fund for Postdoctoral Fellowship, Chulalongkorn University and the Chulalongkorn Academic into Its 2nd Century Project Advancement Project (Thailand); the Kavli Foundation; the Nvidia Corporation; the SuperMicro Corporation; the Welch Foundation, contract C-1845; and the Weston Havens Foundation (USA).

References

[1] P. Minkowski, "$\mu \to e\gamma$ at a rate of one out of 10^9 muon decays?", *Phys. Lett. B* **67** (1977) 421, doi:10.1016/0370-2693(77)90435-X.

[2] R. N. Mohapatra and G. Senjanović, "Neutrino mass and spontaneous parity nonconservation", *Phys. Rev. Lett.* **44** (1980) 912, doi:10.1103/PhysRevLett.44.912.

[3] M. Magg and C. Wetterich, "Neutrino mass problem and gauge hierarchy", *Phys. Lett. B* **94** (1980) 61, doi:10.1016/0370-2693(80)90825-4.

[4] R. N. Mohapatra and G. Senjanović, "Neutrino masses and mixings in gauge models with spontaneous parity violation", *Phys. Rev. D* **23** (1981) 165, doi:10.1103/PhysRevD.23.165.

[5] J. Schechter and J. W. F. Valle, "Neutrino masses in SU(2) x U(1) theories", *Phys. Rev. D* **22** (1980) 2227, doi:10.1103/PhysRevD.22.2227.

[6] J. Schechter and J. W. F. Valle, "Neutrino decay and spontaneous violation of lepton number", *Phys. Rev. D* **25** (1982) 774, doi:10.1103/PhysRevD.25.774.

[7] R. N. Mohapatra, "Mechanism for understanding small neutrino mass in superstring theories", *Phys. Rev. Lett.* **56** (1986) 561, doi:10.1103/PhysRevLett.56.561.

[8] R. N. Mohapatra and J. W. F. Valle, "Neutrino mass and baryon number nonconservation in superstring models", *Phys. Rev. D* **34** (1986) 1642, doi:10.1103/PhysRevD.34.1642.

[9] R. Foot, H. Lew, X. G. He, and G. C. Joshi, "Seesaw neutrino masses induced by a triplet of leptons", *Z. Phys. C* **44** (1989) 441, doi:10.1007/BF01415558.

[10] F. del Aguila and M. J. Bowick, "The possibility of new fermions with δi = 0 mass", *Nucl. Phys. B* **224** (1983) 107, doi:10.1016/0550-3213(83)90316-4.

[11] P. M. Fishbane, R. E. Norton, and M. J. Rivard, "Experimental implications of heavy isosinglet quarks and leptons", *Phys. Rev. D* **33** (1986) 2632, doi:10.1103/PhysRevD.33.2632.

[12] P. M. Fishbane and P. Q. Hung, "Lepton masses in a dynamical model of family symmetry", *Z. Phys. C* **38** (1988) 649, doi:10.1007/BF01624371.

[13] I. Montvay, "Three mirror pairs of fermion families", *Phys. Lett. B* **205** (1988) 315, doi:10.1016/0370-2693(88)91671-1.

[14] F. del Aguila, L. Ametller, G. L. Kane, and J. Vidal, "Vector-like fermion and standard higgs production at hadron colliders", *Nucl. Phys. B* **334** (1990) 1, doi:10.1016/0550-3213(90)90655-W.

[15] K. Fujikawa, "A vector-like extension of the standard model", *Prog. Theor. Phys.* **92** (1994) 1149, doi:10.1143/PTP.92.1149, arXiv:hep-ph/9411258.

[16] F. del Aguila, J. de Blas, and M. Peréz-Victoria, "Effects of new leptons in electroweak precision data", *Phys. Rev. D* **78** (2008) 013010, doi:10.1103/PhysRevD.78.013010, arXiv:0803.4008.

[17] J. C. Pati and A. Salam, "Unified Lepton-Hadron Symmetry and a Gauge Theory of the Basic Interactions", *Phys. Rev. D* **8** (1973) 1240, doi:10.1103/PhysRevD.8.1240.

[18] W. Buchmüller, R. Rückl, and D. Wyler, "Leptoquarks in lepton-quark collisions", *Phys. Lett. B* **191** (1987) 442, doi:10.1016/0370-2693(87)90637-X. [Erratum: doi:10.1016/S0370-2693(99)00014-3].

[19] S. Davidson and P. Verdier, "Leptoquarks decaying to a top quark and a charged lepton at hadron colliders", *Phys. Rev. D* **83** (2011) 115016, doi:10.1103/PhysRevD.83.115016, arXiv:1102.4562.

[20] B. Diaz, M. Schmaltz, and Y.-M. Zhong, "The leptoquark hunter's guide: Pair production", *JHEP* **10** (2017) 097, doi:10.1007/JHEP10(2017)097, arXiv:1706.05033.

[21] "HEPData record for this analysis", 2022. doi:10.17182/hepdata.110691.

[22] C. Biggio and F. Bonnet, "Implementation of the Type-III seesaw model in feynrules/madgraph and prospects for discovery with early LHC data", *Eur. Phys. J. C* **72** (2012) 1899, doi:10.1140/epjc/s10052-012-1899-z, arXiv:1107.3463.

[23] C. Biggio et al., "Global bounds on the Type-III seesaw", *JHEP* **05** (2020) 022, doi:10.1007/JHEP05(2020)022, arXiv:1911.11790.

[24] A. Das and S. Mandal, "Bounds on the triplet fermions in Type-III seesaw and implications for collider searches", *Nucl. Phys. B* **966** (2021) 115374, doi:10.1016/j.nuclphysb.2021.115374, arXiv:2006.04123.

[25] A. Abada et al., "Low energy effects of neutrino masses", *JHEP* **12** (2007) 061, doi:10.1088/1126-6708/2007/12/061, arXiv:0707.4058.

[26] A. Abada et al., "$\mu \to e\gamma$ and $\tau \to \ell\gamma$ decays in the fermion triplet seesaw model", *Phys. Rev. D* **78** (2008) 033007, doi:10.1103/PhysRevD.78.033007, arXiv:0803.0481.

[27] R. Franceschini, T. Hambye, and A. Strumia, "Type-III seesaw at LHC", *Phys. Rev. D* **78** (2008) 033002, doi:10.1103/PhysRevD.78.033002, arXiv:0805.1613.

[28] Y. Cai, T. Han, T. Li, and R. Ruiz, "Lepton number violation: Seesaw models and their collider tests", *Frontiers in Physics* **6** (2018) 40, doi:10.3389/fphy.2018.00040, arXiv:1711.02180.

[29] S. Ashanujjaman and K. Ghosh, "Type-III seesaw: Phenomenological implications of the information lost in decoupling from high-energy to low-energy", *Phys. Lett. B* **819** (2021) 136403, doi:10.1016/j.physletb.2021.136403, arXiv:2102.09536.

[30] ATLAS Collaboration, "Search for type-III seesaw heavy leptons in leptonic final states in pp collisions at $\sqrt{s} = 13$ TeV with the ATLAS detector", 2022. arXiv:2202.02039. Submitted to *Eur. Phys. J. C*.

[31] CMS Collaboration, "Search for physics beyond the standard model in multilepton final states in proton-proton collisions at $\sqrt{s} = 13$ TeV", *JHEP* **03** (2020) 051, doi:10.1007/JHEP03(2020)051, arXiv:1911.04968.

[32] S. P. Martin, "Extra vector-like matter and the lightest higgs scalar boson mass in low-energy supersymmetry", *Phys. Rev. D* **81** (2010) 035004, doi:10.1103/PhysRevD.81.035004, arXiv:0910.2732.

[33] P. W. Graham, A. Ismail, S. Rajendran, and P. Saraswat, "A little solution to the little hierarchy problem: A vector-like generation", *Phys. Rev. D* **81** (2010) 055016, doi:10.1103/PhysRevD.81.055016, arXiv:0910.3020.

[34] M. Endo, K. Hamaguchi, S. Iwamoto, and N. Yokozaki, "Higgs mass and muon anomalous magnetic moment in supersymmetric models with vector-like matters", *Phys. Rev. D* **84** (2011) 075017, doi:10.1103/PhysRevD.84.075017, arXiv:1108.3071.

[35] S. Zheng, "Minimal vectorlike model in supersymmetric unification", *Eur. Phys. J. C* **80** (2020) 273, doi:10.1140/epjc/s10052-020-7843-8, arXiv:1904.10145.

[36] K. Kong, S. C. Park, and T. G. Rizzo, "A vector-like fourth generation with a discrete symmetry from split-ued", *JHEP* **07** (2010) 059, doi:10.1007/JHEP07(2010)059, arXiv:1004.4635.

[37] G.-Y. Huang, K. Kong, and S. C. Park, "Bounds on the fermion-bulk masses in models with universal extra dimensions", *JHEP* **06** (2012) 099, doi:10.1007/JHEP06(2012)099, arXiv:1204.0522.

[38] R. Nevzorov, "e_6 inspired supersymmetric models with exact custodial symmetry", *Phys. Rev. D* **87** (2013) 015029, doi:10.1103/PhysRevD.87.015029, arXiv:1205.5967.

[39] I. Doršner, S. Fajfer, and I. Mustać, "Light vector-like fermions in a minimal SU(5) setup", *Phys. Rev. D* **89** (2014) 115004, doi:10.1103/PhysRevD.89.115004, arXiv:1401.6870.

[40] A. Joglekar and J. L. Rosner, "Searching for signatures of e_6", *Phys. Rev. D* **96** (2017) 015026, doi:10.1103/PhysRevD.96.015026, arXiv:1607.06900.

[41] P. Schwaller, T. M. P. Tait, and R. Vega-Morales, "Dark matter and vectorlike leptons from gauged lepton number", *Phys. Rev. D* **88** (2013) 035001, doi:10.1103/PhysRevD.88.035001, arXiv:1305.1108.

[42] J. Halverson, N. Orlofsky, and A. Pierce, "Vectorlike leptons as the tip of the dark matter iceberg", *Phys. Rev. D* **90** (2014) 015002, doi:10.1103/PhysRevD.90.015002, arXiv:1403.1592.

[43] S. Bahrami et al., "Dark matter and collider studies in the left-right symmetric model with vectorlike leptons", *Phys. Rev. D* **95** (2017) 095024, doi:10.1103/PhysRevD.95.095024, arXiv:1612.06334.

[44] S. Bhattacharya, P. Ghosh, N. Sahoo, and N. Sahu, "Mini review on vector-like leptonic dark matter, neutrino mass, and collider signatures", *Frontiers in Physics* **7** (2019) 80, doi:10.3389/fphy.2019.00080, arXiv:1812.06505.

[45] K. Agashe, T. Okui, and R. Sundrum, "A common origin for neutrino anarchy and charged hierarchies", *Phys. Rev. Lett.* **102** (2009) 101801, doi:10.1103/PhysRevLett.102.101801, arXiv:0810.1277.

[46] M. Redi, "Leptons in composite mfv", *JHEP* **09** (2013) 060, doi:10.1007/JHEP09(2013)060, arXiv:1306.1525.

[47] A. Falkowski, D. M. Straub, and A. Vicente, "Vector-like leptons: Higgs decays and collider phenomenology", *JHEP* **05** (2014) 092, doi:10.1007/JHEP05(2014)092, arXiv:1312.5329.

[48] R. Dermíšek and A. Raval, "Explanation of the muon g-2 anomaly with vectorlike leptons and its implications for higgs decays", *Phys. Rev. D* **88** (2013) 013017, doi:10.1103/PhysRevD.88.013017, arXiv:1305.3522.

[49] E. Megias, M. Quiros, and L. Salas, "Muon g-2 from vector-like leptons in warped space", *JHEP* **05** (2017) 016, doi:10.1007/JHEP05(2017)016, arXiv:1701.05072.

[50] J. Kawamura, S. Raby, and A. Trautner, "Complete vectorlike fourth family and new $u(1)'$ for muon anomalies", *Phys. Rev. D* **100** (2019) 055030, doi:10.1103/PhysRevD.100.055030, arXiv:1906.11297.

[51] G. Hiller, C. Hormigos-Feliu, D. F. Litim, and T. Steudtner, "Model building from asymptotic safety with higgs and flavor portals", *Phys. Rev. D* **102** (2020) 095023, doi:10.1103/PhysRevD.102.095023, arXiv:2008.08606.

[52] Muon g-2 Collaboration, "Final report of the muon e821 anomalous magnetic moment measurement at bnl", *Phys. Rev. D* **73** (2006) 072003, doi:10.1103/PhysRevD.73.072003, arXiv:hep-ex/0602035.

[53] Muon g-2 Collaboration, "Measurement of the positive muon anomalous magnetic moment to 0.46 ppm", *Phys. Rev. Lett.* **126** (2021) 141801, doi:10.1103/PhysRevLett.126.141801, arXiv:2104.03281.

[54] N. Kumar and S. P. Martin, "Vectorlike leptons at the large hadron collider", *Phys. Rev. D* **92** (2015) 115018, doi:10.1103/PhysRevD.92.115018, arXiv:1510.03456.

[55] P. N. Bhattiprolu and S. P. Martin, "Prospects for vectorlike leptons at future proton-proton colliders", *Phys. Rev. D* **100** (2019) 015033, doi:10.1103/PhysRevD.100.015033, arXiv:1905.00498.

[56] R. Dermíšek, A. Raval, and S. Shin, "Effects of vectorlike leptons on $h \to 4\ell$ and the connection to the muon g-2 anomaly", *Phys. Rev. D* **90** (2014) 034023, doi:10.1103/PhysRevD.90.034023, arXiv:1406.7018.

[57] R. Dermíšek, J. P. Hall, E. Lunghi, and S. Shin, "Limits on vectorlike leptons from searches for anomalous production of multi-lepton events", *JHEP* **12** (2014) 013, doi:10.1007/JHEP12(2014)013, arXiv:1408.3123.

[58] CMS Collaboration, "Search for vector-like leptons in multilepton final states in proton-proton collisions at $\sqrt{s} = 13$ TeV", *Phys. Rev. D* **100** (2019) 052003, doi:10.1103/PhysRevD.100.052003, arXiv:1905.10853.

[59] L3 Collaboration, "Search for heavy neutral and charged leptons in e^+e^- annihilation at lep", *Phys. Lett. B* **517** (2001) 75, doi:10.1016/S0370-2693(01)01005-X, arXiv:hep-ex/0107015.

[60] J. C. Pati and A. Salam, "Lepton number as the fourth color", *Phys. Rev. D* **10** (1974) 275, doi:10.1103/PhysRevD.10.275. [Erratum: doi:https://doi.org/10.1103/PhysRevD.11.703.2].

[61] H. Georgi and S. L. Glashow, "Unity of all elementary particle forces", *Phys. Rev. Lett.* **32** (1974) 438, doi:10.1103/PhysRevLett.32.438.

[62] H. Fritzsch and P. Minkowski, "Unified interactions of leptons and hadrons", *Annals Phys.* **93** (1975) 193, doi:10.1016/0003-4916(75)90211-0.

[63] B. Gripaios, M. Nardecchia, and S. A. Renner, "Composite leptoquarks and anomalies in b-meson decays", *JHEP* **05** (2015) 006, doi:10.1007/JHEP05(2015)006, arXiv:1412.1791.

[64] L. Da Rold and F. Lamagna, "Composite higgs and leptoquarks from a simple group", *JHEP* **03** (2019) 135, doi:10.1007/JHEP03(2019)135, arXiv:1812.08678.

[65] S. Weinberg, "Supersymmetry at ordinary energies. Masses and conservation laws", *Phys. Rev. D* **26** (1982) 287, doi:10.1103/PhysRevD.26.287.

[66] R. Barbier et al., "R-parity violating supersymmetry", *Phys. Rept.* **420** (2005) 1, doi:10.1016/j.physrep.2005.08.006, arXiv:hep-ph/0406039.

[67] R. Mandal and A. Pich, "Constraints on scalar leptoquarks from lepton and kaon physics", *JHEP* **12** (2019) 089, doi:10.1007/JHEP12(2019)089, arXiv:1908.11155.

[68] J. K. Mizukoshi, O. J. P. Éboli, and M. C. Gonzalez-Garcia, "Bounds on scalar leptoquarks from z physics", *Nucl. Phys. B* **443** (1995) 20, doi:10.1016/0550-3213(95)00162-L, arXiv:hep-ph/9411392.

[69] E. Alvarez et al., "A composite pngb leptoquark at the LHC", *JHEP* **12** (2018) 027, doi:10.1007/JHEP12(2018)027, arXiv:1808.02063.

[70] A. Angelescu, D. Bečirević, D. A. Faroughy, and O. Sumensari, "Closing the window on single leptoquark solutions to the b-physics anomalies", *JHEP* **10** (2018) 183, doi:10.1007/JHEP10(2018)183, arXiv:1808.08179.

[71] A. Crivellin, D. Müller, and F. Saturnino, "Flavor phenomenology of the leptoquark singlet-triplet model", *JHEP* **06** (2020) 020, doi:10.1007/JHEP06(2020)020, arXiv:1912.04224.

[72] S. Saad and A. Thapa, "Common origin of neutrino masses and $r_{D^{(*)}}$, $r_{K^{(*)}}$ anomalies", *Phys. Rev. D* **102** (2020) 015014, doi:10.1103/PhysRevD.102.015014, arXiv:2004.07880.

[73] U. Haisch and G. Polesello, "Resonant third-generation leptoquark signatures at the large hadron collider", *JHEP* **05** (2021) 057, doi:10.1007/JHEP05(2021)057, arXiv:2012.11474.

[74] BaBar Collaboration, "Measurement of an excess of $\bar{B} \to d^{(*)}\tau^-\bar{\nu}_\tau$ decays and implications for charged higgs bosons", *Phys. Rev. D* **88** (2013) 072012, doi:10.1103/PhysRevD.88.072012, arXiv:1303.0571.

[75] Belle Collaboration, "Measurement of $\mathcal{R}(d)$ and $\mathcal{R}(d^*)$ with a semileptonic tagging method", *Phys. Rev. Lett.* **124** (2020) 161803, doi:10.1103/PhysRevLett.124.161803, arXiv:1910.05864.

[76] LHCb Collaboration, "Measurement of the ratio of branching fractions $\mathcal{B}(b_c^+ \to j/\psi\tau^+\nu_\tau)/\mathcal{B}(b_c^+ \to j/\psi\mu^+\nu_\mu)$", *Phys. Rev. Lett.* **120** (2018) 121801, doi:10.1103/PhysRevLett.120.121801, arXiv:1711.05623.

[77] LHCb Collaboration, "Measurement of the ratio of the $b^0 \to d^{*-}\tau^+\nu_\tau$ and $b^0 \to d^{*-}\mu^+\nu_\mu$ branching fractions using three-prong τ-lepton decays", *Phys. Rev. Lett.* **120** (2018) 171802, doi:10.1103/PhysRevLett.120.171802, arXiv:1708.08856.

[78] LHCb Collaboration, "Test of lepton universality in beauty-quark decays", 2021. arXiv:2103.11769.

[79] Belle Collaboration, "Lepton-flavor-dependent angular analysis of $b \to k^*\ell^+\ell^-$", *Phys. Rev. Lett.* **118** (2017) 111801, doi:10.1103/PhysRevLett.118.111801, arXiv:1612.05014.

[80] LHCb Collaboration, "Test of lepton universality with $b^0 \to k^{*0}\ell^+\ell^-$ decays", *JHEP* **08** (2017) 055, doi:10.1007/JHEP08(2017)055, arXiv:1705.05802.

[81] LHCb Collaboration, "Search for lepton-universality violation in $b^+ \to k^+\ell^+\ell^-$ decays", *Phys. Rev. Lett.* **122** (2019) 191801, doi:10.1103/PhysRevLett.122.191801, arXiv:1903.09252.

[82] ATLAS Collaboration, "Search for pair production of scalar leptoquarks decaying into first- or second-generation leptons and top quarks in proton-proton collisions at $\sqrt{s}$ = 13 TeV with the ATLAS detector", *Eur. Phys. J. C* **81** (2021) 313, doi:10.1140/epjc/s10052-021-09009-8, arXiv:2010.02098.

[83] ATLAS Collaboration, "Search for pair production of third-generation scalar leptoquarks decaying into a top quark and a τ-lepton in pp collisions at $\sqrt{s} = 13$ TeV with the ATLAS detector", *JHEP* **06** (2021) 179, doi:10.1007/JHEP06(2021)179, arXiv:2101.11582.

[84] ATLAS Collaboration, "Searches for third-generation scalar leptoquarks in $\sqrt{s}$ = 13 TeV pp collisions with the ATLAS detector", *JHEP* **06** (2019) 144, doi:10.1007/JHEP06(2019)144, arXiv:1902.08103.

[85] CMS Collaboration, "Search for leptoquarks coupled to third-generation quarks in proton-proton collisions at $\sqrt{s} = 13$ TeV", *Phys. Rev. Lett.* **121** (2018) 241802, doi:10.1103/PhysRevLett.121.241802, arXiv:1809.05558.

[86] CMS Collaboration, "Search for third-generation scalar leptoquarks decaying to a top quark and a τ lepton at $\sqrt{s} = 13$ TeV", *Eur. Phys. J. C* **78** (2018) 707, doi:10.1140/epjc/s10052-018-6143-z, arXiv:1803.02864.

[87] CMS Collaboration, "Search for singly and pair-produced leptoquarks coupling to third-generation fermions in proton-proton collisions at $\sqrt{s} = 13$ TeV", *Phys. Lett. B* **819** (2021) 136446, doi:10.1016/j.physletb.2021.136446, arXiv:2012.04178.

[88] CMS Collaboration, "Constraints on models of scalar and vector leptoquarks decaying to a quark and a neutrino at $\sqrt{s} = 13$ TeV", *Phys. Rev. D* **98** (2018) 032005, doi:10.1103/PhysRevD.98.032005, arXiv:1805.10228.

[89] CMS Collaboration, "Search for heavy neutrinos and third-generation leptoquarks in hadronic states of two τ leptons and two jets in proton-proton collisions at $\sqrt{s} = 13$ TeV", *JHEP* **03** (2019) 170, doi:10.1007/JHEP03(2019)170, arXiv:1811.00806.

[90] CMS Collaboration, "Search for a singly produced third-generation scalar leptoquark decaying to a τ lepton and a bottom quark in proton-proton collisions at $\sqrt{s} = 13$ TeV", *JHEP* **07** (2018) 115, doi:10.1007/JHEP07(2018)115, arXiv:1806.03472.

[91] CMS Collaboration, "The CMS experiment at the CERN LHC", *JINST* **3** (2008) S08004, doi:10.1088/1748-0221/3/08/S08004.

[92] CMS Collaboration, "Performance of the CMS level-1 trigger in proton-proton collisions at $\sqrt{s} = 13$ TeV", *JINST* **15** (2020) P10017, doi:10.1088/1748-0221/15/10/P10017, arXiv:2006.10165.

[93] CMS Collaboration, "The CMS trigger system", *JINST* **12** (2017) P01020, doi:10.1088/1748-0221/12/01/P01020, arXiv:1609.02366.

[94] J. Alwall et al., "The automated computation of tree-level and next-to-leading order differential cross sections, and their matching to parton shower simulations", *JHEP* **07** (2014) 079, doi:10.1007/JHEP07(2014)079, arXiv:1405.0301.

[95] P. Nason, "A new method for combining NLO QCD with shower monte carlo algorithms", *JHEP* **11** (2004) 040, doi:10.1088/1126-6708/2004/11/040, arXiv:hep-ph/0409146.

[96] S. Frixione, P. Nason, and C. Oleari, "Matching NLO QCD computations with parton shower simulations: the POWHEG method", *JHEP* **11** (2007) 070, doi:10.1088/1126-6708/2007/11/070, arXiv:0709.2092.

[97] S. Alioli, P. Nason, C. Oleari, and E. Re, "A general framework for implementing NLO calculations in shower monte carlo programs: the POWHEG BOX", *JHEP* **06** (2010) 043, doi:10.1007/JHEP06(2010)043, arXiv:1002.2581.

[98] J. M. Campbell and R. K. Ellis, "MCFM for the tevatron and the LHC", *Nucl. Phys. B Proc. Suppl.* **205-206** (2010) 10, doi:10.1016/j.nuclphysbps.2010.08.011, arXiv:1007.3492.

[99] Y. Gao et al., "Spin determination of single-produced resonances at hadron colliders", *Phys. Rev. D* **81** (2010) 075022, doi:10.1103/PhysRevD.81.075022, arXiv:1001.3396.

[100] S. Bolognesi et al., "On the spin and parity of a single-produced resonance at the LHC", *Phys. Rev. D* **86** (2012) 095031, doi:10.1103/PhysRevD.86.095031, arXiv:1208.4018.

[101] I. Anderson et al., "Constraining anomalous HVV interactions at proton and lepton colliders", *Phys. Rev. D* **89** (2014) 035007, doi:10.1103/PhysRevD.89.035007, arXiv:1309.4819.

[102] A. V. Gritsan, R. Röntsch, M. Schulze, and M. Xiao, "Constraining anomalous Higgs boson couplings to the heavy flavor fermions using matrix element techniques", *Phys. Rev. D* **94** (2016) 055023, doi:10.1103/PhysRevD.94.055023, arXiv:1606.03107.

[103] T. Sjöstrand et al., "An introduction to PYTHIA 8.2", *Comput. Phys. Commun.* **191** (2015) 159, doi:10.1016/j.cpc.2015.01.024, arXiv:1410.3012.

[104] B. Fuks, M. Klasen, D. R. Lamprea, and M. Rothering, "Gaugino production in proton-proton collisions at a center-of-mass energy of 8 TeV", *JHEP* **10** (2012) 081, doi:10.1007/JHEP10(2012)081, arXiv:1207.2159.

[105] B. Fuks, M. Klasen, D. R. Lamprea, and M. Rothering, "Precision predictions for electroweak superpartner production at hadron colliders with resummino", *Eur. Phys. J. C* **73** (2013) 2480, doi:10.1140/epjc/s10052-013-2480-0, arXiv:1304.0790.

[106] J. Blümlein, E. Boos, and A. Kryukov, "Leptoquark pair production in hadronic interactions", *Z. Phys. C* **76** (1997) 137, doi:10.1007/s002880050538, arXiv:hep-ph/9610408.

[107] M. Krämer, T. Plehn, M. Spira, and P. M. Zerwas, "Pair production of scalar leptoquarks at the CERN LHC", *Phys. Rev. D* **71** (2005) 057503, doi:10.1103/PhysRevD.71.057503, arXiv:hep-ph/0411038.

[108] NNPDF Collaboration, "Parton distributions for the LHC Run II", *JHEP* **04** (2015) 040, doi:10.1007/JHEP04(2015)040, arXiv:1410.8849.

[109] NNPDF Collaboration, "Parton distributions from high-precision collider data", *Eur. Phys. J. C* **77** (2017) 663, doi:10.1140/epjc/s10052-017-5199-5, arXiv:1706.00428.

[110] CMS Collaboration, "Event generator tunes obtained from underlying event and multiparton scattering measurements", *Eur. Phys. J. C* **76** (2016) 155, doi:10.1140/epjc/s10052-016-3988-x, arXiv:1512.00815.

[111] CMS Collaboration, "Extraction and validation of a new set of CMS PYTHIA8 tunes from underlying-event measurements", *Eur. Phys. J. C* **80** (2020) 4, doi:10.1140/epjc/s10052-019-7499-4, arXiv:1903.12179.

[112] S. Hoeche et al., "Matching parton showers and matrix elements", 2006. arXiv:hep-ph/0602031.

[113] R. Frederix and S. Frixione, "Merging meets matching in MC@NLO", *JHEP* **12** (2012) 061, doi:10.1007/JHEP12(2012)061, arXiv:1209.6215.

[114] GEANT4 Collaboration, "GEANT4—a simulation toolkit", *Nucl. Instrum. Meth. A* **506** (2003) 250, doi:10.1016/S0168-9002(03)01368-8.

[115] M. Cacciari, G. P. Salam, and G. Soyez, "The anti-k_{T} jet clustering algorithm", *JHEP* **04** (2008) 063, doi:10.1088/1126-6708/2008/04/063, arXiv:0802.1189.

[116] M. Cacciari, G. P. Salam, and G. Soyez, "Fastjet user manual", *Eur. Phys. J. C* **72** (2012) 1896, doi:10.1140/epjc/s10052-012-1896-2, arXiv:1111.6097.

[117] CMS Collaboration, "Particle-flow reconstruction and global event description with the CMS detector", *JINST* **12** (2017) P10003, doi:10.1088/1748-0221/12/10/P10003, arXiv:1706.04965.

[118] CMS Collaboration, "Electron and photon reconstruction and identification with the CMS experiment at the CERN LHC", *JINST* **16** (2021) P05014, doi:10.1088/1748-0221/16/05/P05014, arXiv:2012.06888.

[119] CMS Collaboration, "Performance of the CMS muon detector and muon reconstruction with proton-proton collisions at $\sqrt{s} = 13$ TeV", *JINST* **13** (2018) P06015, doi:10.1088/1748-0221/13/06/P06015, arXiv:1804.04528.

[120] CMS Collaboration, "Performance of reconstruction and identification of τ leptons decaying to hadrons and ν_τ in pp collisions at $\sqrt{s} = 13$ TeV", *JINST* **13** (2018) P10005, doi:10.1088/1748-0221/13/10/P10005, arXiv:1809.02816.

[121] M. Cacciari, G. P. Salam, and G. Soyez, "The catchment area of jets", *JHEP* **04** (2008) 005, doi:10.1088/1126-6708/2008/04/005, arXiv:0802.1188.

[122] M. Cacciari and G. P. Salam, "Pileup subtraction using jet areas", *Phys. Lett. B* **659** (2008) 119, doi:10.1016/j.physletb.2007.09.077, arXiv:0707.1378.

[123] CMS Collaboration, "Jet energy scale and resolution in the CMS experiment in pp collisions at 8 TeV", *JINST* **12** (2017) P02014, doi:10.1088/1748-0221/12/02/P02014, arXiv:1607.03663.

[124] CMS Collaboration, "Jet algorithms performance in 13 TeV data", CMS Physics Analysis Summary CMS-PAS-JME-16-003, 2017.

[125] CMS Collaboration, "Identification of heavy-flavour jets with the CMS detector in pp collisions at 13 TeV", *JINST* **13** (2018) P05011, doi:10.1088/1748-0221/13/05/P05011, arXiv:1712.07158.

[126] CMS Collaboration, "Performance of missing transverse momentum reconstruction in proton-proton collisions at $\sqrt{s} = 13$ TeV using the CMS detector", *JINST* **14** (2019) P07004, doi:10.1088/1748-0221/14/07/P07004, arXiv:1903.06078.

[127] D. Bertolini, P. Harris, M. Low, and N. Tran, "Pileup per particle identification", *JHEP* **10** (2014) 059, doi:10.1007/JHEP10(2014)059, arXiv:1407.6013.

[128] CMS Collaboration, "Identification of hadronic tau lepton decays using a deep neural network", 2022. arXiv:2201.08458. Submitted to *JINST*.

[129] Particle Data Group Collaboration, "Review of particle physics", *Prog. Theor. Exp. Phys.* **2020** (2020) 083C01, doi:10.1093/ptep/ptaa104.

[130] CMS Collaboration, "Search for third-generation scalar leptoquarks in the tτ channel in proton-proton collisions at $\sqrt{s}$ = 8 TeV", *JHEP* **07** (2015) 042, doi:10.1007/JHEP07(2015)042, arXiv:1503.09049. [Erratum: doi:10.1007/JHEP11(2016)056].

[131] CMS Collaboration, "Measurement of the inclusive W and Z production cross sections in pp collisions at $\sqrt{s} = 7$ TeV", *JHEP* **10** (2011) 132, doi:10.1007/JHEP10(2011)132, arXiv:1107.4789.

[132] H. Voss, A. Höcker, J. Stelzer, and F. Tegenfeldt, "TMVA, the toolkit for multivariate data analysis with ROOT", in *Proceedings of XI International Workshop on Advanced Computing and Analysis Techniques in Physics Research — PoS(ACAT)*, volume 050, p. 040. 2009. arXiv:physics/0703039. doi:10.22323/1.050.0040.

[133] M. Cacciari et al., "The $t\bar{t}$ cross-section at 1.8 and 1.96 TeV: A study of the systematics due to parton densities and scale dependence", *JHEP* **04** (2004) 068, doi:10.1088/1126-6708/2004/04/068, arXiv:hep-ph/0303085.

[134] CMS Collaboration, "Precision luminosity measurement in proton-proton collisions at $\sqrt{s} = 13$ TeV in 2015 and 2016 at CMS", *Eur. Phys. J. C* **81** (2021) 800, doi:10.1140/epjc/s10052-021-09538-2, arXiv:2104.01927.

[135] CMS Collaboration, "CMS luminosity measurement for the 2017 data-taking period at $\sqrt{s} = 13$ TeV", CMS Physics Analysis Summary CMS-PAS-LUM-17-004, 2018.

[136] CMS Collaboration, "CMS luminosity measurement for the 2018 data-taking period at $\sqrt{s} = 13$ TeV", CMS Physics Analysis Summary CMS-PAS-LUM-18-002, 2019.

[137] S. Baker and R. D. Cousins, "Clarification of the use of chi square and likelihood functions in fits to histograms", *Nucl. Instrum. Meth.* **221** (1984) 437, doi:10.1016/0167-5087(84)90016-4.

[138] L. Demortier, "P-values and nuisance parameters", in *Statistical issues for LHC physics. Proceedings, Workshop, PHYSTAT-LHC, Geneva, Switzerland, June 27-29, 2007*, p. 23. 2008. doi:10.5170/CERN-2008-001.

[139] E. Gross and O. Vitells, "Trial factors for the look elsewhere effect in high energy physics", *Eur. Phys. J. C* **70** (2010) 525, doi:10.1140/epjc/s10052-010-1470-8, arXiv:1005.1891.

[140] T. Junk, "Confidence level computation for combining searches with small statistics", *Nucl. Instrum. Meth. A* **434** (1999) 435, doi:10.1016/S0168-9002(99)00498-2, arXiv:hep-ex/9902006.

[141] A. L. Read, "Presentation of search results: The CL_s technique", *J. Phys. G* **28** (2002) 2693, doi:10.1088/0954-3899/28/10/313.

[142] G. Cowan, K. Cranmer, E. Gross, and O. Vitells, "Asymptotic formulae for likelihood-based tests of new physics", *Eur. Phys. J. C* **71** (2011) 1554, doi:10.1140/epjc/s10052-011-1554-0, arXiv:1007.1727. [Erratum: doi:10.1140/epjc/s10052-013-2501-z].

[143] ATLAS and CMS Collaborations, and LHC Higgs Combination Group, "Procedure for the LHC higgs boson search combination in summer 2011", Technical Report CMS-NOTE-2011-005, ATL-PHYS-PUB-2011-011, CERN, 2011.

[144] CMS Collaboration, "Simplified likelihood for the re-interpretation of public CMS results", CMS Note CMS-NOTE-2017-001, 2017.

A The CMS Collaboration

Yerevan Physics Institute, Yerevan, Armenia
A. Tumasyan

Institut für Hochenergiephysik, Vienna, Austria
W. Adam, J.W. Andrejkovic, T. Bergauer, S. Chatterjee, K. Damanakis, M. Dragicevic, A. Escalante Del Valle, R. Frühwirth[1], M. Jeitler[1], N. Krammer, L. Lechner, D. Liko, I. Mikulec, P. Paulitsch, F.M. Pitters, J. Schieck[1], R. Schöfbeck, D. Schwarz, S. Templ, W. Waltenberger, C.-E. Wulz[1]

Institute for Nuclear Problems, Minsk, Belarus
V. Chekhovsky, A. Litomin, V. Makarenko

Universiteit Antwerpen, Antwerpen, Belgium
M.R. Darwish[2], E.A. De Wolf, T. Janssen, T. Kello[3], A. Lelek, H. Rejeb Sfar, P. Van Mechelen, S. Van Putte, N. Van Remortel

Vrije Universiteit Brussel, Brussel, Belgium
F. Blekman, E.S. Bols, J. D'Hondt, M. Delcourt, H. El Faham, S. Lowette, S. Moortgat, A. Morton, D. Müller, A.R. Sahasransu, S. Tavernier, W. Van Doninck, D. Vannerom

Université Libre de Bruxelles, Bruxelles, Belgium
D. Beghin, B. Bilin, B. Clerbaux, G. De Lentdecker, L. Favart, A.K. Kalsi, K. Lee, M. Mahdavikhorrami, I. Makarenko, L. Moureaux, S. Paredes, L. Pétré, A. Popov, N. Postiau, E. Starling, L. Thomas, M. Vanden Bemden, C. Vander Velde, P. Vanlaer

Ghent University, Ghent, Belgium
T. Cornelis, D. Dobur, J. Knolle, L. Lambrecht, G. Mestdach, M. Niedziela, C. Rendón, C. Roskas, A. Samalan, K. Skovpen, M. Tytgat, B. Vermassen, L. Wezenbeek

Université Catholique de Louvain, Louvain-la-Neuve, Belgium
A. Benecke, A. Bethani, G. Bruno, F. Bury, C. Caputo, P. David, C. Delaere, I.S. Donertas, A. Giammanco, K. Jaffel, Sa. Jain, V. Lemaitre, K. Mondal, J. Prisciandaro, A. Taliercio, M. Teklishyn, T.T. Tran, P. Vischia, S. Wertz

Centro Brasileiro de Pesquisas Fisicas, Rio de Janeiro, Brazil
G.A. Alves, C. Hensel, A. Moraes, P. Rebello Teles

Universidade do Estado do Rio de Janeiro, Rio de Janeiro, Brazil
W.L. Aldá Júnior, M. Alves Gallo Pereira, M. Barroso Ferreira Filho, H. Brandao Malbouisson, W. Carvalho, J. Chinellato[4], E.M. Da Costa, G.G. Da Silveira[5], D. De Jesus Damiao, V. Dos Santos Sousa, S. Fonseca De Souza, C. Mora Herrera, K. Mota Amarilo, L. Mundim, H. Nogima, A. Santoro, S.M. Silva Do Amaral, A. Sznajder, M. Thiel, F. Torres Da Silva De Araujo[6], A. Vilela Pereira

Universidade Estadual Paulista (a), Universidade Federal do ABC (b), São Paulo, Brazil
C.A. Bernardes[5], L. Calligaris, T.R. Fernandez Perez Tomei, E.M. Gregores, D.S. Lemos, P.G. Mercadante, S.F. Novaes, Sandra S. Padula

Institute for Nuclear Research and Nuclear Energy, Bulgarian Academy of Sciences, Sofia, Bulgaria
A. Aleksandrov, G. Antchev, R. Hadjiiska, P. Iaydjiev, M. Misheva, M. Rodozov, M. Shopova, G. Sultanov

University of Sofia, Sofia, Bulgaria
A. Dimitrov, T. Ivanov, L. Litov, B. Pavlov, P. Petkov, A. Petrov

Beihang University, Beijing, China
T. Cheng, T. Javaid[7], M. Mittal, L. Yuan

Department of Physics, Tsinghua University, Beijing, China
M. Ahmad, G. Bauer, C. Dozen[8], Z. Hu, J. Martins[9], Y. Wang, K. Yi[10,11]

Institute of High Energy Physics, Beijing, China
E. Chapon, G.M. Chen[7], H.S. Chen[7], M. Chen, F. Iemmi, A. Kapoor, D. Leggat, H. Liao, Z.-A. Liu[7], V. Milosevic, F. Monti, R. Sharma, J. Tao, J. Thomas-Wilsker, J. Wang, H. Zhang, J. Zhao

State Key Laboratory of Nuclear Physics and Technology, Peking University, Beijing, China
A. Agapitos, Y. An, Y. Ban, C. Chen, A. Levin, Q. Li, X. Lyu, Y. Mao, S.J. Qian, D. Wang, J. Xiao, H. Yang

Sun Yat-Sen University, Guangzhou, China
M. Lu, Z. You

Institute of Modern Physics and Key Laboratory of Nuclear Physics and Ion-beam Application (MOE) - Fudan University, Shanghai, China
X. Gao[3], H. Okawa, Y. Zhang

Zhejiang University, Hangzhou, China, Zhejiang, China
Z. Lin, M. Xiao

Universidad de Los Andes, Bogota, Colombia
C. Avila, A. Cabrera, C. Florez, J. Fraga

Universidad de Antioquia, Medellin, Colombia
J. Mejia Guisao, F. Ramirez, J.D. Ruiz Alvarez, C.A. Salazar González

University of Split, Faculty of Electrical Engineering, Mechanical Engineering and Naval Architecture, Split, Croatia
D. Giljanovic, N. Godinovic, D. Lelas, I. Puljak

University of Split, Faculty of Science, Split, Croatia
Z. Antunovic, M. Kovac, T. Sculac

Institute Rudjer Boskovic, Zagreb, Croatia
V. Brigljevic, D. Ferencek, D. Majumder, M. Roguljic, A. Starodumov[12], T. Susa

University of Cyprus, Nicosia, Cyprus
A. Attikis, K. Christoforou, A. Ioannou, G. Kole, M. Kolosova, S. Konstantinou, J. Mousa, C. Nicolaou, F. Ptochos, P.A. Razis, H. Rykaczewski, H. Saka

Charles University, Prague, Czech Republic
M. Finger[13], M. Finger Jr.[13], A. Kveton

Escuela Politecnica Nacional, Quito, Ecuador
E. Ayala

Universidad San Francisco de Quito, Quito, Ecuador
E. Carrera Jarrin

Academy of Scientific Research and Technology of the Arab Republic of Egypt, Egyp-

tian Network of High Energy Physics, Cairo, Egypt
S. Elgammal[14], A. Ellithi Kamel[15]

Center for High Energy Physics (CHEP-FU), Fayoum University, El-Fayoum, Egypt
M.A. Mahmoud, Y. Mohammed

National Institute of Chemical Physics and Biophysics, Tallinn, Estonia
S. Bhowmik, R.K. Dewanjee, K. Ehataht, M. Kadastik, S. Nandan, C. Nielsen, J. Pata, M. Raidal, L. Tani, C. Veelken

Department of Physics, University of Helsinki, Helsinki, Finland
P. Eerola, H. Kirschenmann, K. Osterberg, M. Voutilainen

Helsinki Institute of Physics, Helsinki, Finland
S. Bharthuar, E. Brücken, F. Garcia, J. Havukainen, M.S. Kim, R. Kinnunen, T. Lampén, K. Lassila-Perini, S. Lehti, T. Lindén, M. Lotti, L. Martikainen, M. Myllymäki, J. Ott, H. Siikonen, E. Tuominen, J. Tuominiemi

Lappeenranta University of Technology, Lappeenranta, Finland
P. Luukka, H. Petrow, T. Tuuva

IRFU, CEA, Université Paris-Saclay, Gif-sur-Yvette, France
C. Amendola, M. Besancon, F. Couderc, M. Dejardin, D. Denegri, J.L. Faure, F. Ferri, S. Ganjour, P. Gras, G. Hamel de Monchenault, P. Jarry, B. Lenzi, E. Locci, J. Malcles, J. Rander, A. Rosowsky, M.Ö. Sahin, A. Savoy-Navarro[16], M. Titov, G.B. Yu

Laboratoire Leprince-Ringuet, CNRS/IN2P3, Ecole Polytechnique, Institut Polytechnique de Paris, Palaiseau, France
S. Ahuja, F. Beaudette, M. Bonanomi, A. Buchot Perraguin, P. Busson, A. Cappati, C. Charlot, O. Davignon, B. Diab, G. Falmagne, S. Ghosh, R. Granier de Cassagnac, A. Hakimi, I. Kucher, J. Motta, M. Nguyen, C. Ochando, P. Paganini, J. Rembser, R. Salerno, U. Sarkar, J.B. Sauvan, Y. Sirois, A. Tarabini, A. Zabi, A. Zghiche

Université de Strasbourg, CNRS, IPHC UMR 7178, Strasbourg, France
J.-L. Agram[17], J. Andrea, D. Apparu, D. Bloch, G. Bourgatte, J.-M. Brom, E.C. Chabert, C. Collard, D. Darej, J.-C. Fontaine[17], U. Goerlach, C. Grimault, A.-C. Le Bihan, E. Nibigira, P. Van Hove

Institut de Physique des 2 Infinis de Lyon (IP2I), Villeurbanne, France
E. Asilar, S. Beauceron, C. Bernet, G. Boudoul, C. Camen, A. Carle, N. Chanon, D. Contardo, P. Depasse, H. El Mamouni, J. Fay, S. Gascon, M. Gouzevitch, B. Ille, I.B. Laktineh, H. Lattaud, A. Lesauvage, M. Lethuillier, L. Mirabito, S. Perries, K. Shchablo, V. Sordini, L. Torterotot, G. Touquet, M. Vander Donckt, S. Viret

Georgian Technical University, Tbilisi, Georgia
A. Khvedelidze[13], I. Lomidze, Z. Tsamalaidze[13]

RWTH Aachen University, I. Physikalisches Institut, Aachen, Germany
V. Botta, L. Feld, K. Klein, M. Lipinski, D. Meuser, A. Pauls, N. Röwert, J. Schulz, M. Teroerde

RWTH Aachen University, III. Physikalisches Institut A, Aachen, Germany
A. Dodonova, D. Eliseev, M. Erdmann, P. Fackeldey, B. Fischer, S. Ghosh, T. Hebbeker, K. Hoepfner, F. Ivone, L. Mastrolorenzo, M. Merschmeyer, A. Meyer, G. Mocellin, S. Mondal, S. Mukherjee, D. Noll, A. Novak, T. Pook, A. Pozdnyakov,

Y. Rath, H. Reithler, J. Roemer, A. Schmidt, S.C. Schuler, A. Sharma, L. Vigilante, S. Wiedenbeck, S. Zaleski

RWTH Aachen University, III. Physikalisches Institut B, Aachen, Germany
C. Dziwok, G. Flügge, W. Haj Ahmad[18], O. Hlushchenko, T. Kress, A. Nowack, O. Pooth, D. Roy, A. Stahl[19], T. Ziemons, A. Zotz

Deutsches Elektronen-Synchrotron, Hamburg, Germany
H. Aarup Petersen, M. Aldaya Martin, P. Asmuss, S. Baxter, M. Bayatmakou, O. Behnke, A. Bermúdez Martínez, S. Bhattacharya, A.A. Bin Anuar, K. Borras[20], D. Brunner, A. Campbell, A. Cardini, C. Cheng, F. Colombina, S. Consuegra Rodríguez, G. Correia Silva, V. Danilov, M. De Silva, L. Didukh, G. Eckerlin, D. Eckstein, L.I. Estevez Banos, O. Filatov, E. Gallo[21], A. Geiser, A. Giraldi, A. Grohsjean, M. Guthoff, A. Jafari[22], N.Z. Jomhari, H. Jung, A. Kasem[20], M. Kasemann, H. Kaveh, C. Kleinwort, R. Kogler, D. Krücker, W. Lange, J. Lidrych, K. Lipka, W. Lohmann[23], R. Mankel, I.-A. Melzer-Pellmann, M. Mendizabal Morentin, J. Metwally, A.B. Meyer, M. Meyer, J. Mnich, A. Mussgiller, Y. Otarid, D. Pérez Adán, D. Pitzl, A. Raspereza, B. Ribeiro Lopes, J. Rübenach, A. Saggio, A. Saibel, M. Savitskyi, M. Scham[24], V. Scheurer, S. Schnake, P. Schütze, C. Schwanenberger[21], M. Shchedrolosiev, R.E. Sosa Ricardo, D. Stafford, N. Tonon, M. Van De Klundert, R. Walsh, D. Walter, Q. Wang, Y. Wen, K. Wichmann, L. Wiens, C. Wissing, S. Wuchterl

University of Hamburg, Hamburg, Germany
R. Aggleton, S. Albrecht, S. Bein, L. Benato, P. Connor, K. De Leo, M. Eich, F. Feindt, A. Fröhlich, C. Garbers, E. Garutti, P. Gunnellini, M. Hajheidari, J. Haller, A. Hinzmann, G. Kasieczka, R. Klanner, T. Kramer, V. Kutzner, J. Lange, T. Lange, A. Lobanov, A. Malara, A. Nigamova, K.J. Pena Rodriguez, M. Rieger, O. Rieger, P. Schleper, M. Schröder, J. Schwandt, J. Sonneveld, H. Stadie, G. Steinbrück, A. Tews, I. Zoi

Karlsruher Institut fuer Technologie, Karlsruhe, Germany
J. Bechtel, S. Brommer, M. Burkart, E. Butz, R. Caspart, T. Chwalek, W. De Boer†, A. Dierlamm, A. Droll, K. El Morabit, N. Faltermann, M. Giffels, J.O. Gosewisch, A. Gottmann, F. Hartmann[19], C. Heidecker, U. Husemann, P. Keicher, R. Koppenhöfer, S. Maier, M. Metzler, S. Mitra, Th. Müller, M. Neukum, A. Nürnberg, G. Quast, K. Rabbertz, J. Rauser, D. Savoiu, M. Schnepf, D. Seith, I. Shvetsov, H.J. Simonis, R. Ulrich, J. Van Der Linden, R.F. Von Cube, M. Wassmer, M. Weber, S. Wieland, R. Wolf, S. Wozniewski, S. Wunsch

Institute of Nuclear and Particle Physics (INPP), NCSR Demokritos, Aghia Paraskevi, Greece
G. Anagnostou, G. Daskalakis, A. Kyriakis, D. Loukas, A. Stakia

National and Kapodistrian University of Athens, Athens, Greece
M. Diamantopoulou, D. Karasavvas, P. Kontaxakis, C.K. Koraka, A. Manousakis-Katsikakis, A. Panagiotou, I. Papavergou, N. Saoulidou, K. Theofilatos, E. Tziaferi, K. Vellidis, E. Vourliotis

National Technical University of Athens, Athens, Greece
G. Bakas, K. Kousouris, I. Papakrivopoulos, G. Tsipolitis, A. Zacharopoulou

University of Ioánnina, Ioánnina, Greece
K. Adamidis, I. Bestintzanos, I. Evangelou, C. Foudas, P. Gianneios, P. Katsoulis, P. Kokkas,

N. Manthos, I. Papadopoulos, J. Strologas

MTA-ELTE Lendület CMS Particle and Nuclear Physics Group, Eötvös Loránd University, Budapest, Hungary
M. Csanad, K. Farkas, M.M.A. Gadallah[25], S. Lökös[26], P. Major, K. Mandal, A. Mehta, G. Pasztor, A.J. Rádl, O. Surányi, G.I. Veres

Wigner Research Centre for Physics, Budapest, Hungary
M. Bartók[27], G. Bencze, C. Hajdu, D. Horvath[28,29], F. Sikler, V. Veszpremi

Institute of Nuclear Research ATOMKI, Debrecen, Hungary
S. Czellar, D. Fasanella, F. Fienga, J. Karancsi[27], J. Molnar, Z. Szillasi, D. Teyssier

Institute of Physics, University of Debrecen, Debrecen, Hungary
P. Raics, Z.L. Trocsanyi[30], B. Ujvari

Karoly Robert Campus, MATE Institute of Technology, Gyongyos, Hungary
T. Csorgo[31], F. Nemes[31], T. Novak

Indian Institute of Science (IISc), Bangalore, India
S. Choudhury

National Institute of Science Education and Research, HBNI, Bhubaneswar, India
S. Bahinipati[32], C. Kar, P. Mal, T. Mishra, V.K. Muraleedharan Nair Bindhu[33], A. Nayak[33], P. Saha, N. Sur, S.K. Swain, D. Vats[33]

Panjab University, Chandigarh, India
S. Bansal, S.B. Beri, V. Bhatnagar, G. Chaudhary, S. Chauhan, N. Dhingra[34], R. Gupta, A. Kaur, H. Kaur, M. Kaur, P. Kumari, M. Meena, K. Sandeep, J.B. Singh, A.K. Virdi

University of Delhi, Delhi, India
A. Ahmed, A. Bhardwaj, B.C. Choudhary, M. Gola, S. Keshri, A. Kumar, M. Naimuddin, P. Priyanka, K. Ranjan, A. Shah

Saha Institute of Nuclear Physics, HBNI, Kolkata, India
M. Bharti[35], R. Bhattacharya, S. Bhattacharya, D. Bhowmik, S. Dutta, S. Dutta, B. Gomber[36], M. Maity[37], P. Palit, P.K. Rout, G. Saha, B. Sahu, S. Sarkar, M. Sharan, S. Thakur[35]

Indian Institute of Technology Madras, Madras, India
P.K. Behera, S.C. Behera, P. Kalbhor, J.R. Komaragiri[38], D. Kumar[38], A. Muhammad, L. Panwar[38], R. Pradhan, P.R. Pujahari, A. Sharma, A.K. Sikdar, P.C. Tiwari[38]

Bhabha Atomic Research Centre, Mumbai, India
D. Dutta, V. Jha, V. Kumar, D.K. Mishra, K. Naskar[39], P.K. Netrakanti, L.M. Pant, P. Shukla

Tata Institute of Fundamental Research-A, Mumbai, India
T. Aziz, S. Dugad, M. Kumar, G.B. Mohanty

Tata Institute of Fundamental Research-B, Mumbai, India
S. Banerjee, R. Chudasama, M. Guchait, S. Karmakar, S. Kumar, G. Majumder, K. Mazumdar, S. Mukherjee

Indian Institute of Science Education and Research (IISER), Pune, India
A. Alpana, S. Dube, B. Kansal, A. Laha, S. Pandey, A. Rastogi, S. Sharma

Isfahan University of Technology, Isfahan, Iran
H. Bakhshiansohi[40,41], E. Khazaie[41], M. Zeinali[42]

Institute for Research in Fundamental Sciences (IPM), Tehran, Iran
S. Chenarani[43], S.M. Etesami, M. Khakzad, M. Mohammadi Najafabadi

University College Dublin, Dublin, Ireland
M. Grunewald

INFN Sezione di Bari [a], Bari, Italy, Università di Bari [b], Bari, Italy, Politecnico di Bari [c], Bari, Italy
M. Abbrescia[a,b], R. Aly[a,b,44], C. Aruta[a,b], A. Colaleo[a], D. Creanza[a,c], N. De Filippis[a,c], M. De Palma[a,b], A. Di Florio[a,b], A. Di Pilato[a,b], W. Elmetenawee[a,b], L. Fiore[a], A. Gelmi[a,b], M. Gul[a], G. Iaselli[a,c], M. Ince[a,b], S. Lezki[a,b], G. Maggi[a,c], M. Maggi[a], I. Margjeka[a,b], V. Mastrapasqua[a,b], S. My[a,b], S. Nuzzo[a,b], A. Pellecchia[a,b], A. Pompili[a,b], G. Pugliese[a,c], D. Ramos[a], A. Ranieri[a], G. Selvaggi[a,b], L. Silvestris[a], F.M. Simone[a,b], Ü. Sözbilir[a], R. Venditti[a], P. Verwilligen[a]

INFN Sezione di Bologna [a], Bologna, Italy, Università di Bologna [b], Bologna, Italy
G. Abbiendi[a], C. Battilana[a,b], D. Bonacorsi[a,b], L. Borgonovi[a], R. Campanini[a,b], P. Capiluppi[a,b], A. Castro[a,b], F.R. Cavallo[a], C. Ciocca[a], M. Cuffiani[a,b], G.M. Dallavalle[a], T. Diotalevi[a,b], F. Fabbri[a], A. Fanfani[a,b], P. Giacomelli[a], L. Giommi[a,b], C. Grandi[a], L. Guiducci[a,b], S. Lo Meo[a,45], L. Lunerti[a,b], S. Marcellini[a], G. Masetti[a], F.L. Navarria[a,b], A. Perrotta[a], F. Primavera[a,b], A.M. Rossi[a,b], T. Rovelli[a,b], G.P. Siroli[a,b]

INFN Sezione di Catania [a], Catania, Italy, Università di Catania [b], Catania, Italy
S. Albergo[a,b,46], S. Costa[a,b,46], A. Di Mattia[a], R. Potenza[a,b], A. Tricomi[a,b,46], C. Tuve[a,b]

INFN Sezione di Firenze [a], Firenze, Italy, Università di Firenze [b], Firenze, Italy
G. Barbagli[a], A. Cassese[a], R. Ceccarelli[a,b], V. Ciulli[a,b], C. Civinini[a], R. D'Alessandro[a,b], E. Focardi[a,b], G. Latino[a,b], P. Lenzi[a,b], M. Lizzo[a,b], M. Meschini[a], S. Paoletti[a], R. Seidita[a,b], G. Sguazzoni[a], L. Viliani[a]

INFN Laboratori Nazionali di Frascati, Frascati, Italy
L. Benussi, S. Bianco, D. Piccolo

INFN Sezione di Genova [a], Genova, Italy, Università di Genova [b], Genova, Italy
M. Bozzo[a,b], F. Ferro[a], R. Mulargia[a,b], E. Robutti[a], S. Tosi[a,b]

INFN Sezione di Milano-Bicocca [a], Milano, Italy, Università di Milano-Bicocca [b], Milano, Italy
A. Benaglia[a], G. Boldrini, F. Brivio[a,b], F. Cetorelli[a,b], F. De Guio[a,b], M.E. Dinardo[a,b], P. Dini[a], S. Gennai[a], A. Ghezzi[a,b], P. Govoni[a,b], L. Guzzi[a,b], M.T. Lucchini[a,b], M. Malberti[a], S. Malvezzi[a], A. Massironi[a], D. Menasce[a], L. Moroni[a], M. Paganoni[a,b], D. Pedrini[a], B.S. Pinolini, S. Ragazzi[a,b], N. Redaelli[a], T. Tabarelli de Fatis[a,b], D. Valsecchi[a,b,19], D. Zuolo[a,b]

INFN Sezione di Napoli [a], Napoli, Italy, Università di Napoli 'Federico II' [b], Napoli, Italy, Università della Basilicata [c], Potenza, Italy, Università G. Marconi [d], Roma, Italy
S. Buontempo[a], F. Carnevali[a,b], N. Cavallo[a,c], A. De Iorio[a,b], F. Fabozzi[a,c], A.O.M. Iorio[a,b], L. Lista[a,b,47], S. Meola[a,d,19], P. Paolucci[a,19], B. Rossi[a], C. Sciacca[a,b]

INFN Sezione di Padova [a], Padova, Italy, Università di Padova [b], Padova, Italy, Università di Trento [c], Trento, Italy
P. Azzi[a], N. Bacchetta[a], D. Bisello[a,b], P. Bortignon[a], A. Bragagnolo[a,b], R. Carlin[a,b], P. Checchia[a], T. Dorigo[a], U. Dosselli[a], F. Gasparini[a,b], U. Gasparini[a,b], G. Grosso, S.Y. Hoh[a,b], L. Layer[a,48], E. Lusiani, M. Margoni[a,b], A.T. Meneguzzo[a,b], J. Pazzini[a,b], P. Ronchese[a,b], R. Rossin[a,b], F. Simonetto[a,b], G. Strong[a], M. Tosi[a,b], H. Yarar[a,b], M. Zanetti[a,b], P. Zotto[a,b], A. Zucchetta[a,b], G. Zumerle[a,b]

INFN Sezione di Pavia [a], Pavia, Italy, Università di Pavia [b], Pavia, Italy
C. Aimè[a,b], A. Braghieri[a], S. Calzaferri[a,b], D. Fiorina[a,b], P. Montagna[a,b], S.P. Ratti[a,b], V. Re[a], C. Riccardi[a,b], P. Salvini[a], I. Vai[a], P. Vitulo[a,b]

INFN Sezione di Perugia [a], Perugia, Italy, Università di Perugia [b], Perugia, Italy
P. Asenov[a,49], G.M. Bilei[a], D. Ciangottini[a,b], L. Fanò[a,b], M. Magherini[b], G. Mantovani[a,b], V. Mariani[a,b], M. Menichelli[a], F. Moscatelli[a,49], A. Piccinelli[a,b], M. Presilla[a,b], A. Rossi[a,b], A. Santocchia[a,b], D. Spiga[a], T. Tedeschi[a,b]

INFN Sezione di Pisa [a], Pisa, Italy, Università di Pisa [b], Pisa, Italy, Scuola Normale Superiore di Pisa [c], Pisa, Italy, Università di Siena [d], Siena, Italy
P. Azzurri[a], G. Bagliesi[a], V. Bertacchi[a,c], L. Bianchini[a], T. Boccali[a], E. Bossini[a,b], R. Castaldi[a], M.A. Ciocci[a,b], V. D'Amante[a,d], R. Dell'Orso[a], M.R. Di Domenico[a,d], S. Donato[a], A. Giassi[a], F. Ligabue[a,c], E. Manca[a,c], G. Mandorli[a,c], D. Matos Figueiredo, A. Messineo[a,b], F. Palla[a], S. Parolia[a,b], G. Ramirez-Sanchez[a,c], A. Rizzi[a,b], G. Rolandi[a,c], S. Roy Chowdhury[a,c], A. Scribano[a], N. Shafiei[a,b], P. Spagnolo[a], R. Tenchini[a], G. Tonelli[a,b], N. Turini[a,d], A. Venturi[a], P.G. Verdini[a]

INFN Sezione di Roma [a], Rome, Italy, Sapienza Università di Roma [b], Rome, Italy
P. Barria[a], M. Campana[a,b], F. Cavallari[a], D. Del Re[a,b], E. Di Marco[a], M. Diemoz[a], E. Longo[a,b], P. Meridiani[a], G. Organtini[a,b], F. Pandolfi[a], R. Paramatti[a,b], C. Quaranta[a,b], S. Rahatlou[a,b], C. Rovelli[a], F. Santanastasio[a,b], L. Soffi[a], R. Tramontano[a,b]

INFN Sezione di Torino [a], Torino, Italy, Università di Torino [b], Torino, Italy, Università del Piemonte Orientale [c], Novara, Italy
N. Amapane[a,b], R. Arcidiacono[a,c], S. Argiro[a,b], M. Arneodo[a,c], N. Bartosik[a], R. Bellan[a,b], A. Bellora[a,b], J. Berenguer Antequera[a,b], C. Biino[a], N. Cartiglia[a], M. Costa[a,b], R. Covarelli[a,b], N. Demaria[a], B. Kiani[a,b], F. Legger[a], C. Mariotti[a], S. Maselli[a], E. Migliore[a,b], E. Monteil[a,b], M. Monteno[a], M.M. Obertino[a,b], G. Ortona[a], L. Pacher[a,b], N. Pastrone[a], M. Pelliccioni[a], M. Ruspa[a,c], K. Shchelina[a], F. Siviero[a,b], V. Sola[a], A. Solano[a,b], D. Soldi[a,b], A. Staiano[a], M. Tornago[a,b], D. Trocino[a], A. Vagnerini[a,b]

INFN Sezione di Trieste [a], Trieste, Italy, Università di Trieste [b], Trieste, Italy
S. Belforte[a], V. Candelise[a,b], M. Casarsa[a], F. Cossutti[a], A. Da Rold[a,b], G. Della Ricca[a,b], G. Sorrentino[a,b], F. Vazzoler[a,b]

Kyungpook National University, Daegu, Korea
S. Dogra, C. Huh, B. Kim, D.H. Kim, G.N. Kim, J. Kim, J. Lee, S.W. Lee, C.S. Moon, Y.D. Oh, S.I. Pak, S. Sekmen, Y.C. Yang

Chonnam National University, Institute for Universe and Elementary Particles, Kwangju, Korea

H. Kim, D.H. Moon

Hanyang University, Seoul, Korea
B. Francois, T.J. Kim, J. Park

Korea University, Seoul, Korea
S. Cho, S. Choi, B. Hong, K. Lee, K.S. Lee, J. Lim, J. Park, S.K. Park, J. Yoo

Kyung Hee University, Department of Physics, Seoul, Republic of Korea, Seoul, Korea
J. Goh, A. Gurtu

Sejong University, Seoul, Korea
H.S. Kim, Y. Kim

Seoul National University, Seoul, Korea
J. Almond, J.H. Bhyun, J. Choi, S. Jeon, J. Kim, J.S. Kim, S. Ko, H. Kwon, H. Lee, S. Lee, B.H. Oh, M. Oh, S.B. Oh, H. Seo, U.K. Yang, I. Yoon

University of Seoul, Seoul, Korea
W. Jang, D.Y. Kang, Y. Kang, S. Kim, B. Ko, J.S.H. Lee, Y. Lee, J.A. Merlin, I.C. Park, Y. Roh, M.S. Ryu, D. Song, I.J. Watson, S. Yang

Yonsei University, Department of Physics, Seoul, Korea
S. Ha, H.D. Yoo

Sungkyunkwan University, Suwon, Korea
M. Choi, H. Lee, Y. Lee, I. Yu

College of Engineering and Technology, American University of the Middle East (AUM), Egaila, Kuwait, Dasman, Kuwait
T. Beyrouthy, Y. Maghrbi

Riga Technical University, Riga, Latvia
K. Dreimanis, V. Veckalns[50]

Vilnius University, Vilnius, Lithuania
M. Ambrozas, A. Carvalho Antunes De Oliveira, A. Juodagalvis, A. Rinkevicius, G. Tamulaitis

National Centre for Particle Physics, Universiti Malaya, Kuala Lumpur, Malaysia
N. Bin Norjoharuddeen, W.A.T. Wan Abdullah, M.N. Yusli, Z. Zolkapli

Universidad de Sonora (UNISON), Hermosillo, Mexico
J.F. Benitez, A. Castaneda Hernandez, M. León Coello, J.A. Murillo Quijada, A. Sehrawat, L. Valencia Palomo

Centro de Investigacion y de Estudios Avanzados del IPN, Mexico City, Mexico
G. Ayala, H. Castilla-Valdez, E. De La Cruz-Burelo, I. Heredia-De La Cruz[51], R. Lopez-Fernandez, C.A. Mondragon Herrera, D.A. Perez Navarro, A. Sánchez Hernández

Universidad Iberoamericana, Mexico City, Mexico
S. Carrillo Moreno, C. Oropeza Barrera, F. Vazquez Valencia

Benemerita Universidad Autonoma de Puebla, Puebla, Mexico
I. Pedraza, H.A. Salazar Ibarguen, C. Uribe Estrada

University of Montenegro, Podgorica, Montenegro
J. Mijuskovic[52], N. Raicevic

University of Auckland, Auckland, New Zealand
D. Krofcheck

University of Canterbury, Christchurch, New Zealand
P.H. Butler

National Centre for Physics, Quaid-I-Azam University, Islamabad, Pakistan
A. Ahmad, M.I. Asghar, A. Awais, M.I.M. Awan, H.R. Hoorani, W.A. Khan, M.A. Shah, M. Shoaib, M. Waqas

AGH University of Science and Technology Faculty of Computer Science, Electronics and Telecommunications, Krakow, Poland
V. Avati, L. Grzanka, M. Malawski

National Centre for Nuclear Research, Swierk, Poland
H. Bialkowska, M. Bluj, B. Boimska, M. Górski, M. Kazana, M. Szleper, P. Zalewski

Institute of Experimental Physics, Faculty of Physics, University of Warsaw, Warsaw, Poland
K. Bunkowski, K. Doroba, A. Kalinowski, M. Konecki, J. Krolikowski

Laboratório de Instrumentação e Física Experimental de Partículas, Lisboa, Portugal
M. Araujo, P. Bargassa, D. Bastos, A. Boletti, P. Faccioli, M. Gallinaro, J. Hollar, N. Leonardo, T. Niknejad, M. Pisano, J. Seixas, O. Toldaiev, J. Varela

Joint Institute for Nuclear Research, Dubna, Russia
S. Afanasiev, D. Budkouski, I. Golutvin, I. Gorbunov, V. Karjavine, V. Korenkov, A. Lanev, A. Malakhov, V. Matveev[53,54], V. Palichik, V. Perelygin, M. Savina, D. Seitova, V. Shalaev, S. Shmatov, S. Shulha, V. Smirnov, O. Teryaev, N. Voytishin, B.S. Yuldashev[55], A. Zarubin, I. Zhizhin

Petersburg Nuclear Physics Institute, Gatchina (St. Petersburg), Russia
G. Gavrilov, V. Golovtcov, Y. Ivanov, V. Kim[56], E. Kuznetsova[57], V. Murzin, V. Oreshkin, I. Smirnov, D. Sosnov, V. Sulimov, L. Uvarov, S. Volkov, A. Vorobyev

Institute for Nuclear Research, Moscow, Russia
Yu. Andreev, A. Dermenev, S. Gninenko, N. Golubev, A. Karneyeu, D. Kirpichnikov, M. Kirsanov, N. Krasnikov, A. Pashenkov, G. Pivovarov, A. Toropin

Moscow Institute of Physics and Technology, Moscow, Russia
T. Aushev

National Research Center 'Kurchatov Institute', Moscow, Russia
V. Epshteyn, V. Gavrilov, N. Lychkovskaya, A. Nikitenko[58], V. Popov, A. Stepennov, M. Toms, E. Vlasov, A. Zhokin

National Research Nuclear University 'Moscow Engineering Physics Institute' (MEPhI), Moscow, Russia
M. Chadeeva[59], A. Oskin, P. Parygin, E. Popova, V. Rusinov, D. Selivanova

P.N. Lebedev Physical Institute, Moscow, Russia
V. Andreev, M. Azarkin, I. Dremin, M. Kirakosyan, A. Terkulov

Skobeltsyn Institute of Nuclear Physics, Lomonosov Moscow State University, Moscow, Russia
A. Belyaev, E. Boos, V. Bunichev, M. Dubinin[60], L. Dudko, A. Ershov, A. Gribushin, V. Klyukhin, O. Kodolova, I. Lokhtin, S. Obraztsov, S. Petrushanko, V. Savrin

Novosibirsk State University (NSU), Novosibirsk, Russia
V. Blinov[61], T. Dimova[61], L. Kardapoltsev[61], A. Kozyrev[61], I. Ovtin[61], O. Radchenko[61], Y. Skovpen[61]

Institute for High Energy Physics of National Research Centre 'Kurchatov Institute', Protvino, Russia
I. Azhgirey, I. Bayshev, D. Elumakhov, V. Kachanov, D. Konstantinov, P. Mandrik, V. Petrov, R. Ryutin, S. Slabospitskii, A. Sobol, S. Troshin, N. Tyurin, A. Uzunian, A. Volkov

National Research Tomsk Polytechnic University, Tomsk, Russia
A. Babaev, V. Okhotnikov

Tomsk State University, Tomsk, Russia
V. Borshch, V. Ivanchenko, E. Tcherniaev

University of Belgrade: Faculty of Physics and VINCA Institute of Nuclear Sciences, Belgrade, Serbia
P. Adzic[62], M. Dordevic, P. Milenovic, J. Milosevic

Centro de Investigaciones Energéticas Medioambientales y Tecnológicas (CIEMAT), Madrid, Spain
M. Aguilar-Benitez, J. Alcaraz Maestre, A. Álvarez Fernández, I. Bachiller, M. Barrio Luna, Cristina F. Bedoya, C.A. Carrillo Montoya, M. Cepeda, M. Cerrada, N. Colino, B. De La Cruz, A. Delgado Peris, J.P. Fernández Ramos, J. Flix, M.C. Fouz, O. Gonzalez Lopez, S. Goy Lopez, J.M. Hernandez, M.I. Josa, J. León Holgado, D. Moran, Á. Navarro Tobar, C. Perez Dengra, A. Pérez-Calero Yzquierdo, J. Puerta Pelayo, I. Redondo, L. Romero, S. Sánchez Navas, L. Urda Gómez, C. Willmott

Universidad Autónoma de Madrid, Madrid, Spain
J.F. de Trocóniz, R. Reyes-Almanza

Universidad de Oviedo, Instituto Universitario de Ciencias y Tecnologías Espaciales de Asturias (ICTEA), Oviedo, Spain
B. Alvarez Gonzalez, J. Cuevas, C. Erice, J. Fernandez Menendez, S. Folgueras, I. Gonzalez Caballero, J.R. González Fernández, E. Palencia Cortezon, C. Ramón Álvarez, V. Rodríguez Bouza, A. Soto Rodríguez, A. Trapote, N. Trevisani, C. Vico Villalba

Instituto de Física de Cantabria (IFCA), CSIC-Universidad de Cantabria, Santander, Spain
J.A. Brochero Cifuentes, I.J. Cabrillo, A. Calderon, J. Duarte Campderros, M. Fernandez, C. Fernandez Madrazo, P.J. Fernández Manteca, A. García Alonso, G. Gomez, C. Martinez Rivero, P. Martinez Ruiz del Arbol, F. Matorras, P. Matorras Cuevas, J. Piedra Gomez, C. Prieels, A. Ruiz-Jimeno, L. Scodellaro, I. Vila, J.M. Vizan Garcia

University of Colombo, Colombo, Sri Lanka
M.K. Jayananda, B. Kailasapathy[63], D.U.J. Sonnadara, D.D.C. Wickramarathna

University of Ruhuna, Department of Physics, Matara, Sri Lanka
W.G.D. Dharmaratna, K. Liyanage, N. Perera, N. Wickramage

CERN, European Organization for Nuclear Research, Geneva, Switzerland
T.K. Aarrestad, D. Abbaneo, J. Alimena, E. Auffray, G. Auzinger, J. Baechler, P. Baillon[†], D. Barney, J. Bendavid, M. Bianco, A. Bocci, C. Caillol, T. Camporesi, M. Capeans Garrido, G. Cerminara, N. Chernyavskaya, S.S. Chhibra, M. Cipriani, L. Cristella, D. d'Enterria, A. Dabrowski, A. David, A. De Roeck, M.M. Defranchis, M. Deile, M. Dobson, M. Dünser, N. Dupont, A. Elliott-Peisert, N. Emriskova, F. Fallavollita[64],

A. Florent, L. Forthomme, G. Franzoni, W. Funk, S. Giani, D. Gigi, K. Gill, F. Glege, L. Gouskos, M. Haranko, J. Hegeman, V. Innocente, T. James, P. Janot, J. Kaspar, J. Kieseler, M. Komm, N. Kratochwil, C. Lange, S. Laurila, P. Lecoq, A. Lintuluoto, K. Long, C. Lourenço, B. Maier, L. Malgeri, S. Mallios, M. Mannelli, A.C. Marini, F. Meijers, S. Mersi, E. Meschi, F. Moortgat, M. Mulders, S. Orfanelli, L. Orsini, F. Pantaleo, E. Perez, M. Peruzzi, A. Petrilli, G. Petrucciani, A. Pfeiffer, M. Pierini, D. Piparo, M. Pitt, H. Qu, T. Quast, D. Rabady, A. Racz, G. Reales Gutiérrez, M. Rovere, H. Sakulin, J. Salfeld-Nebgen, S. Scarfi, C. Schäfer, C. Schwick, M. Selvaggi, A. Sharma, P. Silva, W. Snoeys, P. Sphicas[65], S. Summers, K. Tatar, V.R. Tavolaro, D. Treille, P. Tropea, A. Tsirou, G.P. Van Onsem, J. Wanczyk[66], K.A. Wozniak, W.D. Zeuner

Paul Scherrer Institut, Villigen, Switzerland
L. Caminada[67], A. Ebrahimi, W. Erdmann, R. Horisberger, Q. Ingram, H.C. Kaestli, D. Kotlinski, U. Langenegger, M. Missiroli[67], L. Noehte[67], T. Rohe

ETH Zurich - Institute for Particle Physics and Astrophysics (IPA), Zurich, Switzerland
K. Androsov[66], M. Backhaus, P. Berger, A. Calandri, A. De Cosa, G. Dissertori, M. Dittmar, M. Donegà, C. Dorfer, F. Eble, K. Gedia, F. Glessgen, T.A. Gómez Espinosa, C. Grab, D. Hits, W. Lustermann, A.-M. Lyon, R.A. Manzoni, L. Marchese, C. Martin Perez, M.T. Meinhard, F. Nessi-Tedaldi, J. Niedziela, F. Pauss, V. Perovic, S. Pigazzini, M.G. Ratti, M. Reichmann, C. Reissel, T. Reitenspiess, B. Ristic, D. Ruini, D.A. Sanz Becerra, V. Stampf, J. Steggemann[66], R. Wallny, D.H. Zhu

Universität Zürich, Zurich, Switzerland
C. Amsler[68], P. Bärtschi, C. Botta, D. Brzhechko, M.F. Canelli, K. Cormier, A. De Wit, R. Del Burgo, J.K. Heikkilä, M. Huwiler, W. Jin, A. Jofrehei, B. Kilminster, S. Leontsinis, S.P. Liechti, A. Macchiolo, P. Meiring, V.M. Mikuni, U. Molinatti, I. Neutelings, A. Reimers, P. Robmann, S. Sanchez Cruz, K. Schweiger, M. Senger, Y. Takahashi

National Central University, Chung-Li, Taiwan
C. Adloff[69], C.M. Kuo, W. Lin, A. Roy, T. Sarkar[37], S.S. Yu

National Taiwan University (NTU), Taipei, Taiwan
L. Ceard, Y. Chao, K.F. Chen, P.H. Chen, P.s. Chen, H. Cheng, W.-S. Hou, Y.y. Li, R.-S. Lu, E. Paganis, A. Psallidas, A. Steen, H.y. Wu, E. Yazgan, P.r. Yu

Chulalongkorn University, Faculty of Science, Department of Physics, Bangkok, Thailand
B. Asavapibhop, C. Asawatangtrakuldee, N. Srimanobhas

Çukurova University, Physics Department, Science and Art Faculty, Adana, Turkey
F. Boran, S. Damarseckin[70], Z.S. Demiroglu, F. Dolek, I. Dumanoglu[71], E. Eskut, Y. Guler[72], E. Gurpinar Guler[72], C. Isik, O. Kara, A. Kayis Topaksu, U. Kiminsu, G. Onengut, K. Ozdemir[73], A. Polatoz, A.E. Simsek, B. Tali[74], U.G. Tok, S. Turkcapar, I.S. Zorbakir

Middle East Technical University, Physics Department, Ankara, Turkey
G. Karapinar, K. Ocalan[75], M. Yalvac[76]

Bogazici University, Istanbul, Turkey
B. Akgun, I.O. Atakisi, E. Gülmez, M. Kaya[77], O. Kaya[78], Ö. Özçelik, S. Tekten[79], E.A. Yetkin[80]

Istanbul Technical University, Istanbul, Turkey

A. Cakir, K. Cankocak[71], Y. Komurcu, S. Sen[81]

Istanbul University, Istanbul, Turkey
S. Cerci[74], I. Hos[82], B. Isildak[83], B. Kaynak, S. Ozkorucuklu, H. Sert, D. Sunar Cerci[74], C. Zorbilmez

Institute for Scintillation Materials of National Academy of Science of Ukraine, Kharkov, Ukraine
B. Grynyov

National Scientific Center, Kharkov Institute of Physics and Technology, Kharkov, Ukraine
L. Levchuk

University of Bristol, Bristol, United Kingdom
D. Anthony, E. Bhal, S. Bologna, J.J. Brooke, A. Bundock, E. Clement, D. Cussans, H. Flacher, J. Goldstein, G.P. Heath, H.F. Heath, L. Kreczko, B. Krikler, S. Paramesvaran, S. Seif El Nasr-Storey, V.J. Smith, N. Stylianou[84], K. Walkingshaw Pass, R. White

Rutherford Appleton Laboratory, Didcot, United Kingdom
K.W. Bell, A. Belyaev[85], C. Brew, R.M. Brown, D.J.A. Cockerill, C. Cooke, K.V. Ellis, K. Harder, S. Harper, M.-L. Holmberg[86], J. Linacre, K. Manolopoulos, D.M. Newbold, E. Olaiya, D. Petyt, T. Reis, T. Schuh, C.H. Shepherd-Themistocleous, I.R. Tomalin, T. Williams

Imperial College, London, United Kingdom
R. Bainbridge, P. Bloch, S. Bonomally, J. Borg, S. Breeze, O. Buchmuller, V. Cepaitis, G.S. Chahal[87], D. Colling, P. Dauncey, G. Davies, M. Della Negra, S. Fayer, G. Fedi, G. Hall, M.H. Hassanshahi, G. Iles, J. Langford, L. Lyons, A.-M. Magnan, S. Malik, A. Martelli, D.G. Monk, J. Nash[88], M. Pesaresi, B.C. Radburn-Smith, D.M. Raymond, A. Richards, A. Rose, E. Scott, C. Seez, A. Shtipliyski, A. Tapper, K. Uchida, T. Virdee[19], M. Vojinovic, N. Wardle, S.N. Webb, D. Winterbottom

Brunel University, Uxbridge, United Kingdom
K. Coldham, J.E. Cole, A. Khan, P. Kyberd, I.D. Reid, L. Teodorescu, S. Zahid

Baylor University, Waco, Texas, USA
S. Abdullin, A. Brinkerhoff, B. Caraway, J. Dittmann, K. Hatakeyama, A.R. Kanuganti, B. McMaster, N. Pastika, M. Saunders, S. Sawant, C. Sutantawibul, J. Wilson

Catholic University of America, Washington, DC, USA
R. Bartek, A. Dominguez, R. Uniyal, A.M. Vargas Hernandez

The University of Alabama, Tuscaloosa, Alabama, USA
A. Buccilli, S.I. Cooper, D. Di Croce, S.V. Gleyzer, C. Henderson, C.U. Perez, P. Rumerio[89], C. West

Boston University, Boston, Massachusetts, USA
A. Akpinar, A. Albert, D. Arcaro, C. Cosby, Z. Demiragli, E. Fontanesi, D. Gastler, S. May, J. Rohlf, K. Salyer, D. Sperka, D. Spitzbart, I. Suarez, A. Tsatsos, S. Yuan, D. Zou

Brown University, Providence, Rhode Island, USA
G. Benelli, B. Burkle, X. Coubez[20], D. Cutts, M. Hadley, U. Heintz, J.M. Hogan[90],

T. KWON, G. Landsberg, K.T. Lau, D. Li, M. Lukasik, J. Luo, M. Narain, N. Pervan, S. Sagir[91], F. Simpson, E. Usai, W.Y. Wong, X. Yan, D. Yu, W. Zhang

University of California, Davis, Davis, California, USA
J. Bonilla, C. Brainerd, R. Breedon, M. Calderon De La Barca Sanchez, M. Chertok, J. Conway, P.T. Cox, R. Erbacher, G. Haza, F. Jensen, O. Kukral, R. Lander, M. Mulhearn, D. Pellett, B. Regnery, D. Taylor, Y. Yao, F. Zhang

University of California, Los Angeles, California, USA
M. Bachtis, R. Cousins, A. Datta, D. Hamilton, J. Hauser, M. Ignatenko, M.A. Iqbal, T. Lam, W.A. Nash, S. Regnard, D. Saltzberg, B. Stone, V. Valuev

University of California, Riverside, Riverside, California, USA
K. Burt, Y. Chen, R. Clare, J.W. Gary, M. Gordon, G. Hanson, G. Karapostoli, O.R. Long, N. Manganelli, M. Olmedo Negrete, W. Si, S. Wimpenny, Y. Zhang

University of California, San Diego, La Jolla, California, USA
J.G. Branson, P. Chang, S. Cittolin, S. Cooperstein, N. Deelen, D. Diaz, J. Duarte, R. Gerosa, L. Giannini, J. Guiang, R. Kansal, V. Krutelyov, R. Lee, J. Letts, M. Masciovecchio, F. Mokhtar, M. Pieri, B.V. Sathia Narayanan, V. Sharma, M. Tadel, F. Würthwein, Y. Xiang, A. Yagil

University of California, Santa Barbara - Department of Physics, Santa Barbara, California, USA
N. Amin, C. Campagnari, M. Citron, A. Dorsett, V. Dutta, J. Incandela, M. Kilpatrick, J. Kim, B. Marsh, H. Mei, M. Oshiro, M. Quinnan, J. Richman, U. Sarica, F. Setti, J. Sheplock, P. Siddireddy, D. Stuart, S. Wang

California Institute of Technology, Pasadena, California, USA
A. Bornheim, O. Cerri, I. Dutta, J.M. Lawhorn, N. Lu, J. Mao, H.B. Newman, T.Q. Nguyen, M. Spiropulu, J.R. Vlimant, C. Wang, S. Xie, Z. Zhang, R.Y. Zhu

Carnegie Mellon University, Pittsburgh, Pennsylvania, USA
J. Alison, S. An, M.B. Andrews, P. Bryant, T. Ferguson, A. Harilal, C. Liu, T. Mudholkar, M. Paulini, A. Sanchez, W. Terrill

University of Colorado Boulder, Boulder, Colorado, USA
J.P. Cumalat, W.T. Ford, A. Hassani, G. Karathanasis, E. MacDonald, R. Patel, A. Perloff, C. Savard, K. Stenson, K.A. Ulmer, S.R. Wagner

Cornell University, Ithaca, New York, USA
J. Alexander, S. Bright-Thonney, X. Chen, Y. Cheng, D.J. Cranshaw, S. Hogan, J. Monroy, J.R. Patterson, D. Quach, J. Reichert, M. Reid, A. Ryd, W. Sun, J. Thom, P. Wittich, R. Zou

Fermi National Accelerator Laboratory, Batavia, Illinois, USA
M. Albrow, M. Alyari, G. Apollinari, A. Apresyan, A. Apyan, L.A.T. Bauerdick, D. Berry, J. Berryhill, P.C. Bhat, K. Burkett, J.N. Butler, A. Canepa, G.B. Cerati, H.W.K. Cheung, F. Chlebana, K.F. Di Petrillo, V.D. Elvira, Y. Feng, J. Freeman, Z. Gecse, L. Gray, D. Green, S. Grünendahl, O. Gutsche, R.M. Harris, R. Heller, T.C. Herwig, J. Hirschauer, B. Jayatilaka, S. Jindariani, M. Johnson, U. Joshi, T. Klijnsma, B. Klima, K.H.M. Kwok, S. Lammel, D. Lincoln, R. Lipton, T. Liu, C. Madrid, K. Maeshima, C. Mantilla, D. Mason, P. McBride, P. Merkel, S. Mrenna, S. Nahn, J. Ngadiuba, V. O'Dell, V. Papadimitriou, K. Pedro, C. Pena[60], O. Prokofyev,

F. Ravera, A. Reinsvold Hall[92], L. Ristori, E. Sexton-Kennedy, N. Smith, A. Soha, L. Spiegel, S. Stoynev, J. Strait, L. Taylor, S. Tkaczyk, N.V. Tran, L. Uplegger, E.W. Vaandering, H.A. Weber

University of Florida, Gainesville, Florida, USA
P. Avery, D. Bourilkov, L. Cadamuro, V. Cherepanov, F. Errico, R.D. Field, D. Guerrero, B.M. Joshi, M. Kim, E. Koenig, J. Konigsberg, A. Korytov, K.H. Lo, K. Matchev, N. Menendez, G. Mitselmakher, A. Muthirakalayil Madhu, N. Rawal, D. Rosenzweig, S. Rosenzweig, J. Rotter, K. Shi, J. Wang, Z. Wu, E. Yigitbasi, X. Zuo

Florida State University, Tallahassee, Florida, USA
T. Adams, A. Askew, R. Habibullah, V. Hagopian, K.F. Johnson, R. Khurana, T. Kolberg, G. Martinez, H. Prosper, C. Schiber, O. Viazlo, R. Yohay, J. Zhang

Florida Institute of Technology, Melbourne, Florida, USA
M.M. Baarmand, S. Butalla, T. Elkafrawy[93], M. Hohlmann, R. Kumar Verma, D. Noonan, M. Rahmani, F. Yumiceva

University of Illinois at Chicago (UIC), Chicago, Illinois, USA
M.R. Adams, H. Becerril Gonzalez, R. Cavanaugh, S. Dittmer, O. Evdokimov, C.E. Gerber, D.A. Hangal, D.J. Hofman, A.H. Merrit, C. Mills, G. Oh, T. Roy, S. Rudrabhatla, M.B. Tonjes, N. Varelas, J. Viinikainen, X. Wang, Z. Ye

The University of Iowa, Iowa City, Iowa, USA
M. Alhusseini, K. Dilsiz[94], L. Emediato, R.P. Gandrajula, O.K. Köseyan, J.-P. Merlo, A. Mestvirishvili[95], J. Nachtman, H. Ogul[96], Y. Onel, A. Penzo, C. Snyder, E. Tiras[97]

Johns Hopkins University, Baltimore, Maryland, USA
O. Amram, B. Blumenfeld, L. Corcodilos, J. Davis, M. Eminizer, A.V. Gritsan, S. Kyriacou, P. Maksimovic, J. Roskes, M. Swartz, T.Á. Vámi

The University of Kansas, Lawrence, Kansas, USA
A. Abreu, J. Anguiano, C. Baldenegro Barrera, P. Baringer, A. Bean, A. Bylinkin, Z. Flowers, T. Isidori, S. Khalil, J. King, G. Krintiras, A. Kropivnitskaya, M. Lazarovits, C. Le Mahieu, C. Lindsey, J. Marquez, N. Minafra, M. Murray, M. Nickel, C. Rogan, C. Royon, R. Salvatico, S. Sanders, E. Schmitz, C. Smith, J.D. Tapia Takaki, Q. Wang, Z. Warner, J. Williams, G. Wilson

Kansas State University, Manhattan, Kansas, USA
S. Duric, A. Ivanov, K. Kaadze, D. Kim, Y. Maravin, T. Mitchell, A. Modak, K. Nam

Lawrence Livermore National Laboratory, Livermore, California, USA
F. Rebassoo, D. Wright

University of Maryland, College Park, Maryland, USA
E. Adams, A. Baden, O. Baron, A. Belloni, S.C. Eno, N.J. Hadley, S. Jabeen, R.G. Kellogg, T. Koeth, Y. Lai, S. Lascio, A.C. Mignerey, S. Nabili, C. Palmer, M. Seidel, A. Skuja, L. Wang, K. Wong

Massachusetts Institute of Technology, Cambridge, Massachusetts, USA
D. Abercrombie, G. Andreassi, R. Bi, W. Busza, I.A. Cali, Y. Chen, M. D'Alfonso, J. Eysermans, C. Freer, G. Gomez Ceballos, M. Goncharov, P. Harris, M. Hu, M. Klute, D. Kovalskyi, J. Krupa, Y.-J. Lee, C. Mironov, C. Paus, D. Rankin, C. Roland, G. Roland, Z. Shi, G.S.F. Stephans, J. Wang, Z. Wang, B. Wyslouch

University of Minnesota, Minneapolis, Minnesota, USA
R.M. Chatterjee, A. Evans, J. Hiltbrand, Sh. Jain, M. Krohn, Y. Kubota, J. Mans, M. Revering, R. Rusack, R. Saradhy, N. Schroeder, N. Strobbe, M.A. Wadud

University of Nebraska-Lincoln, Lincoln, Nebraska, USA
K. Bloom, M. Bryson, S. Chauhan, D.R. Claes, C. Fangmeier, L. Finco, F. Golf, C. Joo, I. Kravchenko, M. Musich, I. Reed, J.E. Siado, G.R. Snow†, W. Tabb, A. Wightman, F. Yan, A.G. Zecchinelli

State University of New York at Buffalo, Buffalo, New York, USA
G. Agarwal, H. Bandyopadhyay, L. Hay, I. Iashvili, A. Kharchilava, C. McLean, D. Nguyen, J. Pekkanen, S. Rappoccio, A. Williams

Northeastern University, Boston, Massachusetts, USA
G. Alverson, E. Barberis, Y. Haddad, Y. Han, A. Hortiangtham, A. Krishna, J. Li, G. Madigan, B. Marzocchi, D.M. Morse, V. Nguyen, T. Orimoto, A. Parker, L. Skinnari, A. Tishelman-Charny, T. Wamorkar, B. Wang, A. Wisecarver, D. Wood

Northwestern University, Evanston, Illinois, USA
S. Bhattacharya, J. Bueghly, Z. Chen, A. Gilbert, T. Gunter, K.A. Hahn, Y. Liu, N. Odell, M.H. Schmitt, M. Velasco

University of Notre Dame, Notre Dame, Indiana, USA
R. Band, R. Bucci, M. Cremonesi, A. Das, N. Dev, R. Goldouzian, M. Hildreth, K. Hurtado Anampa, C. Jessop, K. Lannon, J. Lawrence, N. Loukas, D. Lutton, J. Mariano, N. Marinelli, I. Mcalister, T. McCauley, C. Mcgrady, K. Mohrman, C. Moore, Y. Musienko[53], R. Ruchti, A. Townsend, M. Wayne, M. Zarucki, L. Zygala

The Ohio State University, Columbus, Ohio, USA
B. Bylsma, L.S. Durkin, B. Francis, C. Hill, M. Nunez Ornelas, K. Wei, B.L. Winer, B.R. Yates

Princeton University, Princeton, New Jersey, USA
F.M. Addesa, B. Bonham, P. Das, G. Dezoort, P. Elmer, A. Frankenthal, B. Greenberg, N. Haubrich, S. Higginbotham, A. Kalogeropoulos, G. Kopp, S. Kwan, D. Lange, D. Marlow, K. Mei, I. Ojalvo, J. Olsen, D. Stickland, C. Tully

University of Puerto Rico, Mayaguez, Puerto Rico, USA
S. Malik, S. Norberg

Purdue University, West Lafayette, Indiana, USA
A.S. Bakshi, V.E. Barnes, R. Chawla, S. Das, L. Gutay, M. Jones, A.W. Jung, D. Kondratyev, A.M. Koshy, M. Liu, G. Negro, N. Neumeister, G. Paspalaki, S. Piperov, A. Purohit, J.F. Schulte, M. Stojanovic[16], J. Thieman, F. Wang, R. Xiao, W. Xie

Purdue University Northwest, Hammond, Indiana, USA
J. Dolen, N. Parashar

Rice University, Houston, Texas, USA
D. Acosta, A. Baty, T. Carnahan, M. Decaro, S. Dildick, K.M. Ecklund, S. Freed, P. Gardner, F.J.M. Geurts, A. Kumar, W. Li, B.P. Padley, R. Redjimi, W. Shi, A.G. Stahl Leiton, S. Yang, L. Zhang[98], Y. Zhang

University of Rochester, Rochester, New York, USA
A. Bodek, P. de Barbaro, R. Demina, J.L. Dulemba, C. Fallon, T. Ferbel, M. Galanti,

A. Garcia-Bellido, O. Hindrichs, A. Khukhunaishvili, E. Ranken, R. Taus

Rutgers, The State University of New Jersey, Piscataway, New Jersey, USA
B. Chiarito, J.P. Chou, M. Christos, A. Gandrakota, Y. Gershtein, E. Halkiadakis, A. Hart, M. Heindl, O. Karacheban[23], I. Laflotte, A. Lath, R. Montalvo, K. Nash, M. Osherson, S. Salur, S. Schnetzer, S. Somalwar, R. Stone, S.A. Thayil, S. Thomas, H. Wang

University of Tennessee, Knoxville, Tennessee, USA
H. Acharya, A.G. Delannoy, S. Fiorendi, S. Spanier

Texas A&M University, College Station, Texas, USA
O. Bouhali[99], M. Dalchenko, A. Delgado, R. Eusebi, J. Gilmore, T. Huang, T. Kamon[100], H. Kim, S. Luo, S. Malhotra, R. Mueller, D. Overton, D. Rathjens, A. Safonov

Texas Tech University, Lubbock, Texas, USA
N. Akchurin, J. Damgov, V. Hegde, S. Kunori, K. Lamichhane, S.W. Lee, T. Mengke, S. Muthumuni, T. Peltola, I. Volobouev, Z. Wang, A. Whitbeck

Vanderbilt University, Nashville, Tennessee, USA
E. Appelt, S. Greene, A. Gurrola, W. Johns, A. Melo, H. Ni, K. Padeken, F. Romeo, P. Sheldon, S. Tuo, J. Velkovska

University of Virginia, Charlottesville, Virginia, USA
M.W. Arenton, B. Cardwell, B. Cox, G. Cummings, J. Hakala, R. Hirosky, M. Joyce, A. Ledovskoy, A. Li, C. Neu, C.E. Perez Lara, B. Tannenwald, S. White

Wayne State University, Detroit, Michigan, USA
N. Poudyal

University of Wisconsin - Madison, Madison, WI, Wisconsin, USA
S. Banerjee, K. Black, T. Bose, S. Dasu, I. De Bruyn, P. Everaerts, C. Galloni, H. He, M. Herndon, A. Hervé, U. Hussain, A. Lanaro, A. Loeliger, R. Loveless, J. Madhusudanan Sreekala, A. Mallampalli, A. Mohammadi, D. Pinna, A. Savin, V. Shang, V. Sharma, W.H. Smith, D. Teague, S. Trembath-Reichert, W. Vetens

†: Deceased
1: Also at TU Wien, Wien, Austria
2: Also at Institute of Basic and Applied Sciences, Faculty of Engineering, Arab Academy for Science, Technology and Maritime Transport, Alexandria, Egypt
3: Also at Université Libre de Bruxelles, Bruxelles, Belgium
4: Also at Universidade Estadual de Campinas, Campinas, Brazil
5: Also at Federal University of Rio Grande do Sul, Porto Alegre, Brazil
6: Also at The University of the State of Amazonas, Manaus, Brazil
7: Also at University of Chinese Academy of Sciences, Beijing, China
8: Also at Department of Physics, Tsinghua University, Beijing, China
9: Also at UFMS, Nova Andradina, Brazil
10: Also at Nanjing Normal University Department of Physics, Nanjing, China
11: Now at The University of Iowa, Iowa City, Iowa, USA
12: Also at National Research Center 'Kurchatov Institute', Moscow, Russia
13: Also at Joint Institute for Nuclear Research, Dubna, Russia
14: Now at British University in Egypt, Cairo, Egypt
15: Now at Cairo University, Cairo, Egypt
16: Also at Purdue University, West Lafayette, Indiana, USA

17: Also at Université de Haute Alsace, Mulhouse, France
18: Also at Erzincan Binali Yildirim University, Erzincan, Turkey
19: Also at CERN, European Organization for Nuclear Research, Geneva, Switzerland
20: Also at RWTH Aachen University, III. Physikalisches Institut A, Aachen, Germany
21: Also at University of Hamburg, Hamburg, Germany
22: Also at Isfahan University of Technology, Isfahan, Iran
23: Also at Brandenburg University of Technology, Cottbus, Germany
24: Also at Forschungszentrum Jülich, Juelich, Germany
25: Also at Physics Department, Faculty of Science, Assiut University, Assiut, Egypt
26: Also at Karoly Robert Campus, MATE Institute of Technology, Gyongyos, Hungary
27: Also at Institute of Physics, University of Debrecen, Debrecen, Hungary
28: Also at Institute of Nuclear Research ATOMKI, Debrecen, Hungary
29: Now at Universitatea Babes-Bolyai - Facultatea de Fizica, Cluj-Napoca, Romania
30: Also at MTA-ELTE Lendület CMS Particle and Nuclear Physics Group, Eötvös Loránd University, Budapest, Hungary
31: Also at Wigner Research Centre for Physics, Budapest, Hungary
32: Also at IIT Bhubaneswar, Bhubaneswar, India
33: Also at Institute of Physics, Bhubaneswar, India
34: Also at Punjab Agricultural University, Ludhiana, India
35: Also at Shoolini University, Solan, India
36: Also at University of Hyderabad, Hyderabad, India
37: Also at University of Visva-Bharati, Santiniketan, India
38: Also at Indian Institute of Science (IISc), Bangalore, India
39: Also at Indian Institute of Technology (IIT), Mumbai, India
40: Also at Deutsches Elektronen-Synchrotron, Hamburg, Germany
41: Now at Department of Physics, Isfahan University of Technology, Isfahan, Iran
42: Also at Sharif University of Technology, Tehran, Iran
43: Also at Department of Physics, University of Science and Technology of Mazandaran, Behshahr, Iran
44: Now at INFN Sezione di Bari, Università di Bari, Politecnico di Bari, Bari, Italy
45: Also at Italian National Agency for New Technologies, Energy and Sustainable Economic Development, Bologna, Italy
46: Also at Centro Siciliano di Fisica Nucleare e di Struttura Della Materia, Catania, Italy
47: Also at Scuola Superiore Meridionale, Università di Napoli Federico II, Napoli, Italy
48: Also at Università di Napoli 'Federico II', Napoli, Italy
49: Also at Consiglio Nazionale delle Ricerche - Istituto Officina dei Materiali, Perugia, Italy
50: Also at Riga Technical University, Riga, Latvia
51: Also at Consejo Nacional de Ciencia y Tecnología, Mexico City, Mexico
52: Also at IRFU, CEA, Université Paris-Saclay, Gif-sur-Yvette, France
53: Also at Institute for Nuclear Research, Moscow, Russia
54: Now at National Research Nuclear University 'Moscow Engineering Physics Institute' (MEPhI), Moscow, Russia
55: Also at Institute of Nuclear Physics of the Uzbekistan Academy of Sciences, Tashkent, Uzbekistan
56: Also at St. Petersburg Polytechnic University, St. Petersburg, Russia
57: Also at University of Florida, Gainesville, Florida, USA
58: Also at Imperial College, London, United Kingdom
59: Also at P.N. Lebedev Physical Institute, Moscow, Russia
60: Also at California Institute of Technology, Pasadena, California, USA

61: Also at Budker Institute of Nuclear Physics, Novosibirsk, Russia
62: Also at Faculty of Physics, University of Belgrade, Belgrade, Serbia
63: Also at Trincomalee Campus, Eastern University, Sri Lanka, Nilaveli, Sri Lanka
64: Also at INFN Sezione di Pavia, Università di Pavia, Pavia, Italy
65: Also at National and Kapodistrian University of Athens, Athens, Greece
66: Also at Ecole Polytechnique Fédérale Lausanne, Lausanne, Switzerland
67: Also at Universität Zürich, Zurich, Switzerland
68: Also at Stefan Meyer Institute for Subatomic Physics, Vienna, Austria
69: Also at Laboratoire d'Annecy-le-Vieux de Physique des Particules, IN2P3-CNRS, Annecy-le-Vieux, France
70: Also at Şırnak University, Sirnak, Turkey
71: Also at Near East University, Research Center of Experimental Health Science, Nicosia, Turkey
72: Also at Konya Technical University, Konya, Turkey
73: Also at Piri Reis University, Istanbul, Turkey
74: Also at Adiyaman University, Adiyaman, Turkey
75: Also at Necmettin Erbakan University, Konya, Turkey
76: Also at Bozok Universitetesi Rektörlügü, Yozgat, Turkey
77: Also at Marmara University, Istanbul, Turkey
78: Also at Milli Savunma University, Istanbul, Turkey
79: Also at Kafkas University, Kars, Turkey
80: Also at Istanbul Bilgi University, Istanbul, Turkey
81: Also at Hacettepe University, Ankara, Turkey
82: Also at Istanbul University - Cerrahpasa, Faculty of Engineering, Istanbul, Turkey
83: Also at Ozyegin University, Istanbul, Turkey
84: Also at Vrije Universiteit Brussel, Brussel, Belgium
85: Also at School of Physics and Astronomy, University of Southampton, Southampton, United Kingdom
86: Also at Rutherford Appleton Laboratory, Didcot, United Kingdom
87: Also at IPPP Durham University, Durham, United Kingdom
88: Also at Monash University, Faculty of Science, Clayton, Australia
89: Also at Università di Torino, Torino, Italy
90: Also at Bethel University, St. Paul, Minneapolis, USA
91: Also at Karamanoğlu Mehmetbey University, Karaman, Turkey
92: Also at United States Naval Academy, Annapolis, N/A, USA
93: Also at Ain Shams University, Cairo, Egypt
94: Also at Bingol University, Bingol, Turkey
95: Also at Georgian Technical University, Tbilisi, Georgia
96: Also at Sinop University, Sinop, Turkey
97: Also at Erciyes University, Kayseri, Turkey
98: Also at Institute of Modern Physics and Key Laboratory of Nuclear Physics and Ion-beam Application (MOE) - Fudan University, Shanghai, China
99: Also at Texas A&M University at Qatar, Doha, Qatar
100: Also at Kyungpook National University, Daegu, Korea